RHODES UNIVERSITY

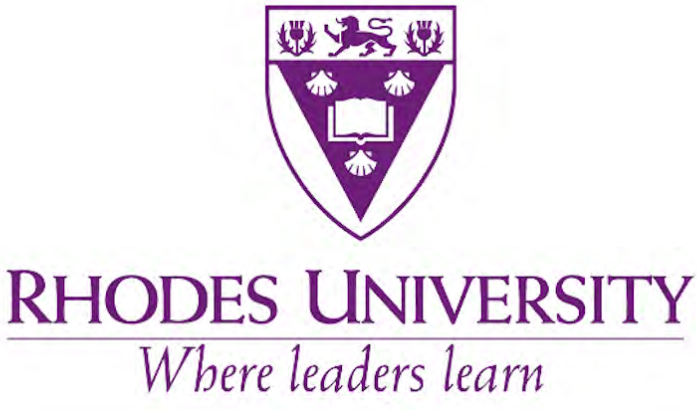

Thermoluminescence and Phototransferred Thermoluminescence of Tanzanite

by: Kingsley Acheampong Opoku

supervisor: Professor Makaiko L. Chithambo

Submitted in fulfilment of the requirements for the degree of

Master of Science

in

Physics

January 2024

Abstract

The thermoluminescence (TL) and phototransferred thermoluminescence (PTTL) properties of tanzanite, an extremely rare gem mineral, have been investigated. While tanzanite shows sensitivity to thermal and optical stimulation of luminescence techniques used for defect probing in insulators, it has received little attention in this regard. A glow curve corresponding to 70 Gy and measured at 1 °C s^{-1} revealed a high intensity peak at 74 °C (peak I) and two secondary peaks at 138 and 186 °C (peaks II and III). All the peaks exhibit a first order kinetics characteristics, as their positions remained unaffected by changes in either dose or partial heating $(T_m - T_{stop})$. For variable doses from 10 to 200 Gy, the dose response of each peak is sublinear from the analysis of supralinearity indices. Peak I fades at room temperature when readout is delayed following irradiation, and this loss is due to thermal fading. The secondary peaks do not fade. Various methods of kinetic analysis were used to compute the kinetic parameters. For the respective peaks, the activation energy is about 0.84, 1.00 and 1.19 eV. All the peaks suffer thermal quenching with increasing heating rate. Continuous wave optically stimulated luminescence measurements were conducted to supplement the TL analysis with the aim of evaluating the kinetic parameters activation energy of thermal assistance (E_a) and quenching (ΔE). The OSL source traps are the same as the TL source traps and occur within 40 to 90 °C, 110 to 145 °C and 160 to 220 °C. The kinetic parameter ΔE when luminescence from all the source traps is considered is comparable to that when source traps within 110 to 220 °C are measured and does not depend on the dose (10, 50 or 70Gy). Except for irradiation to 10 Gy, E_a is also comparable. For traps within 160 to 220 °C, ΔE is comparable for the different doses but higher than that of the other traps, and a similar pattern was observed for E_a. Measurement of the PTTL signal induced by 470 nm blue LEDs following irradiation to 150 Gy and preheating to 158 °C showed that the TL peaks I and II were reproduced under phototransfer. The analysis for order of kinetics and dose response yielded the same results as the convention TL peaks. The model used to describe the PTTL intensity time response profiles shows that the PTTL emanates from a system of one acceptor and three donors, where the latter is a conglomerate of an unknown number of peaks.

Acknowledgement

I would like to express my profound gratitude to my supervisor, Prof. Chithambo, for his immense support, guidance, patience and encouragement throughout my study period. It was a great privilege to work under your supervision. Thank you very much, Prof. Chithambo, for helping me to achieve this significant milestone in my life.

I extend my sincere appreciation to the Ghana Education Trust Fund (GETFund) for the financial support towards my studies. Without this assistance, I could not have realized my dream of furthering my education.

I appreciate the support and companionship of my colleagues: Godfred, Fiindje, Cyndie, Lexy and Victoria. I also thank all the teaching and non-teaching staff at the Department of Physics and Electronics for their assistance. Special thanks to Afia, Biya, Gershon, David, Kyerewaa and Priscilla for your encouragement and well wishes.

My research could not have been successful without the unflinching prayers, love and encouragement received from my family. To my dad, John, my mum, Agnes, and my sisters, Suzzy, Dora and Abi, I love you all. Thank you for being so supportive.

Content

List of Figures

Chapter 1

Introduction

Luminescence is defined as light emitted from an insulator or semiconductor following absorption of energy from ionizing radiation such as x-rays, alpha particles, beta particles or gamma radiation [1]. The energy from the ionizing source excites electrons from the valence band to the conduction band. Ultra-violet light can also trigger excitation [2]. For an ideal crystalline solid with no defects, some of the excited electrons may transit back into the valence band and give off excess energy as luminescence. Lattice defects in semiconductors and insulators act as charge trapping centres where some of the excited charges are trapped. The presence of defects introduces localised energy levels within the band gap. Luminescence is produced when the trapped charges return to ground state by optical or thermal stimulation.

The period between irradiation and emission of light is the characteristics time τ_c [1]. The excited charges may immediately return to the ground state or reside in the traps for few seconds or many years depending on the excitation temperature or trap depth. The characteristics time is used to categorise the luminescence process into fluorescence and phosphorescence. Figure 1 illustrates both the fluorescence and phosphorescence mechanisms. The ground and excited levels are represented as *g* and *e* respectively. For fluorescence, τ_c is less than 10^{-8} s hence the excited electrons (transition a) immediately return to the ground level (transition b) with the emission of light [2]. No light is emitted with the cessation of excitation. For phosphorescence, τ_c is greater than 10^{-8} s [2]. The excited electrons are trapped at defect sites (transition c). Luminescence occurs when the trapped electrons transit into the excited level (transition d) and return to ground level (transition b). If the energy source that induced the transition of trapped electrons into the excited level is heat, thermoluminescence is said to have occurred [2]. On the other hand, if the energy source is light, optically stimulated luminescence is the case [3]. Phosphorescence is further divided into short period where τ_c is less than 10^{-4} s and long period where τ_c is greater than 10^{-4} s [1]. Our work shall focus on long period phosphorescence.

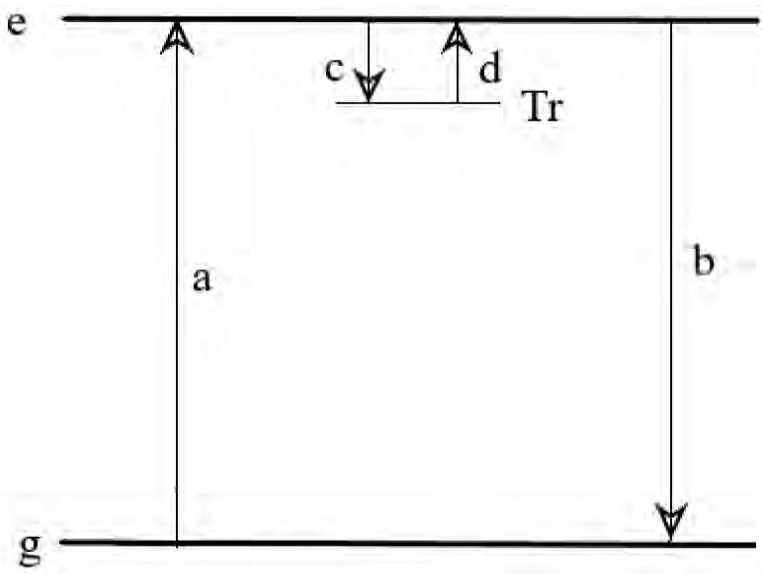

Figure 1.1: Energy level diagram showing the mechanisms of fluorescence and phosphorescence. The ground and excited energy levels are represented as *g* and *e* respectively. *Tr* is a trap level. The arrows show the directions of electron transitions.

Luminescence research has been a useful tool in studying imperfections and impurities present in insulators and semiconductors. A large volume of published works has mainly focused on thermoluminescence and optically stimulated luminescence of materials such as carbon-doped aluminium oxide (Al_2O_3:C), beryllium oxide (BeO), lithium fluoride (LiF), calcium fluoride (CaF_2), quartz and feldspar since most of these materials exhibit high sensitivity to stimulated luminescence and linearity over wide range of doses which are desirable properties in dosimetry [4, 5]. These luminescence materials are applied in such areas as environmental and workplace radiation monitoring, personal dosimetry, space dosimetry and dating. The luminescence mechanism of most of these materials is however not fully understood which poses challenges in dosimetry applications. An example is the case of Al_2O_3:C where the changes in luminescence sensitivity with irradiation history caused by competitor traps is still unclear [6]. The quest to broaden our current understanding has catalysed extensive studies on the luminescence dynamics of both well-established and recently discovered luminescence materials such as tanzanite.

Tanzanite is a rare gem mineral mostly known for its aesthetic purposes. The splendid pleochroism display of the gem at different crystallographic orientations is one reason tanzanite

is highly sought after commercially. Tanzania is the only country with tanzanite deposits. Details of the crystal structure and properties of tanzanite shall be provided later. The few luminescence studies of tanzanite have shown that the gem is sensitive to thermal and optical stimulation of luminescence [7, 8, 9].

1.1 Aims and objectives

The aim of this work is to understand the dynamics of thermoluminescence and phototransferred thermoluminescence in tanzanite. Optically stimulated luminescence measurements were made to supplement the thermoluminescence and obtain analytical information otherwise not possible using thermoluminescence alone. The specific objectives are as follows:

(i) Perform comprehensive kinetic analysis of the thermoluminescence and analyse the dosimetric features.
(ii) Investigate how different doses and measurement temperatures affect the optically stimulated luminescence properties of tanzanite.
(iii) Study the non-radiative recombination processes in thermoluminescence, optically stimulated luminescence and phototransferred thermoluminescence.
(iv) Analyse the role deep electron traps play in the luminescence mechanism in tanzanite.
(v) Study the mechanism of electron transfer from deep electron traps to empty shallow traps under optical stimulation by blue LEDs.

1.2 Research justification

Tanzanite is sensitive to thermal and optical stimulation of luminescence techniques used to study point defects in insulators. Notwithstanding, only two works [7, 8] have been reported on the luminescence properties of the gem. The kinetic analysis of the primary thermoluminescence peak was reported in the first work [7] but the secondary peaks were excluded. In addition to that, the optically stimulated luminescence properties in terms of the dose response, source traps of the luminescence signal, thermal assistance and quenching of luminescence signal have not

been reported. This thesis seeks to provide more insight into the thermoluminescence and phototransferred thermoluminescence processes in tanzanite.

1.3 Thesis outline

This work is grouped into 7 chapters. The current chapter has introduced the mechanism of luminescence, the aims and objectives of this work, the research justification and the synopsis of the thesis.

Chapter 2 covers the theory of thermoluminescence, optically stimulated luminescence and phototransferred thermoluminescence. The various analytical methods used to compute the kinetic parameters are covered in this section.

Chapter 3 discusses the instruments and details of the sample used for this work.

Chapters 4,5 and 6 present the results and discussions of the thermoluminescence, optically stimulated luminescence and phototransferred thermoluminescence measurements.

Chapter 7 concludes the whole thesis and outlines some recommendations for future work.

Chapter 2

Theoretical background

2.1 Thermoluminescence

The mechanism of thermoluminescence is explained using the band theory of solids. Figure 2.1 shows the energy band structure of an insulator. At equilibrium state, the conduction band has no electrons whereas the valence band is full of electrons. In between the valence band and the conduction band is an energy gap or band gap. The value of the band gap for an insulator can be up to 2.5 eV [10]. For an ideal crystalline material with no defects, there would be no energy levels in the band gap. The presence of defects creates localised energy centres inside the energy gap which act as charge traps (*Tr* and *R*). The defects may be vacancies at lattice points (example: Frenkel defects) or impurities that distort the periodicity of the crystal structure [11]. Metals have no band gap and therefore are not considered luminescence materials. At equilibrium state, the fermi energy level, defined as the maximum energy level at zero Kelvin [11] lies above the valence band. The stages for thermoluminescence emission, namely, irradiation and heating are elaborated below.

During irradiation, electrons (solid circles) in the valence band gain energy greater than the band gap and transit into the conduction band (transition a). The transition creates a hole (open circle) in the valence band. The excited electrons transit into the trap *Tr* and holes move into the recombination centre *R* (transition b) creating a metastable state. A metastable state is a non-equilibrium energy level. The potential barrier between the edge of the conduction band and the trap is the trap depth or activation energy (*E*) [2]. The trapped electrons are liberated by gaining energy greater than the trap depth. Shallow electron traps located near the edge of the conduction band are very unstable hence electron detrapping can occur at room temperature. The irradiation temperature may also be sufficient to cause detrapping of electrons from shallow traps. Deep traps on the other hand are stable hence require higher amount of energy to cause electron detrapping.

In thermoluminescence, the material is heat treated at a constant rate resulting in thermal agitation and subsequent release of trapped electrons into the conduction band (transition c). The temperature of the system as a function of time can be expressed as

$$T(t) = T_0 + \beta t \tag{2.1}$$

where T_0 is the initial temperature prior to heating and $\beta = dT/dt$ is the heating rate in units of K/s. The electron escape from the trap (Tr) is modulated by

$$p = sexp^{-\frac{E}{kT}} \tag{2.2}$$

where p is the thermal excitation probability, E is the activation energy, k is Boltzmann's constant, T is the temperature and s is the frequency factor [12]. The frequency factor is the number of times per second the electrons interacts with lattice phonons [12] and its magnitude is in the order of the Debye vibration frequency($\sim 10^{12} - 10^{14}\ s^{-1}$) [13].

Following detrapping into the conduction band, the electrons return to equilibrium level by recombining with trapped hole at the recombination centre (transition d) with emission of light or luminescence which is characterized by glow curves. A glow curve is a plot of the luminescence signal against temperature [14]. The glow curve peaks at temperatures corresponding to different trap depths. A broad peak representing a collocation of trap depths that are very close to each other may also be observed.

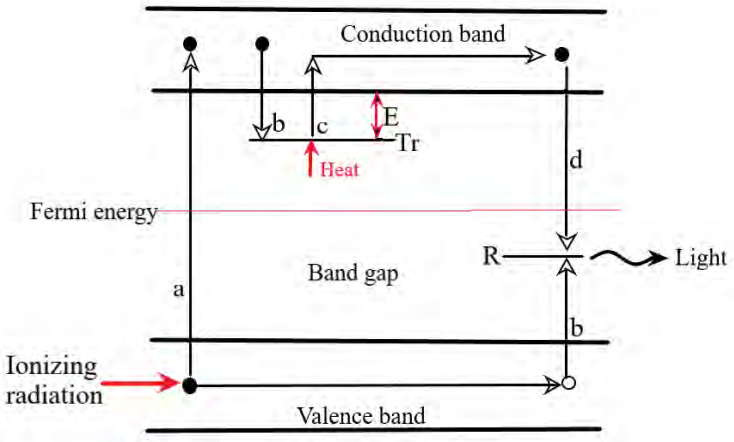

Figure 2.1: Energy band diagram of an insulator illustrating the thermoluminescence mechanism. The solid and open circles represent electrons and holes respectively. The straight black arrows show the direction of the charges.

2.1.1 Mathematical treatment of thermoluminescence

Figure 2.2 is a simple energy band diagram with one electron trap and one recombination centre (OTOR model) [2]. The total concentration of electron traps is represented by N (cm^{-3}), the total concentration of hole traps is represented by M (cm^{-3}), and n (cm^{-3}) and m (cm^{-3}) are the concentrations of trapped electrons and holes respectively. The concentrations of free electrons and holes in the conduction and valence bands are n_c (cm^{-3}) and n_v (cm^{-3}) respectively.

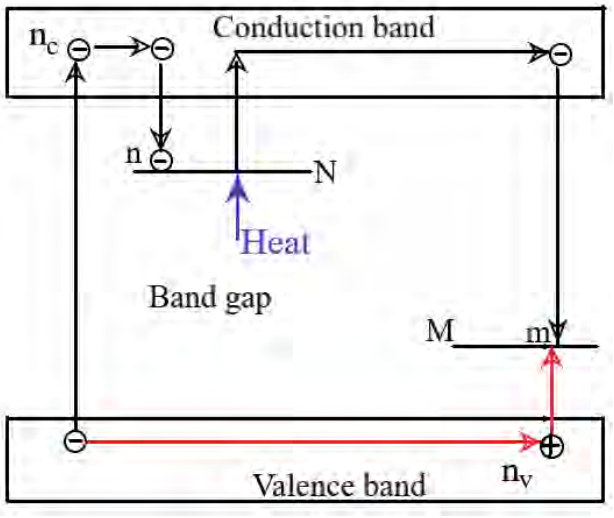

Figure 2.2: An energy band diagram of one trap and one recombination centre (OTOR). The negative circles and positive circle represent electrons and holes. The electron trap and recombination centre are respectively denoted as N and M whereas n and m are the concentrations of trapped electrons and holes respectively. The black and red arrows show the transition paths of the electron and hole.

The rate of electron detrapping is given by

$$\frac{dn^-}{dt} = np \tag{2.3}$$

and the rate of electron trapping can be represented as

$$\frac{dn^+}{dt} = n_c(N-n)A_n \tag{2.4}$$

where A_n is the electron trapping probability in $cm^3 s^{-1}$ [15].

The net change of electrons in trap during excitation by ionizing radiation is given by

$$\frac{dn}{dt} = \frac{dn^+}{dt} - \frac{dn^-}{dt} = n_c(N-n)A_n - np. \tag{2.5}$$

The excitation temperature is usually low (approximately at room temperature) hence the term np can be ignored and the probability of electron detrapping during excitation is considered negligible.

Following the same argument leading to equation (2.5), the net change in trapped holes will be

$$\frac{dm}{dt} = \frac{dm^+}{dt} - \frac{dm^-}{dt} = n_v(M-m)B - mn_cA_m. \tag{2.6}$$

where B is hole trapping probability in $cm^3 s^{-1}$ and A_m is the probability of electron-hole recombination at the recombination centre in units of $cm^3 s^{-1}$.

The change of free holes in the valence band is given by

$$\frac{dn_v}{dt} = \frac{dn}{dt} + \frac{dn_c}{dt} - \frac{dm}{dt} \tag{2.7}$$

and the net change of free electrons in the conduction band is expressed as

$$\frac{dn_c}{dt} = X - n_c(N-n)A_n - mn_cA_m \tag{2.8}$$

where X is the rate of electron-hole pair creation. For the charges in the system to remain neutral, the total concentration of holes must balance the total concentration of electrons hence

$$n + n_c = m + m_v\,. \tag{2.9}$$

When irradiation ceases, no electron-hole pairs are further created meaning $X = 0$. The concentration of electrons in the conduction band and holes in the valence band also becomes zero.

Following the application of heat at a linear rate to the system, the thermal stimulation probability becomes greater than zero, the concentration of electrons in the conduction band

becomes greater than zero and the concentration of holes in the valence band remains zero since no holes are thermally stimulated. The heating stage can be mathematically represented as

$$\frac{dn}{dt} = n_c(N-n)A_n - np \tag{2.10}$$

$$I(T) = -\frac{dm}{dt} = mn_cA_m \tag{2.11}$$

$$\frac{dm}{dt} = \frac{dn}{dt} + \frac{dn_c}{dt}. \tag{2.12}$$

The change in the concentration of trapped holes in equation (2.11) is due to recombination of electrons and holes at the recombination centre, resulting in thermoluminescence $I(T)$.

Two assumptions are made to solve the coupled non-linear differential equations (2.10) – (2.12). They are expressed as

$$\left|\frac{dn}{dt}\right|, \left|\frac{dm}{dt}\right| \gg \left|\frac{dn_c}{dt}\right|, \left|\frac{dm_v}{dt}\right| \tag{2.13}$$

and

$$n, m \gg n_c, m_v. \tag{2.14}$$

Equations (2.13) – (2.14) are known as the quasi-equilibrium assumption which states that the rate at which the concentration of free charges change is insignificant compared to that of the trapped charges, and the concentration of free charges is insignificant compared to that of the trapped charges [2]. The parameter $dn_c/dt \cong 0$ in equation (2.12). The parameters dn/dt and $-dm/dt$ in equations (2.10) and (2.11) respectively are substituted into equation (2.12) to yield

$$n_c = \frac{sn\ exp\left(\frac{-E}{kT}\right)}{mA_m + (N-n)A_n}. \tag{2.15}$$

The thermoluminescence intensity $I(T)$ can then be expressed as

$$I = -\frac{dm}{dt} = \frac{mA_m\ sn\ exp\left(\frac{-E}{kT}\right)}{mA_m + (N-n)A_n}. \tag{2.16}$$

Equation (2.16) has been arrived at by substituting equation (2.15) into equation (2.11).

2.1.1.1 First order kinetics

First order kinetics is the case where electron-hole recombination is assumed to be dominant in comparison with electron retrapping. Hence, $A_n(N-n) \ll mA_m$. Moreover, $n \cong m$ and $dn/dt \cong dm/dt$. The thermoluminescence intensity equation (2.16) becomes

$$I = -\frac{dm}{dt} = -\frac{dn}{dt} = sn\ exp\left(\frac{-E}{kT}\right). \tag{2.17}$$

The integral of equation (2.17) from initial temperature T_0 to temperature T at a constant heating rate β is given as

$$I(T) = n_0 s\ exp\left(\frac{-E}{kT}\right)\ exp\left[-\left(\frac{s}{\beta}\right)\int_{T_0}^{T} exp\left(\frac{-E}{k\Theta}\right)d\Theta\right] \tag{2.18}$$

where n_0 is the initial concentration of trapped charges at $T = T_0$ and Θ is a dummy variable representing temperature. Equation (2.18) is the first order kinetics equation as proposed by Randall and Wilkins [16].

2.1.1.2 Second order kinetics

For second order kinetics, Garlick and Gibson [17] considered the case where electron retrapping is dominant compared with recombination, that is, $A_n(N-n) \gg mA_m$. The thermoluminescence intensity equation (2.16) now becomes

$$I = -\frac{dm}{dt} = \frac{mA_m\ sn\ exp\left(\frac{-E}{kT}\right)}{(N-n)A_n}. \tag{2.19}$$

Also, the electron trap N is assumed to be nowhere near saturation hence $N \gg n$. Equation (2.19) is rewritten as

$$I = -\frac{dm}{dt} = \frac{mA_m\ sn\ exp\left(\frac{-E}{kT}\right)}{NA_n}. \tag{2.20}$$

The condition $m = n$ is also imposed on equation (2.20) hence,

$$I = -\frac{dn}{dt} = \frac{n^2 A_m \, s \, exp\left(\frac{-E}{kT}\right)}{N A_n}. \tag{2.21}$$

If the probability of hole and electron retrapping is assumed to be equal, that is, $A_m = A_n$, equation (2.21) turns into

$$I = -\frac{dn}{dt} = \frac{n^2 \, s \, exp\left(\frac{-E}{kT}\right)}{N}. \tag{2.22}$$

For a linear heating rate, the integral of equation (2.22) gives

$$I(T) = \frac{n_o^2 s}{N} \, exp\left(\frac{-E}{kT}\right)\left[1 + \frac{n_o s}{N\beta}\int_{T_o}^{T} exp\left(\frac{-E}{k\Theta}\right) d\Theta\right]^{-2} \tag{2.23}$$

where all symbols are as previously defined. Equation (2.23) can be expressed as

$$I(T) = n_o s'' \, exp\left(\frac{-E}{kT}\right)\left[1 + \frac{s''}{\beta}\int_{T_o}^{T} exp\left(\frac{-E}{k\Theta}\right) d\Theta\right]^{-2} \tag{2.24}$$

where $s'' = sn_0/N$ is the effective pre-exponential factor with unit of s^{-1}.

2.1.1.3 General order kinetics

The general order kinetics is the case where both the first order kinetics equation (2.18) and second order kinetics equation (2.23) does not hold. The thermoluminescence intensity in this case was empirically expressed by May and Patridge [18] as

$$I = \frac{dn}{dt} = s' n^b \, exp\left(\frac{-E}{kT}\right) \tag{2.25}$$

where s' is a constant with dimensions of $m^{3(b-1)}s^{-1}$ and b is a dimensionless quantity termed kinetic order [2]. The parameter b usually lies between 1 and 2. For a linear heating function, the integral of equation (2.25) yields

$$I(T) = n_o s'' \, exp\left(\frac{-E}{kT}\right)\left[1 + (b-1)\frac{s''}{\beta}\int_{T_o}^{T} exp\left(\frac{-E}{k\Theta}\right) d\Theta\right]^{-\left(\frac{b}{b-1}\right)} \tag{2.26}$$

where $s'' = s' n_o^{(b-1)}$ with unit of s^{-1} and all other parameters are as previously defined. Equation (2.26) is the general order kinetics equation. Suppose the kinetic order $b \approx 1$ is inserted into equation (2.26), the final expression will be the first order kinetics equation whereas if $b = 2$ is inserted, the resultant expression is the second order kinetics equation.

2.2 Kinetic analysis for trap parameters

Kinetic analysis is generally performed to evaluate the trap parameters associated with the TL glow curve. The parameters of interest in this study are the activation energy (*E*), the frequency factor (*s*) and the kinetic order (*b*). These three parameters give insight into the thermoluminescence processes. The analytical methods used for the kinetic analysis in this work are elaborated below:

2.2.1 Initial rise method

The initial rise method provides a means of evaluating the activation energy of a glow peak. This analysis is concerned with the initial rising part of a thermoluminescence glow peak. The changes in the concentration of trapped charges at the low temperature region of the rising part is assumed to be negligible [2]. This assumption is valid only within a limited range of temperatures corresponding to the initial rise region. The application of this method requires that the peak is well isolated, and the region is well defined. A common criterion is to consider the part of the initial rise that corresponds to 5-15% of the maximum TL intensity [19]. This method is applicable to any order of kinetics.

The activation energy (*E*) is evaluated by first considering the first order TL equation (2.18). Assuming the temperature change T_0 to T within the region of interest is small,

$$exp\left[-\left(\frac{s}{\beta}\right)\int_{T_o}^{T} exp\left(\frac{-E}{k\Theta}\right)d\Theta\right] \cong 1 \tag{2.27}$$

and equation (2.18) becomes

$$I(T) = n_o s\, exp^{\left(-\frac{E}{kT}\right)} \tag{2.28}$$

where all symbols retain their previous meanings. Equation (2.28) can be rewritten as

$$I(T) = c\ exp^{\left(-\frac{E}{kT}\right)} \tag{2.29}$$

where $c = n_o s$ is a constant. Applying the natural logarithm on both sides of equation (2.29) yields

$$\ln[I(T)] = \ln(c) - \frac{E}{kT}. \tag{2.30}$$

A plot of $\ln(I)$ against $1/kT$ will produce a straight line with a gradient equal to $-E$ and intercept equal to $\ln(c)$.

Following the same assumption leading to equation (2.28), the thermoluminescence intensity for second and general order kinetics can be respectively represented as

$$I(T) = \frac{n_o^2}{N} s\ exp^{\left(-\frac{E}{kT}\right)} \tag{2.31}$$

and

$$I(T) = n_o s''\ exp^{\left(-\frac{E}{kT}\right)}. \tag{2.32}$$

Equations (2.31) and (2.32) can be rewritten in the form of equation (2.30) from which the activation energy can be evaluated from the slope of the plot of $\ln(I)$ against $1/kT$.

2.2.2 Whole glow peak method

Unlike the initial rise method where only a small portion of the glow curve is used for analysis, the whole glow peak method is concerned with the total area under the TL glow peak. The integral $n(T)$ from temperature T_0 to T_f of the TL intensity is estimated to represent the total area under the glow peak. Figure 2.3 shows an example of such a plot. The shaded portion represents the area under the glow curve.

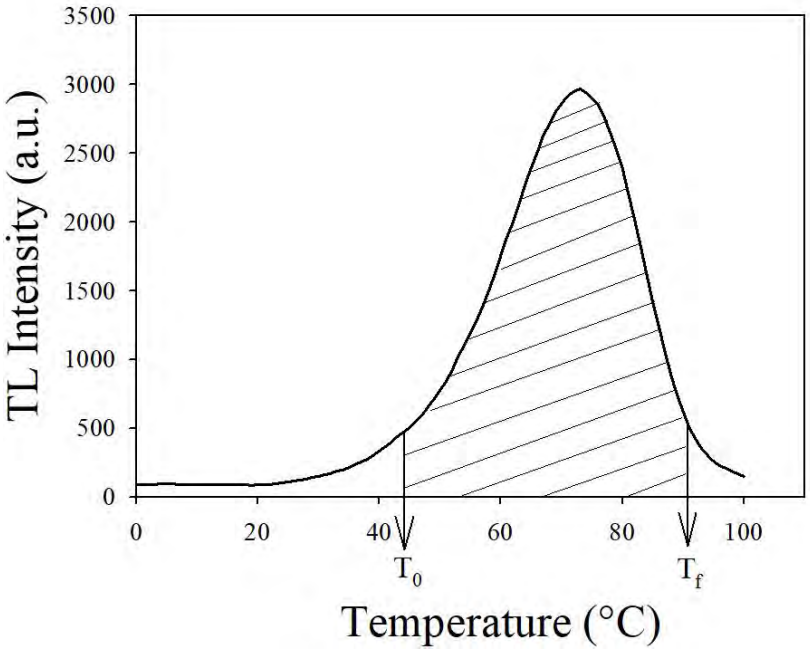

Figure 2.3: Area under a TL peak for whole glow peak analysis. The shaded portion between the initial temperature T_0 and the final temperature T_f is the area.

The integral is expressed as

$$n(T) = \int_{t_o}^{t_f} I dt = \frac{1}{\beta} \int_{T_o}^{T_f} I dT \tag{2.33}$$

where $n(T)$ represents the area under the TL peak within the temperature range T_0 to T_f and all other parameters are as previously defined [1].

The first order kinetics equation (2.17) can be written as a function of temperature T to give

$$I(T) = \frac{ns}{\beta}\, exp\left(-\frac{E}{kT}\right) \tag{2.34}$$

where the meaning of each symbol remains unchanged [15]. Equation (2.34) is rearranged, and the natural logarithm is applied on both sides to yield

$$\ln\left[\frac{I(T)}{n}\right] = \ln\left(\frac{s}{\beta}\right) - \frac{E}{kT} \tag{2.35}$$

where a plot of $\mathrm{In}[I(T)/n]$ against $1/kT$ will give a straight line. The activation energy and frequency factor are evaluated from the gradient and intercept respectively.

The assumptions made to arrive at equation (2.35) can be extended to the general order kinetics equation (2.25) to give

$$\mathrm{In}\left[\frac{I(T)}{n^b}\right] = In\left(\frac{s'}{\beta}\right) - \frac{E}{kT} \tag{2.36}$$

where all symbols have their usual meanings. Various values of b are used in the plot of $\mathrm{In}[I(T)/n^b]$ versus $1/kT$ to obtain several straight lines. The activation energy and frequency factor are computed from the most linear line, that is, the line with the greatest coefficient of determination (r^2) value.

2.2.3 Curve fitting method

For curve fitting procedure, functions that fit well the recorded glow curve are used to compute the activation energy, kinetic order and the frequency factor. The analysis can be applied on collocated TL glow peaks to compute the activation energy and the frequency factor of each peak [20]. Appropriate thermoluminescence functions for the curve fitting procedure have been developed by Kitis et al [21] as follows. For first order kinetics,

$$I(T) = I_m exp\left[1 + \frac{E}{kT}\frac{T - T_m}{T_m} - \frac{T^2}{T_m^2}\left(1 - \frac{2kT_m}{E}\right) exp\left(\frac{E}{kT}\frac{T - T_m}{T_m}\right) - \frac{2kT_m}{E}\right] \tag{2.37}$$

where I_m is the intensity at peak maximum, T_m is the temperature that corresponds to the peak maximum and all other symbols retain their usual definitions.

For second order kinetics,

$$I(T) = 4I_m exp\left(\frac{E}{kT}\frac{T - T_m}{T_m}\right) \times \left[\frac{T^2}{T_m^2}\left(1 - \frac{2kT}{E}\right) exp\left(\frac{E}{kT}\frac{T - T_m}{T_m}\right) + 1 + \frac{2kT_m}{E}\right]^{-2} \tag{2.38}$$

and for general order kinetics,

$$I(T) = I_m b^{\frac{b}{b-1}} exp\left(\frac{E}{kT}\frac{T-T_m}{T_m}\right)\left[1 + (b-1)\frac{2kT_m}{E}\right.$$
$$\left. + (b-1)\left(1 - \frac{2kT}{E}\right)\frac{T^2}{T_m^2} \times exp\left(\frac{E}{kT}\frac{T-T_m}{T_m}\right)\right]^{\frac{-b}{b-1}}. \quad (2.39)$$

The function $I(T)$ is fitted to the glow curve by first determining the values of the parameters I_m and T_m from the experimental TL peak and guessing the value of E. A good guess of E can be obtained from other methods of analysis. The parameters E and s are made to vary until a best fit that minimizes the difference between the experimental data and the predicted data is obtained. Applying equation (2.39) makes the evaluation of both E and b possible as compared with equations (2.37) and (2.38). In case equation (2.39) is used, the parameter b is also guessed and varied until a good fit is obtained.

The figure of merit (FOM) can be used to numerically confirm the goodness of the fitting procedure. The FOM is expressed as

$$FOM = \frac{\sum|y_{exp} - y_{fit}|}{\sum y_{fit}} \quad (2.40)$$

where y_{exp} represents the experimental luminescence data and y_{fit} represents the predicted data points of the fitted function [22]. Generally, FOM value less than 0.035 is acceptable [23].

In practice, several computer software packages are available for conveniently performing the curve fitting procedure. The results for the kinetic parameters however should agree with those obtained from other methods of analysis.

The frequency factor s for the first, second and third order kinetics is evaluated by setting $dI/dT = 0$ in equations (2.18), (2.23) and (2.26) respectively. The peak maximum is where $dI/dT = 0$. Hence,

$$s = \frac{\beta E}{kT_M^2} exp\left(\frac{E}{kT_M}\right) \quad (2.41)$$

$$s = \frac{\beta E}{kT_M^2\left(1 + \frac{2kT_M}{E}\right)} \exp\left(\frac{E}{kT_M}\right) \quad (2.42)$$

and

$$s = \frac{\beta E}{kT_M^2\left(1 + \frac{2kT_M(b-1)}{E}\right)} \exp\left(\frac{E}{kT_M}\right) \tag{2.43}$$

where all terms have been previously defined.

2.2.4 Phosphorescence decay method

Phosphorescence decay is concerned with the measurement of thermoluminescence intensity as a function of time at a fixed temperature [2]. The time dependent function provides a way of evaluating the decay rate of the trapped electrons [19]. Randall and Wilkins [24] were the first to demonstrate the phosphorescence decay method. For first order kinetics, the phosphorescence decay can be represented by an exponential decay function of the form:

$$I(t) = I_0\, exp(-mt) \tag{2.44}$$

where I is the TL intensity as a function of time t, I_0 represents the initial TL intensity and m represents the thermal stimulation probability. The parameter m can be expressed as

$$m = s\, exp\left(-\frac{E}{kT}\right) \tag{2.45}$$

where the meaning of each term remains unchanged [2]. The natural logarithm can be applied to equation (2.44) to get

$$\ln I(t) = \ln I_0 - mt\,. \tag{2.46}$$

A plot of $\ln I(t)$ against t will yield a straight line with gradient equal to $-m$. For phosphorescence measurement taken at two different temperatures T_1 and T_2, their respective gradients m_1 and m_2 can be expressed as

$$\ln\left(\frac{m_1}{m_2}\right) = \frac{E}{k}\left(\frac{1}{T_2} - \frac{1}{T_1}\right). \tag{2.47}$$

The activation energy E can be evaluated from equation (2.47). Subsequently, s can be computed by substituting E into equation (2.45). Alternatively, a number of phosphorescence

measurements at variable temperatures can be recorded and for each measurement, the gradient can be determined from equation (2.46). Equation (2.45) can be written in the form

$$\ln(m) = \ln(s) - \frac{E}{kT} \tag{2.48}$$

where a plot of $\ln(m)$ against $1/kT$ will produce a straight line with gradient equal to -E. The parameter s is computed from the intercept on the y-axis.

For second order kinetics, the TL intensity can be expressed as

$$I(t) = \frac{-dn}{dt} = m'n^2 \tag{2.49}$$

where m' is the probability of thermal stimulation and all other symbols are as earlier defined [2]. The parameter m' is given as

$$m' = s' \, exp\left(-\frac{E}{kT}\right). \tag{2.50}$$

The integral of equation (2.49) gives

$$I(t) = \frac{I_0}{(1 + m'n_0 t)^2}. \tag{2.51}$$

Equation (2.51) can be rearranged as

$$\sqrt{\frac{I_0}{I(t)}} = 1 + m'n_0 t \tag{2.52}$$

where a plot of $\sqrt{I_0/I(t)}$ against t will yield a straight line whose gradient is equal to $m'n_0$. From equation (2.50), the gradient can be expressed as

$$m'n_0 = n_0 s' \, exp\left(-\frac{E}{kT}\right) \tag{2.53}$$

and the natural logarithm can be introduced to get

$$\ln(m'n_0) = \ln(n_0 s') - \frac{E}{kT}. \tag{2.54}$$

According to equation (2.54), several phosphorescence measurements can be taken at different temperatures and the parameters E and $n_0 s$ evaluated by plotting $\ln(m' n_0)$ against $1/kT$.

The integral of the general order kinetics equation (2.26) with respect to time at constant temperature gives

$$I(t) = I_0 \left[1 + m' n_0^{b-1}(b-1)t\ exp\left(-\frac{E}{kT}\right)\right]^{\frac{b}{1-b}}. \tag{2.55}$$

The initial thermoluminescence intensity I_0 can be expressed as

$$I_0 = m' n_0^b exp\left(-\frac{E}{kT}\right) \tag{2.56}$$

where the meaning of each parameter remains unchanged [2]. Equation (2.55) is rearranged to give

$$\left(\frac{I(t)}{I_0}\right)^{\frac{1-b}{b}} = \left[1 + m' n_0^{b-1}(b-1)t\ exp\left(-\frac{E}{kT}\right)\right]. \tag{2.57}$$

A straight line is obtained from the plot of $(I/I_0)^{(1-b)/b}$ against t where the gradient $(m) = m' n_0^{b-1}(b-1)\ \exp(-E/kT)$ provided the value of b is suitable. It is hence convenient to use value of b obtained from other methods of kinetic analysis as an initial estimate. By taking several phosphorescence measurements at different temperatures, numerous gradients can be obtained and a plot of $\ln(m)$ against $1/kT$ will produce a straight line whose gradient is equal to $-E$.

2.2.5 Phosphorescence area method

This method of analysis was introduced by Chithambo [25] to evaluate the activation energy for first order kinetics peaks and the activation energy of thermal quenching ΔE of the thermoluminescence signal. For some limited cases of general order kinetics, the activation energy can be evaluated. The dependence of a small area under a phosphorescence decay on the measurement temperature is of interest for this analysis. From the first order kinetics equation (2.17), the area under the phosphorescence decay can be represented as

$$\frac{d\Phi}{dt'} = -\Phi p \tag{2.58}$$

where t' represents time and is given as $t - t_a$ where $t_a > t$ [25]. This implies $t' < 0$. The parameter Φ represents the area below the segment $|t - t_a|$ of the phosphorescence decay. Hence, we can write

$$\Phi = \Phi_m \exp(-pt') \tag{2.59}$$

where Φ_m represents the total area and all other parameters are as defined before [25]. From the notion that $t' < 0$ and applying the approximation $e^x \approx (1 + x)$, we have

$$\Phi_m(1 - pt') \sim \Phi_m pt'. \tag{2.60}$$

Hence, equation (2.59) can be written as

$$\Phi = -\Phi_m(\mathrm{t} - t_m)\mathrm{s} \exp\left(\frac{-E}{kT}\right). \tag{2.61}$$

Equation (2.61) is simplified to arrive at

$$\Phi = C \exp\left(\frac{-E}{kT}\right) \tag{2.62}$$

where C is a constant equal to $-\Phi_m(\mathrm{t} - t_m)s$. The activation energy is evaluated from the plot of $\mathrm{In}(\Phi)$ against $1/kT$. In applying this method of analysis, the time interval $t - t_a$ selected from the area under the phosphorescence decay curve has to be small enough for the approximation $e^x \approx (1 + x)$ to be valid, or else the computed activation energy will be inaccurate. Figure 2.4 shows an example of a phosphorescence decay curve where only a segment (the solid red line) of the area under the curve is considered.

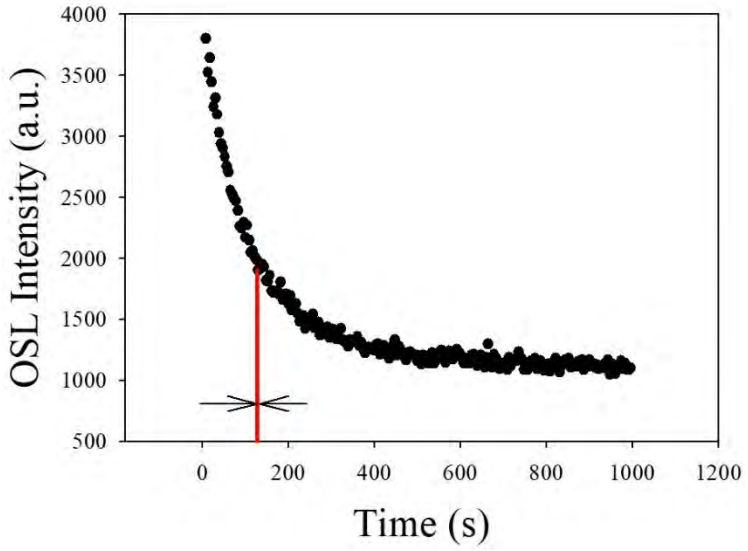

Figure 2.4: Area under a phosphorescence decay curve. The solid red line represents the area within a very small time interval under the decay curve.

The phosphorescence area method can be further applied in a different way to evaluate the activation energy and the kinetic order. The area under the phosphorescence decay Φ is plotted against the measurement temperature. A number of measurements are made at different temperatures to generate several data points of areas against measurement temperatures. Since phosphorescence is simply thermoluminescence recorded at a fixed temperature [2], a pseudo glow peak is generated from the plot of area against temperature. The pseudo peak is then fitted with the Kitis et al. general order curve fitting equation [21], expressed in equation (2.39) to evaluate the activation energy and the kinetic order.

2.2.6 Variable heating rate method

The measurement of thermoluminescence at different heating rates alters the position of the peak. The activation energy and the frequency factor can be computed from this behaviour. For the peak maximum ($dI/dT = 0$), the first order kinetics equation (2.18) reduces to

$$\beta = \frac{kT_m^2}{E} s exp\left(-\frac{E}{kT_m}\right). \tag{2.63}$$

Here, T_m replaces T in equation (2.18). The peak position T_m increases with heating rate β according to equation (2.63). Also, T_m does not depend on the initial concentration of trapped charges. For two variable heating rates β_1 and β_2 and their respective peak temperatures T_{m1} and T_{m2}, the activation energy E can be expressed as

$$E = \frac{kT_{m1}\,T_{m2}}{T_{m1} - T_{m2}}\ \mathrm{In}\left[\frac{\beta_1}{\beta_2}\left(\frac{T_{m2}}{T_{m1}}\right)^2\right] \tag{2.64}$$

where all symbols are as previously defined [12, 26, 27]. The computed activation energy can be substituted into equation (2.63) to calculate the frequency factor s.

Alternatively, TL at several heating rates can be measured and the activation energy evaluated from the relation

$$\mathrm{In}\left(\frac{T_m^2}{\beta}\right) = \frac{E}{kT_m} + \ \mathrm{In}\left(\frac{E}{sk}\right). \tag{2.65}$$

where a plot of $\mathrm{In}(T_m^2/\beta)$ against $1/kT_m$ will yield a straight line [19, 28]. The value of the gradient is the activation energy, and the frequency factor is evaluated from the intercept on the y-axis.

For any kinetic order *b*, the variable heating rate method can be applied to evaluate the activation energy as follows. By differentiating the general order kinetics equation (2.26), the maximum peak intensity I_m can be expressed with respect to the heating rate as

$$I_m^{b-1}\left(\frac{T_m^2}{\beta}\right)^b = \left(\frac{E}{bks}\right)^b exp\left(\frac{E}{kT_m}\right). \tag{2.66}$$

The natural logarithm is applied to equation (2.66) to arrive at

$$\mathrm{In}\left[I_m^{b-1}\left(\frac{T_m^2}{\beta}\right)^b\right] = In\left[\left(\frac{E}{bks}\right)^b\right] + \left(\frac{E}{kT_m}\right) \tag{2.67}$$

where a plot of $\mathrm{In}[I_m^{b-1}(T_m^2/\beta)^b]$ versus $(1/kT_m)$ will yield a straight line for an appropriate value of *b*. The value of the slope is the activation energy. The frequency factor can be calculated from the intercept on the y-axis. Several thermoluminescence measurements are recorded at different heating rates for such a plot.

2.2.7 Peak shape method

The peak shape method is concerned with the geometry of the TL glow peak. Chen [29] proposed mathematical expressions for evaluating the activation energy and the kinetic order for both first and second order kinetics by extracting parameters that correspond to the shape of the TL glow peak. The shape of the glow peak for first order kinetics is not symmetrical while that of second order kinetics is nearly symmetrical [19]. Figure 2.5 shows a TL glow curve and the geometric parameters. The parameter T_M represents the peak temperature, T_1 is the temperature on the left side of T_M that corresponds to half the intensity value $(I_M/2)$ and T_2 represents the temperature on the right side of T_M that corresponds to half the intensity value $(I_M/2)$. The parameters τ, δ, ω, and μ are evaluated as

$$\tau = T_M - T_1 \tag{2.68}$$

$$\delta = T_2 - T_M \tag{2.69}$$

$$\omega = T_2 - T_1 \tag{2.70}$$

and

$$\mu = \frac{\delta}{\omega} \tag{2.71}$$

where τ represents the half-width towards the low temperature region of the peak, δ represents the half-width towards the high temperature region of the peak, ω represents the total half-width and μ represents the geometrical shape factor [19, 29]. For first order kinetics, $\mu = 0.42$ and for second order kinetics, $\mu = 0.52$ [12].

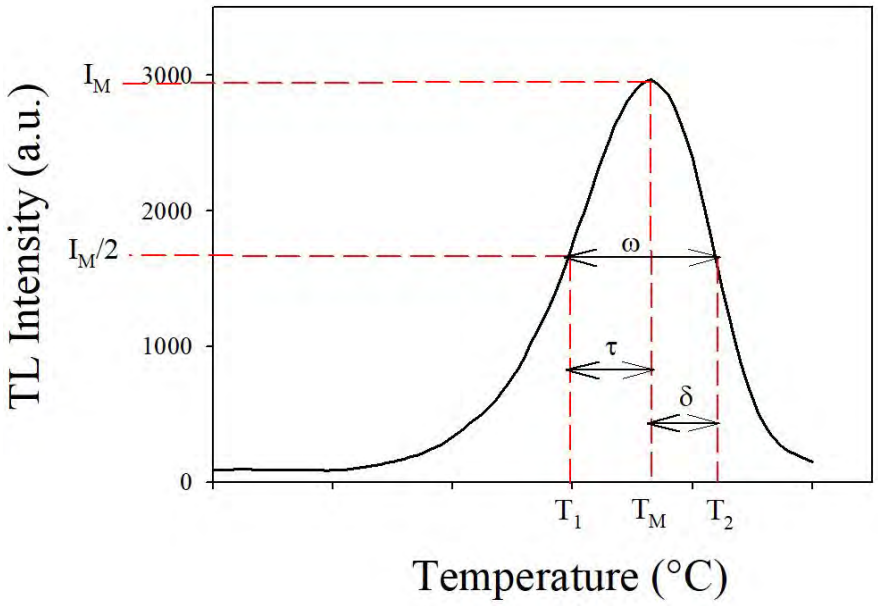

Figure 2.5: A TL glow curve showing the geometric features T_M, T_1, T_2, I_m, $\left(\frac{I_M}{2}\right)$, τ, δ, and ω. The meaning of each term has been explained in the text.

The expression for evaluating the activation energy is given by

$$E_\alpha = C_\alpha\left(\frac{kT_M^2}{\alpha}\right) - b_\alpha(2kT_M) \tag{2.72}$$

where α is any of the parameters τ, δ, or ω [29]. The coefficients C_α and b_α are expressed as

$$C_\tau = 1.51 + 3(\mu - 0.42), \qquad b_\tau = 1.58 + 4.2(\mu - 0.42) \tag{2.73}$$

$$C_\delta = 0.976 + 7.3(\mu - 0.42), \qquad b_\delta = 0 \tag{2.74}$$

and

$$C_\omega = 2.52 + 10.2(\mu - 0.42), \qquad b_\omega = 1. \tag{2.75}$$

For first order kinetics, $\mu = 0.42$ and equation (2.72) can be rewritten in the forms

$$E_\tau = \frac{1.51kT_M^2}{\tau} - 1.58(2kT_M) \tag{2.76}$$

$$E_{\delta} = \frac{0.976kT_M^2}{\delta} \tag{2.77}$$

$$E_{\omega} = \frac{2.52kT_M^2}{\omega} - (2kT_M)\,. \tag{2.78}$$

For second order kinetics, $\mu = 0.52$ and equation (2.72) is rewritten in the forms

$$E_{\tau} = \frac{1.81kT_M^2}{\tau} - 2(2kT_M) \tag{2.79}$$

$$E_{\delta} = \frac{1.71kT_M^2}{\delta} \tag{2.80}$$

$$E_{\omega} = \frac{3.54kT_M^2}{\omega} - (2kT_M)\,. \tag{2.81}$$

The peak shape method therefore yields three parameters (E_{τ}, E_{δ}, and E_{ω}) for the activation energy.

2.3 Glow peak resolution techniques

The recorded glow curve may be a collocation of a number of peaks in cases where more than one electron traps are involved in the luminescence mechanism. Moreover, very high intensity peaks cause low intensity peaks to appear less prominent in the glow curve. The initial rise, variable heating rate and the peak shape methods of kinetic analysis are carried out on well isolated peaks. In cases of overlapping peaks, the following methods are applied to resolve them.

2.3.1 Thermal cleaning

Thermal cleaning [1] is a peak separation procedure used to ascertain the number of glow peaks present. The procedure involves preheating an irradiated sample to a temperature just above the range at which an identified peak occurs. Thermoluminescence measurement is made afterwards. Preheating ensures that the trapped charges contributing to the luminescence of the identified peak are depleted while those of the subsequent peaks, if any, are kept intact. As such, subsequent TL measurement clearly reveals hidden or less prominent peaks.

2.3.2 Partial heating ($T_m - T_{stop}$)

The partial heating technique ($T_m - T_{stop}$) analyses the dependence of the peak position (T_m) on preheat temperature (T_{stop}). An irradiated sample is preheated to T_{stop} following which the thermoluminescence glow curve is measured and the peak position T_m noted. The procedure is repeated but at a different T_{stop} each time. The selected range of T_{stop} values fall below the peak position T_m. For first order kinetics, the peak position T_m does not depend on the initial concentration of trapped charges hence shows no variation with partial heating T_{stop}. For second order kinetics, T_m changes with T_{stop} because the peak position depends on the initial concentration of trapped charges [1]. For peaks which are very close to each other, a plot of T_m against T_{stop} will show different levels of T_m where each level is associated with a particular peak.

2.4 Thermal quenching

Thermal quenching is associated with a decrease in luminescence intensity as the temperature of measurement is increased [30]. The variable heating rate method discussed earlier showed that any variation in the heating rate causes changes to the peak position. The luminescence efficiency (η) is also affected according to the relation

$$\eta = \frac{\Gamma_{rad}}{\Gamma_{rad} + \Gamma_{nrad}} \tag{2.82}$$

where Γ_{rad} is the radiative transition probability and Γ_{nrad} is the non-radiative transition probability. The luminescence efficiency expresses the radiative transition probability to the total transition probability. A decrease in the probability of radiative transition means a reduction in η. The parameter η can also be written as a function of temperature as

$$\eta(T) = \frac{1}{1 + Cexp\left(\frac{W}{kT}\right)} \tag{2.83}$$

where C is a constant, W is activation energy of thermal quenching and all other symbols are as previously defined [15]. The parameter Γ_{rad} in equation (2.82) is equated to 1 in equation (2.83).

Thermal quenching becomes more prominent with increasing heating rate. Assuming the effect of thermal quenching at the lowest heating rate is the least and increases with heating rate, the luminescence efficiency can be represented by the equation

$$\eta(T) = \frac{I_{qn}}{I_{un}} \tag{2.84}$$

where I_{qn} is the quenched TL intensity and I_{un} is the unquenched TL intensity [25]. The parameters I_{qn} and I_{un} represent the integral under the quenched and unquenched TL peak respectively. Hence, equation (2.83) can be rewritten as

$$\frac{I_{un}}{I_{qn}} - 1 = Cexp\left(-\frac{W}{kT_m}\right) \tag{2.85}$$

and the natural logarithm is applied to both sides of equation (2.85) to yield

$$\ln\left[\left(\frac{I_{un}}{I_{qn}}\right) - 1\right] = \ln C - \frac{W}{kT_m}. \tag{2.86}$$

A plot of $\ln(I_{un}/I_{qn} - 1)$ against $1/(kT_m)$ will give a straight line of gradient equal to $-W$. The y-intercept is equal to $\ln C$.

The mechanism of thermal quenching in luminescence materials has been elaborated in many research [31 - 34] using the Mott-Seitz configurational coordinate model. Figure 2.6 presents the various decay processes in the configurational coordinate model. The recombination pathway for an electron in an excited state within the recombination centre consists of radiative and non-radiative decay processes. The recombination centre is made up of the ground state and the excited state. The symbols E_e and E_g represent the excited state and the ground state energy levels. Strong electron-lattice coupling causes the energy curves to cross at point *F.* An electron in its relaxed excited state can transit to position *Qe* of the ground state (transition b) with the emission of photon and such transition is considered as radiative recombination. Thereafter, the electron undergoes multiphonon relaxation to position *Qg* of the ground state. Alternatively, the excited electron may gain energy via phonon interactions at high temperature and undergo

transition c. The energy absorbed (W) is the activation energy of thermal quenching. The meeting point F is degenerate to both the ground and excited states. The electron then undergoes transition to position Qg (transition d) of the ground state and because this relaxation probability is much greater than transition to Qe (transition b), the former is non-radiative and is associated with the dissipation of heat [35].

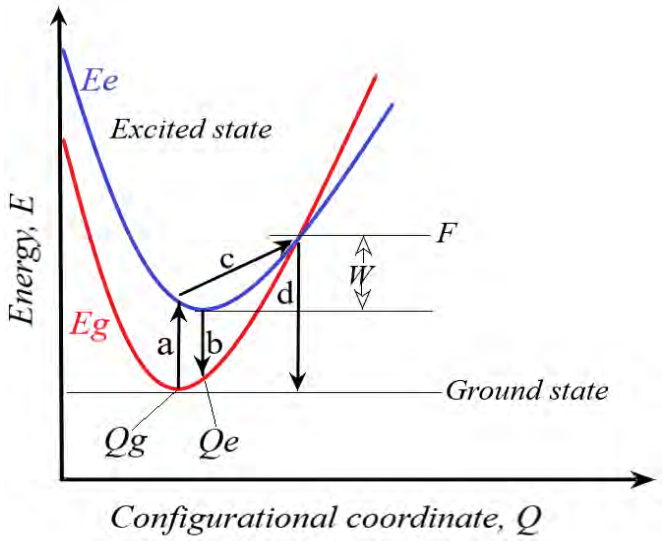

Figure 2.6: The configurational coordinate diagram illustrating the energy levels at the recombination centre. The excited and ground energy states are indicated E_e and E_g. Transition b is radiative recombination whereas transition d is non-radiative. The parameter W is the activation energy of the non-radiative transition.

Thermoluminescence measured at increasing heating rates shifts the glow peak to higher temperature values and decreases the luminescence intensity. This behaviour has been reported in several studies where luminescence intensity is recorded as a function of temperature (TL, radioluminescence, OSL, photoluminescence) [30, 32, 36, 37]. As a consequence, the kinetic parameters evaluated from the initial rise, curve fitting and peak shape methods could be inaccurate as a result of the temperature effect on the shape of the glow peak [38, 39]. Other luminescence studies have reported an inverse quenching behaviour where the luminescence intensity has been found to increase with increasing heating rate [40, 41].

2.5 Optically Stimulated Luminescence

2.5.1 Continuous wave optically stimulated luminescence (CW-OSL)

Optically stimulated luminescence (OSL) has a mechanism similar to thermoluminescence, but the variation is with the stimulation source. For OSL, light of an appropriate wavelength is the stimulation source. Heat is replaced with light in Figure 2.1 to describe the flow of charges in OSL. A semiconductor or insulator is exposed to ionizing radiation which causes excitation of electrons from the valence band to the conduction band (transition a). Holes are created in the valence band by the absence of electrons. A number of these electrons immediately de-excite and return to the equilibrium state (valence band) through electron-hole recombination. Some of the excited electrons however get trapped in the band gap just below the conduction band (transition b). In a similar fashion, holes are trapped inside the band gap just above the valence band. The trapped charges are said to be in a metastable state and are localized at defect sites in the crystal lattice [10]. Shallow electron traps and hole traps are located closer to the conduction band and valence band respectively. Upon exposure of the material to light of an appropriate wavelength, the trapped electrons are detrapped into the conduction band (transition c) following which electron-hole recombination occur at the recombination centre (transition d) with the emission of light. Thus, optically induced luminescence is termed OSL. The luminescence signal emitted provides a history of the absorbed radiation dose by the material [2]. Application of OSL has mainly been in the fields of dosimetry and dating [42, 43].

Continuous wave optically stimulated luminescence (CW-OSL) measurement is a technique where the OSL signal is recorded by providing a constant light intensity from the stimulation source throughout the measurement period [43]. The measurement is also made at a constant temperature. Appropriate filters are placed between the stimulating source and the sample to discriminate between the light from the source and the emitted luminescence from the sample. The luminescence signal appears as a simple monotonic decay with time. The kinetics governing the transition of charges are elaborated in the next section.

2.5.1.1 Mathematical analysis

The one trap and one recombination centre (OTOR) model used to explain the rate equations in thermoluminescence is utilized here to explain the OSL mechanism. Figure 2.7 shows an energy band diagram for the OTOR model. All the parameters retain their previous definitions. The rate equations (2.5) – (2.8) during the excitation of electrons by ionizing radiation in TL also hold for OSL.

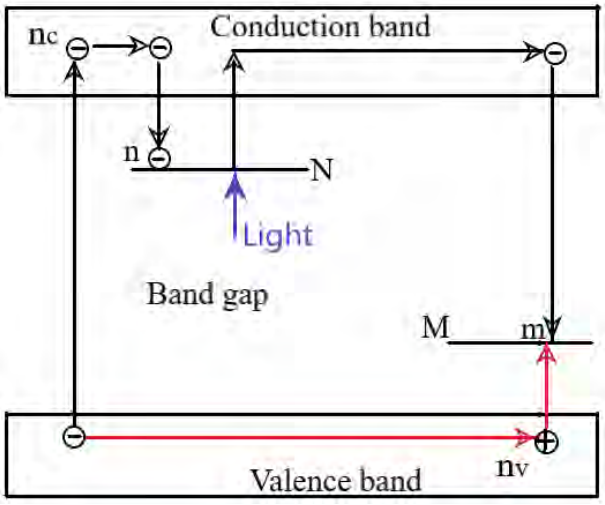

Figure 2.7: An energy band diagram of one trap and one recombination centre (OTOR). The holes and electrons are the positive and negative circles. The parameters N and M are the electron trap and recombination centre, n and m are the concentrations of trapped electrons and holes. The black and red arrows show the transition paths of the electrons and holes.

At the optical exposure stage, the concentration of charges can be represented as

$$\frac{dn}{dt} = n_c A_n (N - n) - nf \tag{2.87}$$

$$\frac{dm}{dt} = -mA_m n_c \tag{2.88}$$

$$\frac{dm}{dt} = \frac{dn_c}{dt} + \frac{dn}{dt}. \tag{2.89}$$

The parameter $f(s^{-1})$ is the optical stimulation rate of electrons and can be expressed as

$$f = \sigma\Phi \tag{2.90}$$

where $\Phi(m^{-2}s^{-1})$ is the light intensity and $\sigma(m^2)$ is the photoionization cross section of the depleted traps [43]. By inference from equation (2.89), the concentration of electrons and holes remains balanced. Equations (2.87) – (2.89) can be combined to give

$$\frac{dn_c}{dt} = nf - n_c A_n(N-n) - mA_m n_c. \tag{2.91}$$

Imposing the quasi-equilibrium condition as expressed in equation (2.13), the parameter dn_c/dt in equations (2.89) and (2.91) approaches zero. The parameter n_c in equation (2.91) is substituted into equation (2.87) to arrive at the general OTOR equation for the OSL mechanism expressed as

$$I_{OSL} = -\frac{dn}{dt} = nf\left(1 - \frac{A_n(N-n)}{mA_m + A_n(N-n)}\right) \tag{2.92}$$

2.5.1.1.1 First order kinetics

The probability of electron retrapping once liberated from its trap as against the probability of electron recombination with trapped holes at the recombination centre determines the order of kinetics. Electron-hole recombination is more probable than electron retrapping for first order kinetics [1]. This means $A_n(N-n)$ in equation (2.92) approaches zero, hence,

$$I_{OSL} = nf\ . \tag{2.93}$$

The solution to equation (2.93) is

$$I_{OSL} = I_0 \exp(-\lambda t) \tag{2.94}$$

where $I_0 = n_0 f$ represents the initial OSL intensity, λ represents the decay constant and t is time. For experimental data, the decay curve can be fitted by a sum of several exponential components, and this technique has been extensively applied to study the OSL decay curve of quartz [44, 45, 46]. The components provide a mathematically convenient way of describing the shape of the decay curve and are not necessarily linked to any separate physical mechanism.

2.5.1.1.2 Second order kinetics

For second order kinetics, electron retrapping is taken into consideration, hence $A_m = A_n$ and $m = n$. The OSL intensity then becomes

$$I_{OSL} = -\frac{dn}{dt} = \frac{n^2 f}{N} \tag{2.95}$$

and the integral of equation (2.95) yields

$$I_{OSL} = -\frac{f n_0^2}{N\left(1 + \frac{n_0 f t}{N}\right)^2} \tag{2.96}$$

where all symbols are as previously defined.

2.5.1.1.3 General order Kinetics

For general order kinetics, the OSL intensity can be expressed as

$$I_{OSL} = -\frac{dn}{dt} = \frac{n^b f}{N^{b-1}} \tag{2.97}$$

where each term retains its previous definition [10]. Equation (2.97) is analogous to the general order TL equation (2.25). The integral of equation (2.97) gives

$$I_{OSL} = \frac{f n_0^b}{N^{(b-1)}}\left[1 + (b-1)\left(\frac{n_0}{N}\right)^{b-1} f t\right]^{-\frac{b}{b-1}}. \tag{2.98}$$

Equation (2.98) yields the first order kinetics equation (2.94) when $b \sim 1$ and the second order kinetics equation (2.96) when $b = 2$.

2.5.2 Linearly modulated optically stimulated luminescence (LM-OSL)

The procedure for recording the OSL signal can be done in a variety of ways aside from CW-OSL. We begin with the expression for the optical stimulation probability f given in equation (2.90). For linearly modulated optically stimulated luminescence (LM-OSL), the light intensity

from the stimulation source is increased at a constant rate during the OSL measurement [47]. Equation (2.90) is now rewritten as

$$f = \sigma(\Phi_0 + \Upsilon_\Phi t) \tag{2.99}$$

where Φ_0 is the initial light intensity, Υ_Φ is the rate at which the light intensity changes and t is time. For a linear increase in light intensity within $t = 0$ and $t = t_q$, the intensity variation can be represented by $\Upsilon_\Phi = \Phi_q/t_q$ and the OSL intensity is expressed as

$$\frac{dn}{dt} = -n\sigma\frac{\Phi_q}{t_q}t\,. \tag{2.100}$$

The integral of equation (2.100) yields

$$I(t)_{OSL} = n_0\sigma\frac{\Phi_q}{t_q}t\,exp\left(\frac{\Phi_q}{2t_q}\sigma t^2\right) \tag{2.101}$$

where the meaning of each parameter remains the same. The LM-OSL signal shows an initial linear increase owing to electron detrapping and subsequent recombination with holes, following which the signal gradually decreases due to the decreased concentration of trapped charges [10]. The shape therefore appears as a peak. The presence of multiple traps will show multiple peaks where each peak is associated with a trap. As such, LM-OSL measurement provides a convenient way of resolving overlapping OSL components from multiple traps. Traps of large photoionization cross section are quickly depleted of charges followed by those with relatively lower photoionization cross section. The recorded luminescence signal hence will show series of peaks if the difference in photoionization cross section is sufficient otherwise a single broad peak will be observed. The depleted traps in some cases are the same as those associated with the thermoluminescence peaks [14].

2.5.3 Time-resolved optically stimulated luminescence (TR-OSL)

The OSL measurement modalities considered so far are premised on recording the luminescence at the onset of optical exposure and assume any delay prior to luminescence emission is negligible. For time-resolved optically stimulated luminescence (TR-OSL), the illumination source is pulsed within a short period, and the luminescence is recorded during and after the

pulse [35]. This technique offers a way of gaining information such as the luminescence lifetime and the various recombination sites involved in the luminescence mechanism [48, 49].

If the initial concentration of electron trap is represented by A, the optical stimulation probability is represented by s, and the radiative recombination probability is λ, we can write

$$\frac{dN}{dt} = sA - \lambda N \tag{2.102}$$

where dN/dt is the rate of change of the number of stimulation electrons during illumination [50]. Equation (2.102) is integrated to yield

$$N(t) = \frac{As}{\lambda}[1 - \exp(-\lambda t)]. \tag{2.103}$$

Radiative decay to produce luminescence can be represented as

$$dL(t) = N\lambda(t)dt. \tag{2.104}$$

Hence, the rate of luminescence emission during each pulse is given by

$$L_1(t) = sA[1 - \exp(-\lambda t)]. \tag{2.105}$$

Equation (2.105) implies that the intensity rises towards a maximum.

After each pulse of duration t_1, the rate of luminescence emission with reference to equation (2.104) can be represented as

$$L_2(t) = \lambda N(t_1)\exp[-\lambda(t - t_1)]. \tag{2.106}$$

where t_1 represent the pulse duration. Equation (2.103) is substituted into equation (2.106) to give

$$L_2(t) = sA\exp(-\lambda t)\,[\exp(\lambda t_1) - 1)]. \tag{2.107}$$

Equation (2.107) is an exponential decay function.

The experimental data following each pulse can also be fitted to the function

$$L(t) = \sum_j D_j \exp\left(-\frac{t}{\tau_j}\right) + C \tag{2.108}$$

where D is a scaling parameter of component j, τ is the luminescence lifetime, t is time and C is a constant representing the background [10].

2.6 Phototransferred thermoluminescence

Phototransferred thermoluminescence (PTTL) generally describes the mechanism of how trapped electrons from stable deep traps are transported to empty shallow traps by optical stimulation prior to TL measurement [43]. Traps of smaller depth are generally considered as shallow traps while deep traps are those with large trap depth. The PTTL mechanism provides insight into the optical sensitivity of the traps. For PTTL to occur, the sample is first irradiated to cause trap population following which shallow traps are depopulated. The sample is then illuminated and finally stimulated by heat. Each of these steps is elaborated below.

Sample irradiation by ionizing radiation causes excitation of electrons into the conduction band. The presence of defects within the crystal creates charge trapping centres where electrons are trapped just below the conduction band whereas holes are trapped at the recombination centres. For this process, it is necessary to ensure that the dose is sufficient to fill the deep traps else PTTL may not be observed.

The next procedure is to depopulate the shallow traps without altering the population of deep traps. This can be achieved in a variety of ways. A common characteristic of shallow trap is luminescence loss at room temperature hence the sample can be made to undergo phosphorescence decay at room temperature. This process however may be time consuming if the duration for luminescence fading is long. Alternatively, the sample can be preheated to depopulate the shallow electron traps while keeping the deep traps intact.

The next stage is to expose the sample to light of a single wavelength for some duration. The illumination is to cause liberation of trapped electrons from deep traps (donors) into the conduction band where retrapping into shallow traps (acceptors) can occur. The sensitivity of a trap to optical stimulation is dependent on the optical energy. The presence of multiple shallow traps which act as charge acceptors and other deep traps may compete for charges from donor trap.

The sample is finally heated to liberate trapped electrons from shallow traps into the conduction band following which they undergo recombination with trapped holes at the recombination centre, thus thermoluminescence. The recorded glow curve will show a decrease in the TL intensity of donor trap since some of its trapped electrons are lost to the shallow traps during the illumination stage. The TL intensity of competitor traps on the other hand will show an increase.

2.6.1 Mathematical models of PTTL

The charge transfer mechanism and its accompanying rate equations in PTTL are described below with the simple PTTL model [2] and the phenomenological model of Chithambo et al. [51].

2.6.1.1 The simple PTTL model

A mechanism of PTTL was mathematically modelled by Chen and McKeever [2] by considering the presence of one shallow electron trap acting as charge acceptor, one deep electron trap acting as charge donor and one recombination centre. Figure 2.8 illustrates the simple PTTL model. The parameter N_1 represents the shallow trap concentration, n_1 represents the concentration of electrons in the shallow trap, N_2 represents the deep trap concentration, n_2 represents the concentration of electrons in deep trap, M represents the concentration of recombination centre, m represents the concentration of holes in recombination centre, A_1 is the electron trapping probability into the shallow trap, A_2 is the electron trapping probability into the deep trap, A_m is the recombination probability and n_c represents the population of free electrons in the conduction band.

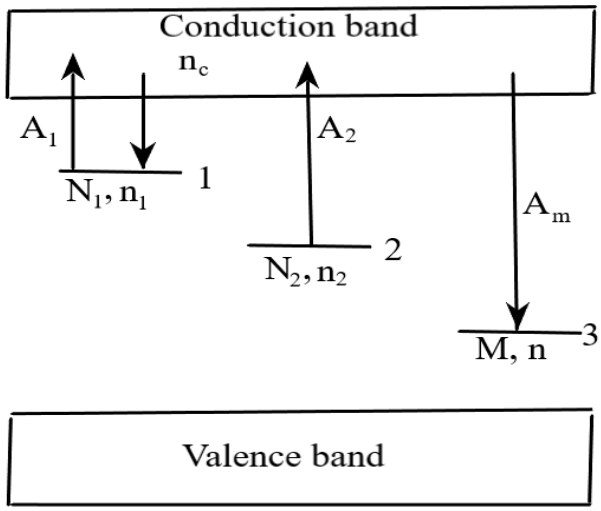

Figure 2.8: A simple PTTL model consisting of one shallow trap at level 1 (acceptor), one deep trap at level 2 (donor) and one recombination site at level 3. The image is adopted from Chen and McKeever [2].

The sample undergoes irradiation followed by preheating or phosphorescence decay at room temperature. The initial concentration of electronss in the shallow trap and deep trap can be respectively expressed as

$$n_{10} = 0 \tag{2.109}$$

and

$$n_{20} = m_0 . \tag{2.110}$$

At the stage of sample exposure to light, electron transfer from the deep trap into the shallow trap via the conduction band is governed by the following rate equations

$$\frac{dn_1}{dt} = n_c(N_1 - n_1)A_1 - n_1 s_1 exp\left(\frac{-E_1}{kT}\right) - n_1 f_1 \tag{2.111}$$

$$\frac{dn_2}{dt} = n_c(N_2 - n_2)A_2 - n_2 f_2 \tag{2.112}$$

$$\frac{dm}{dt} = -n_c m A_m \tag{2.113}$$

$$\frac{dn_c}{dt} = \frac{dm}{dt} - \frac{dn_1}{dt} - \frac{dn_2}{dt} \tag{2.114}$$

where f_1 and f_2 represent the rate of optical excitation of electrons out of the shallow and deep traps respectively [52]. The thermal excitation rate of the shallow trap is represented as $n_1 s_1 exp(-E_1/kT)$. Optical stimulation is normally done at room temperature where the rate of thermal excitation is negligible, hence the thermal excitation rate component of equation (2.111) turns to zero. Also, the parameter f_1 turns to zero since optical stimulation of shallow electron trap is negligible at this stage.

Charge neutrality implies that

$$\mathrm{m} = n_1 + n_2 + n_c \,. \tag{2.115}$$

Imposing the quasi-equilibrium condition expressed as

$$\left|\frac{dn_c}{dt}\right| << \left|\frac{dm}{dt}\right| \; where \; \left|\frac{dn_c}{dt}\right| \approx 0 \tag{2.116}$$

and under the condition of no charge retrapping into deep trap where $n_2 f_2 >> n_c(N_2 - n_2)A_2$, the integral of equations (2.111) – (2.113) gives

$$n_1(t) = N_1[1 - exp(-Bt)] \tag{2.117}$$

$$n_2(t) = n_{20} exp(-f_2 t) \tag{2.118}$$

$$m(t) = m_0 exp\left(\frac{-t}{\tau}\right) \tag{2.119}$$

where τ and B are constants expressed respectively as $(n_c A_m)^{-1}$ and $n_c A_1$ [2].

The next stage after sample illumination is thermal stimulation where trapped charges in shallow traps are liberated into the conduction band. The set of differential equations describing the transition of charges are similar to equations (2.111) – (2.114) with the difference being a replacement of the optical stimulation rate f with thermal stimulation probability p. The resulting differential equations are as follows

$$\frac{dn_1}{dt} = n_c(N_1 - n_1)A_1 - n_1 p_1 \tag{2.120}$$

$$\frac{dn_2}{dt} = n_c(N_2 - n_2)A_2 - n_2 p_2 \tag{2.121}$$

$$\mathrm{I} = \frac{dm}{dt} = -n_c m A_m \tag{2.122}$$

$$\frac{dn_c}{dt} = \frac{dm}{dt} - \frac{dn_1}{dt} - \frac{dn_2}{dt}. \tag{2.123}$$

The thermal stimulation term p_2 for the donor trap is ignored since the temperature range is within the region of the shallow trap [2]. The terms $n_2 p_2$ in equation (2.121) hence turn to zero.

The change in PTTL intensity with illumination time under the conditions of quasi-equilibrium and negligible retrapping $(n_1(t) \ll N_2 - n_2(t))$ predicts a saturation for a system of one acceptor and one donor [2]. However, the PTTL intensity with time of most real luminescence materials shows an initial increase to a maximum value followed by a continuous decrease [52, 53]. Hence, the assumptions made to predict a PTTL intensity increase towards a saturation level are not always the case, giving room for further refinement of our understanding of PTTL.

Also, the simple model described above is limited in explaining several experimental data where more than one active donor or acceptor traps are involved in the PTTL processes. For the case of tanzanite, it is reported [8] that a minimum of two donors and one acceptor are active in the PTTL process. A model that best describes how the PTTL intensity changes with illumination time for the case of one acceptor trap and multiple donor traps is adopted for this work. The same model has been used to successively describe experimental results of PTTL intensity dependence on illumination time for tanzanite [8], α-Al_2O_3:C [51], quartz [54] and CaF_2 [55].

2.6.1.2 Phenomenological model of Chithambo et al. (2017)

The phenomenological model was introduced by Chithambo et al. [51] to describe the PTTL intensity changes with illumination time in α-Al_2O_3:C based on the number of donor and acceptor traps. It was reported [51] that the preheat temperature which is intended to deplete shallow traps (acceptor), and the duration of illumination intended to cause transfer of electrons from deep traps (donor) to shallow empty traps determine the number of active traps serving as donors or acceptors. The TL peak II was reproduced by phototransfer when preheated to 800 °C

for 6 mins. However, no PTTL signal was observed for an extended preheat time to 15 mins. Moreover, a shallow trap can play the role of a donor depending on the preheat temperature. As such, the experimental procedures (preheat temperature, duration of preheat and duration of light exposure) essentially affect the flow of charges between acceptor and donor traps.

Figure 2.9 shows an energy band diagram that illustrates the PTTL mechanism for a system of multiple electron acceptors and donors. The diagram is shown for qualitative description of electron transfer from donor traps to acceptor traps at the illumination stage. Solutions to the various differential equations during the illumination stage are formulated thereafter. The shallow traps are represented as I and II. The deep traps are represented by III and IV. The recombination centre is represented as R. The instantaneous concentration of electrons in traps I-IV are represented by n_1, n_2, n_3 and n_4 respectively. The optical stimulation rate of traps I-IV are respectively represented as f_1, f_2, f_3 and f_4. For the phenomenological model, we assume that during the illumination process, some proportion of electrons liberated from the donor traps are transferred to acceptor traps. Moreover, all traps loose a proportion of charges during illumination, and retrapping into the donor traps is negligible [55].

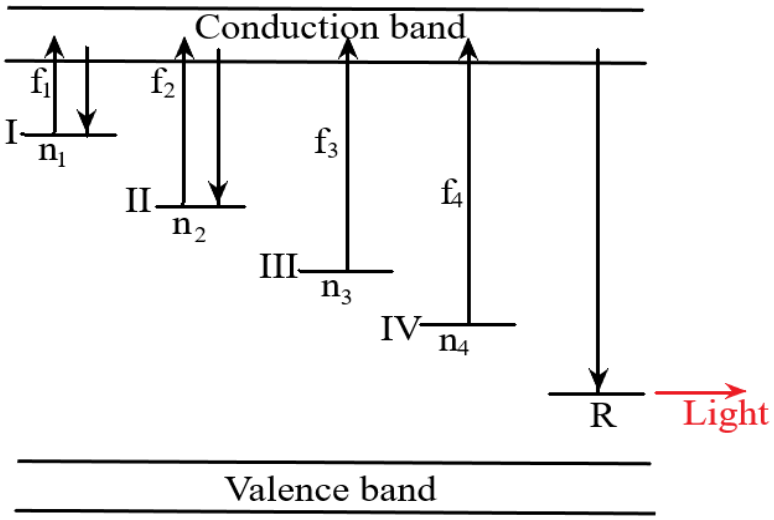

Figure 2.9: An energy level diagram of the phenomenological PTTL model consisting of shallow traps (I and II), deep traps (III and IV) and recombination centre (R). Preheating determines the number of donor and acceptor traps.

We first analyse the PPTL following preheating to deplete the trapped electrons of peak I while keeping peaks II-IV intact. A system of one acceptor (peak I) and three donors (peak II-IV) is hence considered here. The set of differential equations that describe the flow of charges is given by

$$\frac{dn_2}{dt} = -f_2 n_2 \tag{2.124}$$

$$\frac{dn_3}{dt} = -f_3 n_3 \tag{2.125}$$

$$\frac{dn_4}{dt} = -f_4 n_4 \tag{2.126}$$

$$\frac{dn_1}{dt} = -f_1 n_1 + \varrho_2 f_2 n_2 + \varrho_3 f_3 n_3 + \varrho_4 f_4 n_4 \tag{2.127}$$

where ϱ_2, ϱ_3, and ϱ_4 represent proportionality constants. Equations (2.124) – (2.126) describe the liberation of trapped electrons from donor traps into the conduction band. In equation (2.127), the parameters $f_1 n_1$ denote the liberation of trapped electrons from the acceptor trap (peak I) and the remaining terms denote electron retrapping at the acceptor trap. The solution to the set of differential equations (2.124) – (2.127) is formulated using matrix and Eigenvalue method as detailed in the following:

Equations (2.124) – (2.127) are a coupled system of first-order linear differential equations which can be represented by the matrix notation

$$\frac{dn}{dt} = \begin{bmatrix} -f_2 & 0 & 0 & 0 \\ 0 & -f_3 & 0 & 0 \\ 0 & 0 & -f_4 & 0 \\ \varrho_2 f_2 & \varrho_3 f_3 & \varrho_4 f_4 & -f_1 \end{bmatrix} \begin{bmatrix} n_2 \\ n_3 \\ n_4 \\ n_1 \end{bmatrix} \tag{2.128}$$

where dn/dt expresses the changes in electron concentration with time. Equation (2.128) can be written in the matrix form

$$\frac{dn}{dt} = \boldsymbol{An} \tag{2.129}$$

where $\boldsymbol{A}$ represents a coefficient matrix and $\boldsymbol{n}$ represents a column vector [56]. Solutions to equation (2.128) exist if the determinant of the coefficient matrix $\boldsymbol{A}$ can be expressed as

$$|\boldsymbol{A} - \Lambda\, \boldsymbol{I}| = 0 \tag{2.130}$$

where $\boldsymbol{I}$ is an identity matrix and Λ is eigenvalues of the coefficient matrix $\boldsymbol{A}$ [56]. Equations (2.128) and (2.130) are put together to give

$$\begin{vmatrix} -f_2 - \Lambda & 0 & 0 & 0 \\ 0 & -f_3 - \Lambda & 0 & 0 \\ 0 & 0 & -f_4 - \Lambda & 0 \\ \varrho_2 f_2 & \varrho_3 f_3 & \varrho_4 f_4 & -f_1 - \Lambda \end{vmatrix} = 0 \tag{2.131}$$

which implies $\Lambda = -f_2, -f_3, -f_4$ and $-f_1$. The general solution to equation (2.128) can be represented as

$$\begin{aligned} \boldsymbol{n} = k_1[(f_1 - f_2) \quad 0 \quad 0 \quad \varrho_2 f_2\,]^T\, e^{-f_2 t} \;+\; k_2[0 \quad (f_1 - f_3) \quad 0 \quad \varrho_3 f_3\,]^T\, e^{-f_3 t} \\ + k_3[0 \quad 0 \quad (f_1 - f_4) \quad \varrho_4 f_4\,]^T\, e^{-f_4 t} \;+\; k_4[0 \quad 0 \quad 0 \quad 1\,]^T\, e^{-f_1 t} \end{aligned} \tag{2.132}$$

where k_1, k_2, k_3 and k_4 are integration constants. The symbol T is the transpose of the matrix. Equation (2.132) is an initial-value problem hence the solution for the PTTL at the shallow trap (peak I) can be written as

$$n_1 = A_1(e^{-f_2 t} - e^{-f_1 t}) + A_2(e^{-f_3 t} - e^{-f_1 t}) + A_3(e^{-f_4 t} - e^{-f_1 t}) \tag{2.133}$$

where A_1, A_2 and A_3 are constants expressed as $A_1 = (\varrho_2 f_2 n_{ai})/(f_1 - f_2)$, $A_2 = (\varrho_3 f_3 n_{bi})/(f_1 - f_3)$, and $A_3 = (\varrho_4 f_4 n_{ci})/(f_1 - f_4)$. The parameters n_{ai}, n_{bi} and n_{ci} represent the initial concentration of electrons in traps II, III and IV respectively.

If the preheat temperature is increased to depopulate traps I and II only, the set of differential equations that describe the flow of charges for such a system at the illumination stage is written as

$$\frac{dn_3}{dt} = -f_3 n_3 \tag{2.134}$$

$$\frac{dn_4}{dt} = -f_4 n_4 \tag{2.135}$$

$$\frac{dn_1}{dt} = -f_1 n_1 + \text{Б}_3 f_3 n_3 + \text{Б}_4 f_4 n_4 \tag{2.136}$$

where Б$_3$ and Б$_4$ are proportionality constants. Equations (2.134) – (2.136) represent a system of one acceptor (peak I) and two donors (peaks III and IV). Following the steps in equations (2.128) – (2.132), the solution for the PTTL at peak I is given by

$$n_1 = B_2(e^{-f_3 t} - e^{-f_1 t}) + B_3(e^{-f_4 t} - e^{-f_1 t}) \tag{2.137}$$

where B_2 and B_3 are constants expressed as $B_2 = (\text{Б}_3 f_3 n_{bi})/(f_1 - f_3)$ and $B_3 = (\text{Б}_4 f_4 n_{ci})/(f_1 - f_4)$. All other parameters retain their previous definitions.

Moreover, if peak II is reproduced by phototransfer, we can write the set of differential equations

$$\frac{dn_3}{dt} = -f_3 n_3 \tag{2.138}$$

$$\frac{dn_4}{dt} = -f_4 n_4 \tag{2.139}$$

$$\frac{dn_2}{dt} = -f_2 n_2 + \alpha_3 f_3 n_3 + \alpha_4 f_4 n_4 \tag{2.140}$$

where α_3 and α_4 are proportionality constants. A system of one acceptor (peak II) and two donors (peaks III and IV) is represented in equations (2.138) – (2.140). The PTTL at peak II is given by

$$n_2 = +C_2(e^{-f_3 t} - e^{-f_2 t}) + C_3(e^{-f_4 t} - e^{-f_2 t})\,. \tag{2.141}$$

The constants $C_2 = (\alpha_3 f_3 n_{bi})/(f_2 - f_3)$ and $C_3 = (\alpha_4 f_4 n_{ci})/(f_2 - f_4)$.

Following preheating to deplete electron traps in peaks I-III, a system of one acceptor and one donor (peak IV) is created. The PPTL (n_a) at any of the acceptor traps is given by

$$n_a = D_3(e^{-f_4 t} - e^{-f_a t}) \tag{2.142}$$

where a represent any acceptor trap (peak I, II or III), $D_3 = (\text{q}_4 f_4 n_{ci})/(f_a - f_4)$, q_4 is proportionality constant and all other parameters retain the previous definitions.

The phenomenological model above describes the transport of electrons in the PTTL process only at the optical stimulation stage unlike the simple model which includes the irradiation and thermal stimulation stages. Moreover, only a proportion of the optically stimulated electrons

from donor traps are captured into acceptor traps resulting in a system of linear differential equations whose solutions can be directly applied to any experiment PTTL data.

Chapter 3

Experimental procedures

This chapter covers the details of the instrument used for recording the thermoluminescence, the optically stimulated luminescence and the phototransferred thermoluminescence. The latter part describes the sample under study.

3.1 Instrumentation

The RISØ TL/OSL Reader model DA-20 was used to measure the thermoluminescence, the optically stimulated luminescence and the phototransferred thermoluminescence. Figure 3.1 shows the various parts of the RISØ TL/OSL Reader. The main units of the Reader are the controller, the stimulation system, the irradiation component and the luminescence detection unit. Except for the controller, all the other units are linked to a vacuum chamber where the sample carousel is. The sample carousel can accommodate a maximum of 48 stainless steel sample discs. The diameter of each sample disc is 10 mm. The following is a description of each of the main units.

(a)

(b)

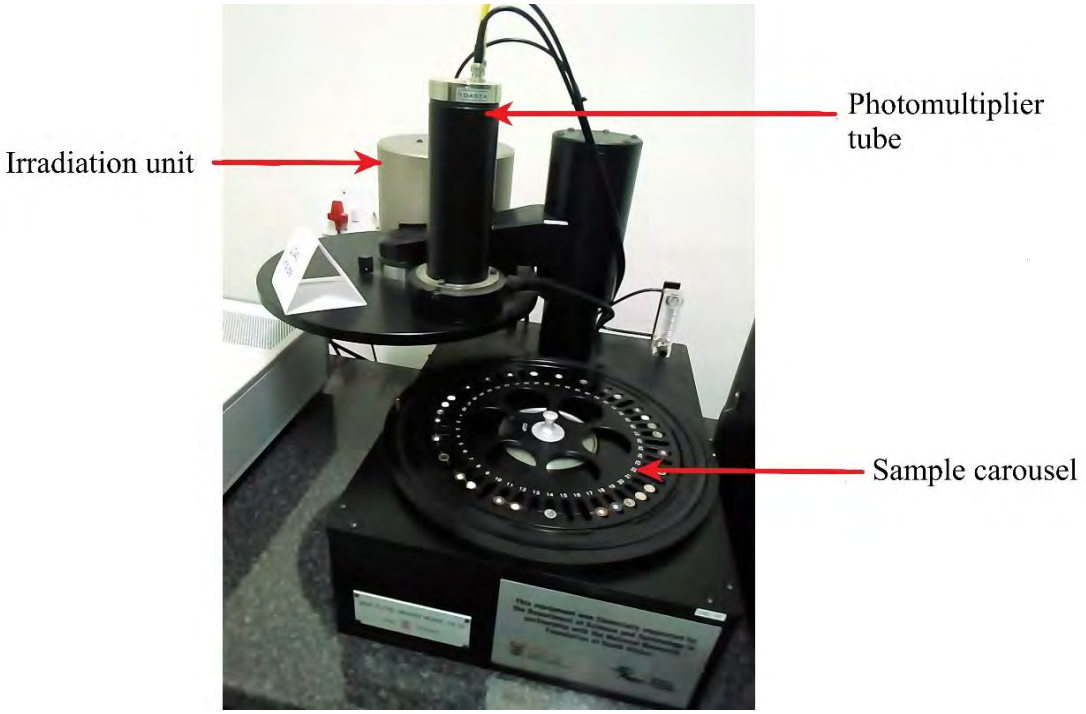

Figure 3.1: An image of the RISØ TL/OSL DA-20 Luminescence Reader showing the controller (a), the irradiation unit and the photomultiplier tube (b). The sample carousel spins and positions the sample disc vertically above the heating unit.

3.1.1 The controller unit

The controller is the heart of the Reader. All the hardware commands are initiated by the controller. The controller is programmed to activate the irradiation unit, nitrogen flow, the stimulation unit and the detection unit. The digital display on the controller shows the current status of the system which includes the sample position, the irradiation time, error messages and invalid commands. The Risø software programs can be installed on any standard desktop computer and connected to the controller via external ports.

3.1.2 The stimulation system

The stimulation system consists of the heating and the optical units. The heating unit comprises of a heater strip that lifts the sample into the measurement position and heats the sample. The heater strip is a high resistance alloy (kanthal) which is designed to accommodate the sample disc and ensure efficient thermal transmission to the sample [57]. The heat is generated by passing a controlled current through the heater strip. The temperature supplied by the heater strip ranges from room temperature up to 700 °C. The lowest heating rate is 0.1 °C s^{-1} and the highest is 10 °C s^{-1}. A solenoid pipe supplies nitrogen to cool the heater strip and to prevent oxidation of the heating unit at elevated temperatures [57].

The optical unit is located around a circular perimeter above the sample. LEDs are used as the optical source due to their stability and long lifespan [58]. The standard optical wavelengths available are 470 nm (blue) and 850 nm (infrared). The blue LEDs were used for every optical stimulation in this work, and they deliver a maximum power density of 80 mW/cm^2 at sample position. Stimulation can be done either at a constant intensity (CW-OSL) or at varying intensity (LM-OSL). The former was used for this work.

3.1.3 The irradiation unit

The irradiation unit is mounted on top of the sample carousel. Inside the unit is a $^{90}Sr/^{90}Y$ beta radiation source. The half-life of the beta source is 28 years. For this work, irradiation was done *in-situ* at a dose rate of 0.10 Gy s^{-1} and at room temperature.

3.1.4 The luminescence detection unit

The luminescence is detected by a bialkali photomultiplier tube model EMI 9235QB. The maximum detection efficiency of the photomultiplier tube is between 200 and 400 nm [57]. A 7 mm Hoya U-340 filter (transmission band 250 – 390 nm) is placed between the photomultiplier tube and the sample to discriminate between the stimulation wavelength and the luminescence, and to prevent scattered luminescence from reaching the detector.

3.2 Sample details

The sample under study is commercially available tanzanite (African Gems and Minerals Inc., Cape Town). Previous luminescence studies of the same sample were on the thermoluminescence properties [7] and the phototransferred thermoluminescence mechanism [8].

The Merelani Hills in northeastern Tanzania is the only location of tanzanite gem mineral deposit. Tanzanite is the blue variety of zoisite, a metamorphic mineral with orthorhombic crystal structure [59]. Zoisite has the chemical formula $Ca_2Al_3(Si_2O_7)(SiO_4)O(OH)$ and is a member of the epidote group [60, 61]. The crystal symmetry of all other members of the epidote group is monoclinic which accounts for the exclusion of zoisite as a member of the epidote group [62]. Zoisite is rather considered by a latter classification system as a polymorph of clinozoisite, a subgroup of the epidote groups [63]. Figure 3.2 shows the crystal structure of zoisite in the polyhedral model. Octahedral chains are connected by single tetrahedra of SiO_4 and double tetrahedra of Si_2O_7 groups. The octahedral sites are occupied by Al or Ca ions [59]. In zoisite, Ti or Al can substitute for Si but the latter occurs only to a smaller extent [60]. There are sevenfold oxygen coordination cavity sites occupied by Ca ions.

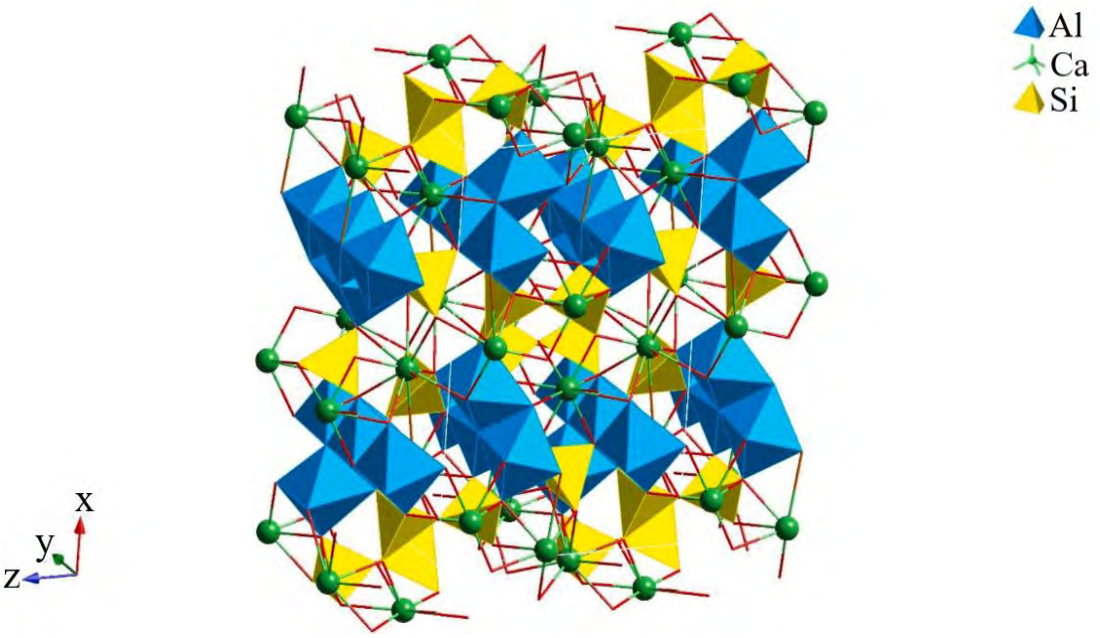

Figure 3.2: Polyhedral representation of the crystal structure of zoisite. Image reproduced from Chithambo [8].

The trichroism of tanzanite (blue, violet, red or green aesthetic display) is evident at different crystallographic orientations. Minor and trace elements like iron, titanium, chromium and vanadium that replace Al or Ca are responsible for the colour variety [64]. Annealing of tanzanite is done to enhance its blue hue for commercial reasons. The process involves heating the sample to about 600 to 650 ^{o}C and holding the sample at that temperature for some period before cooling to room temperature [65]. Early research [66, 67] indicated that the alterations in the valence state of V^{3+} to V^{4+} is the underlying phenomena of the blue colourization but this has been contested by Olivier [68] who attributed the change to titanium oxidation from Ti^{3+} to Ti^{4+}. The former is supported by a recent study [61] that utilized X-ray absorption spectroscopy analysis, and reported an increase in the oxidation state of vanadium whereas titanium exhibited a decrease in oxidation state following heat treatment.

3.3 Sample preparation

The tanzanite samples were prepared in coarse grain form (~100 – 300 μm) and used *as received*. An aliquot of mass 0.041 g was loaded on a stainless steel disc. All measurements were made in a nitrogen atmosphere to improve thermal contact between the heater plate and the sample disc. Unless specified otherwise, all thermoluminescence recordings were made at 1 °C s^{-1}.

Chapter 4

Thermoluminescence analysis

This chapter provides information on the glow curve characteristics, dose response, fading and kinetic analysis of thermoluminescence (TL) of tanzanite.

4.1 Glow curve features

Following irradiation to 70 Gy, the TL was recorded by heating the sample to 500 °C. The sample was heated the second time to record the background signal. Figure 4.1 shows a TL glow curve of tanzanite corresponding to 70 Gy. A high intensity peak occurs at 74 °C and two lower intensity peaks are observed at 138 and 186 °C. These peaks are referenced as I, II and III throughout this work. The peak temperatures are consistent with those reported by Chithambo and Folley [7]

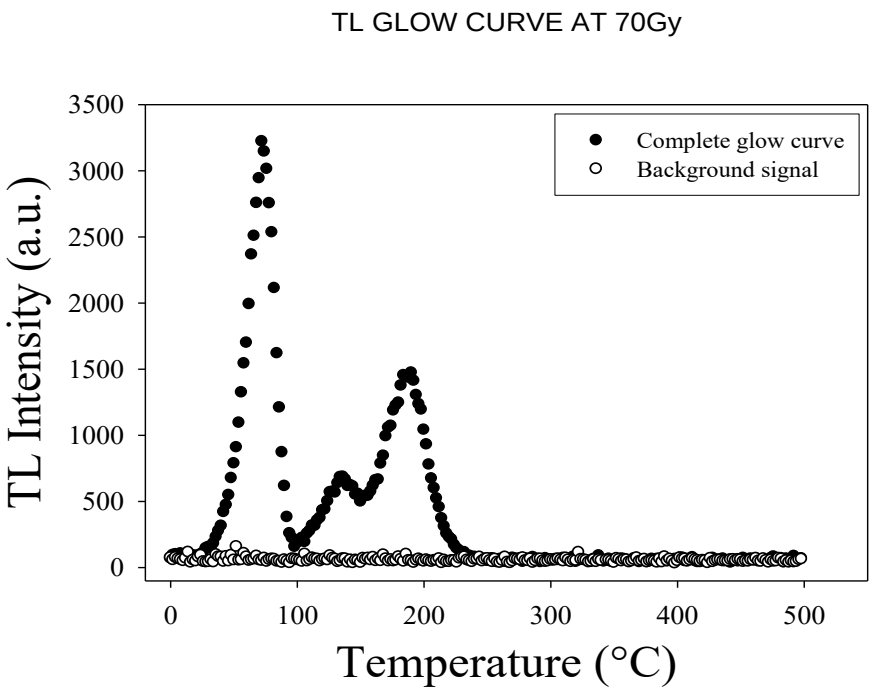

Figure 4.1: TL glow curve of tanzanite following 70 Gy irradiation. Three peaks are noticed at 74, 138 and 186 °C. The background signal is included for comparison.

4.2 Thermal cleaning

Thermal cleaning procedure reveals hidden or less prominent peaks in the glow curve. The sample was irradiated to 70 Gy, preheated to 98 °C and heated to 500 °C to record the glow curve. Two additional measurements were made but the sample was preheated to 148 °C for the first run and 228 °C for the second run. Irradiation to 70 Gy was done prior to every preheat. Figure 4.2(a) compares the complete glow curve in Figure 4.1 to those recorded following preheat to 98 and 148 °C. The complete glow curve shows three peaks at 74, 138 and 186 °C. After preheating to 98 °C, the trapped charges responsible for peak I are depleted and the recorded TL shows peaks II and III only. Following preheating to 148 °C, the trapped charges associated with peaks I and II are depleted and only peak III is revealed in the glow curve. Figure 4.2(b) compares the measured glow curve following preheating to 228 °C to the background signal. No peak is revealed and the TL measured is essentially that of the background signal. Hence, the thermal cleaning procedure shows three TL peaks at 74, 138 and 186 °C.

A total of four measurements of the complete glow curve was carried out to analyse the reproducibility of the peaks. The peak positions were averagely computed as 72.0, 133.5 ± 2.5 and 187.5 ± 1.9 °C for peaks I-III respectively. The percentage difference of the maximum and the minimum intensity gave 2.4, 2.1 and 2.5 % for peaks I-III. This result means that all the peaks are reproducible.

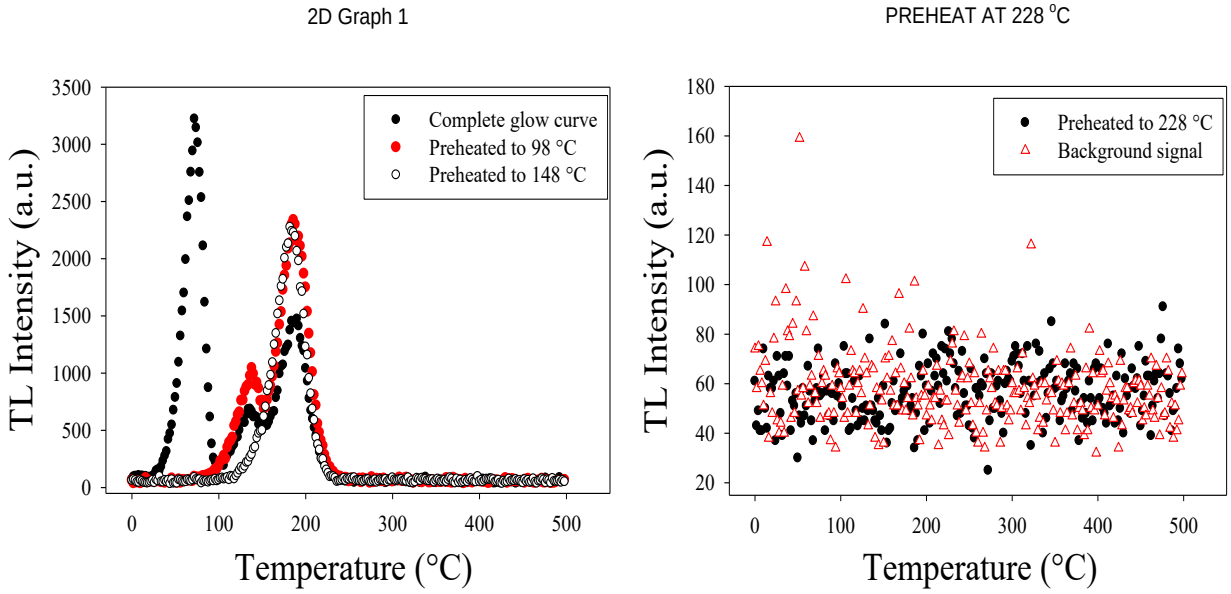

Figure 4.2: Thermal cleaning of TL peaks. The TL was measured following irradiation to 70 Gy and in turn preheating to 98, 148 °C (a) and 228 °C (b).

4.3 Analysis for order of kinetics

The order of kinetics of all the peaks was analysed using the peak position T_m dependence on dose and on partial heating ($T_m - T_{stop}$).

4.3.1 Peak position (T_m) dependence on dose

The sample was irradiated to variable doses from 10 to 200 Gy and the glow curve was recorded following each irradiation. The peak position T_m at each dose was noted for each peak. Figure 4.3 shows the dependence of T_m on dose. Each data point represents an average of four measurements and their standard deviation. For all the peaks, no systematic variation of T_m on dose is observed. The average T_m values are 73.3 ± 1.0, 137.6 ± 2.7, and 186.3 ± 2.0 °C for peaks I-III respectively. This result implies that the peak positions do not depend on the initial concentration of trapped charges hence all the peaks are of first order kinetics [1].

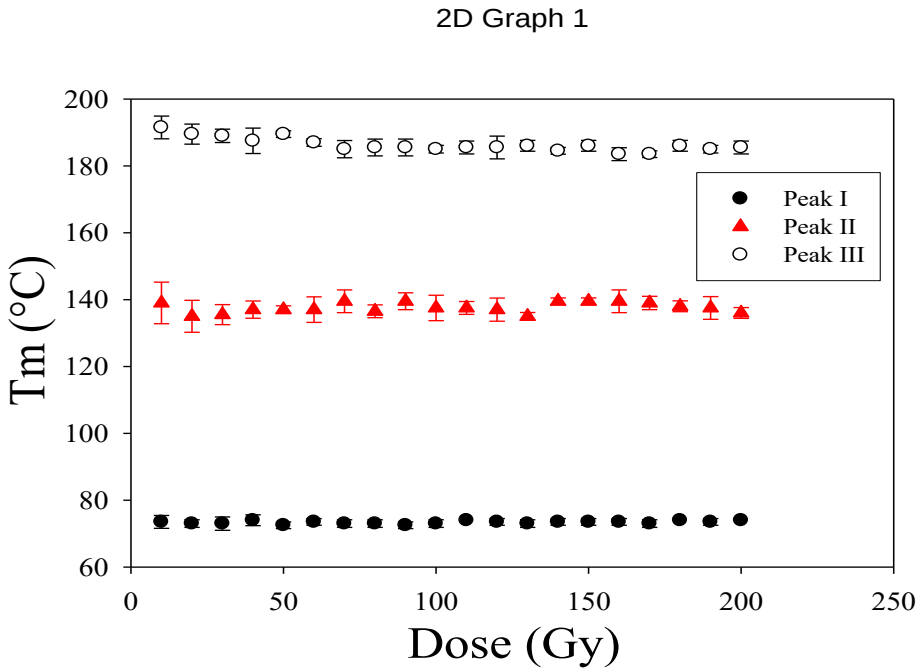

Figure 4.3: Peak position T_m dependence on dose for peaks I-III. For each peak, T_m remains stable with dose. Each data point represents an average of four measurements.

4.3.2 Peak position dependence on partial heating ($T_m - T_{stop}$)

The dependence of the peak position on partial heating for peak I was analysed by irradiating the sample to 30 Gy, preheating to 35 °C (T_{stop}), followed by heating to 500 °C to record the glow curve. The peak position T_m was noted afterwards. The procedure above was repeated except for T_{stop} which was increased at 3 °C intervals for each subsequent measurement up to 71 °C. Peaks II and III were subjected to the same measurement procedures from T_{stop} values of 106 – 130 °C and 158 – 182 °C respectively at 2 °C intervals. Three additional measurements at each T_{stop} were made for each peak to get an average value of T_m. Figure 4.4 shows a plot of T_m against T_{stop} for peaks I-III. Each data point is an average of the four measurements and the error bars represent the standard deviation. The peak positions are stable and do not vary systematically with partial heating. The average T_m is 73.7 ± 1.4 °C for peak I, 138.9 ± 3.0 °C for peak II and 190.6 ± 2.8 °C for peak III. The stability of T_m with T_{stop} for all the peaks is a characteristic of first order kinetics [1].

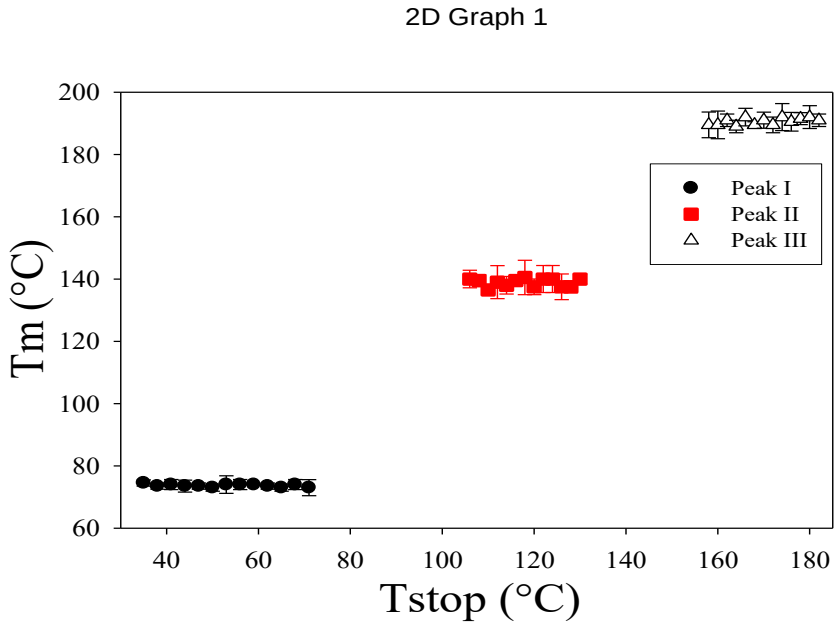

Figure 4.4: Peak position T_m dependence on partial preheating ($T_m - T_{stop}$) for peaks I-III. The peak positions show no dependence on partial heating. Each data point is the mean of four measurements and their standard deviation.

4.4 Dosimetric features

4.4.1 Dose response

The dependence of luminescence intensity on dose is of interest in radiation protection dosimetry and dating. Among the factors to consider in the choice of a material as a dosimeter, stability of luminescence signal over a wide range of dose is often desired. The glow curve was recorded following irradiation to variable doses from 10 to 200 Gy. The area under each glow peak was evaluated to represent the TL intensity. Figure 4.5 shows how the TL intensity vary with dose for peaks I-III. The intensity increases nonlinearly with dose for each peak. The data is best fitted with the empirical function

$$y(D) = a(1 - e^{-bD}) \tag{4.1}$$

where D is dose, a is intensity at saturation level and b is a constant.

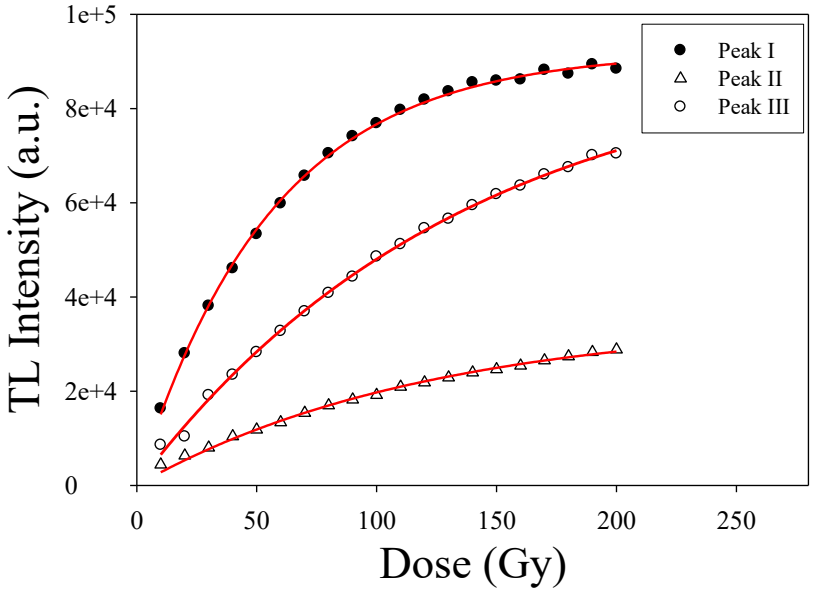

Figure 4.5: TL dose response for peaks I-III. The intensity increases with dose for each peak. The solid lines are the best fits of equation (4.1).

Qualitative analysis of the dose response was carried out using the supralinearity index function $f(D)$, expressed as

$$f(D) = \frac{y(D)/D}{y(D_1)/D_1} \tag{4.2}$$

where D_1 represents the normalization dose and $y(D_1)$ represents an analytical expression that defines y as a function of the normalization dose. The supralinearity index quantitatively indicates deviation from linear response. Values of $f(D) < 1$ indicates sublinear response, $f(D) \sim 0$ indicates saturation response and $f(D) > 1$ indicates supralinearity response [69]. Figure 4.6 shows a plot of $f(D)$ against dose for all the peaks. The parameter $f(D)$ decreases continuously with dose from 1 to values of 0.30, 0.54 and 0.51 for peaks I-III respectively. A sublinear dose response is hence exhibited by each peak. Nonlinear dose response is attributed to competition between charge traps during excitation by ionizing radiation and readout, and details of the underlying mechanisms have been extensively discussed elsewhere [12]. In our case, we may rule out competition during readout since electron-hole recombination is dominant over retrapping.

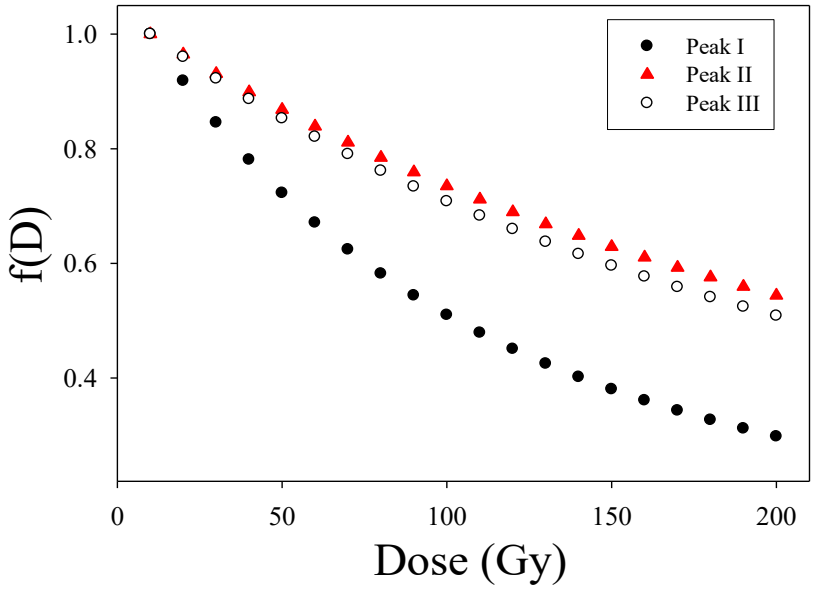

Figure 4.6: Plot of supralinearity index function $f(D)$ versus dose for peaks I-III. The dose response is sublinear for each peak.

4.5 Fading

Following sample irradiation, luminescence fading occurs as a loss of luminescence signal prior to readout which results in the reduction of luminescence intensity. Fading can be thermal (thermal fading) or anomalous (anomalous fading). For thermal fading, shallow electron traps are depleted at room temperature or at the excitation temperature when readout is delayed [2]. The liberated charges move into the conduction band followed by their recombination with trapped holes at the recombination centre. The consequence is a reduced number of trapped charges prior to stimulation. Peaks occurring close to room temperature are more susceptible to fade thermally. Anomalous fading on the other hand is the loss of luminescence signal between irradiation and readout at temperature well below the peak temperature [2]. Anomalous fading is attributed to direct recombination of trapped charges of opposite signs (localised transition) or quantum mechanical tunnelling of trapped electrons to the recombination centre [70, 71].

For fading analysis, the sample was irradiated in turn to 10, 50 and 100 Gy, and stimulation was delayed from 0 to 10,000 s. The TL was measured immediately the delay elapsed. The sample was freshly irradiated prior to each delay and stimulation. The area under each peak was

calculated to represent the TL intensity. Figure 4.7 shows a plot of TL intensity against delay corresponding to 10, 50 and 100 Gy for peak I. The intensity reduces with time to a minimum value at 10,000 s and at this time, only about 27% of its intensity remains. This behaviour is consistent for all the three doses. The data points are best fitted with the empirical function

$$I(t) = a + I_0 e^{-t\lambda} \tag{4.3}$$

where I represents intensity as a function of delay t, a is a constant, I_0 represents initial intensity and λ represents decay constant. The mean lifetimes (λ^{-1}) are 3426, 3571 and 3441 s corresponding to

FADING OF PEAK 1

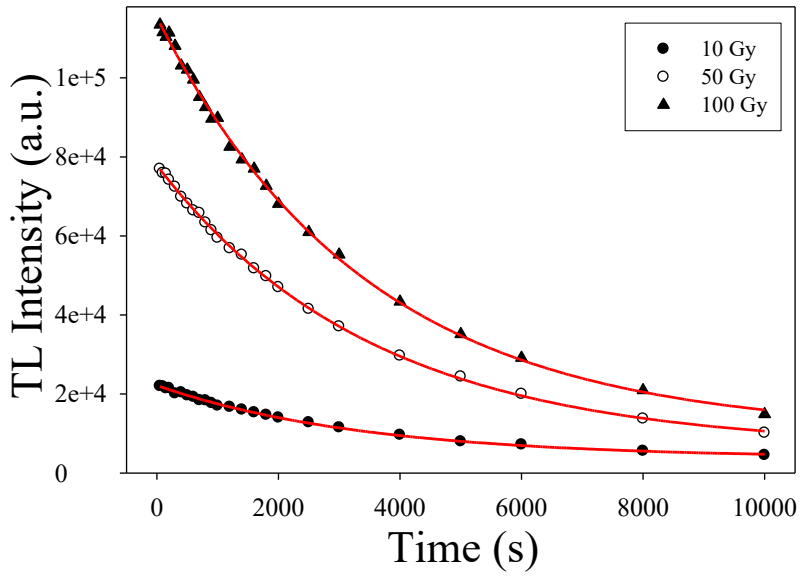

Figure 4.7: TL intensity dependence on delay between irradiation and readout for peak I. The solid lines are the fits of equation (4.3).

Figure 4.8(a) shows the dependence of TL intensity on delay for peak II corresponding to 10, 50 and 100 Gy. The intensity remains stable throughout and shows no fading. This means there is no decrease in the number of trapped charges at room temperature when stimulation is delayed. Peak III shows a similar outcome as seen in Figure 4.8(b). Therefore, peaks II and III are stable and are not associated with shallow electron traps.

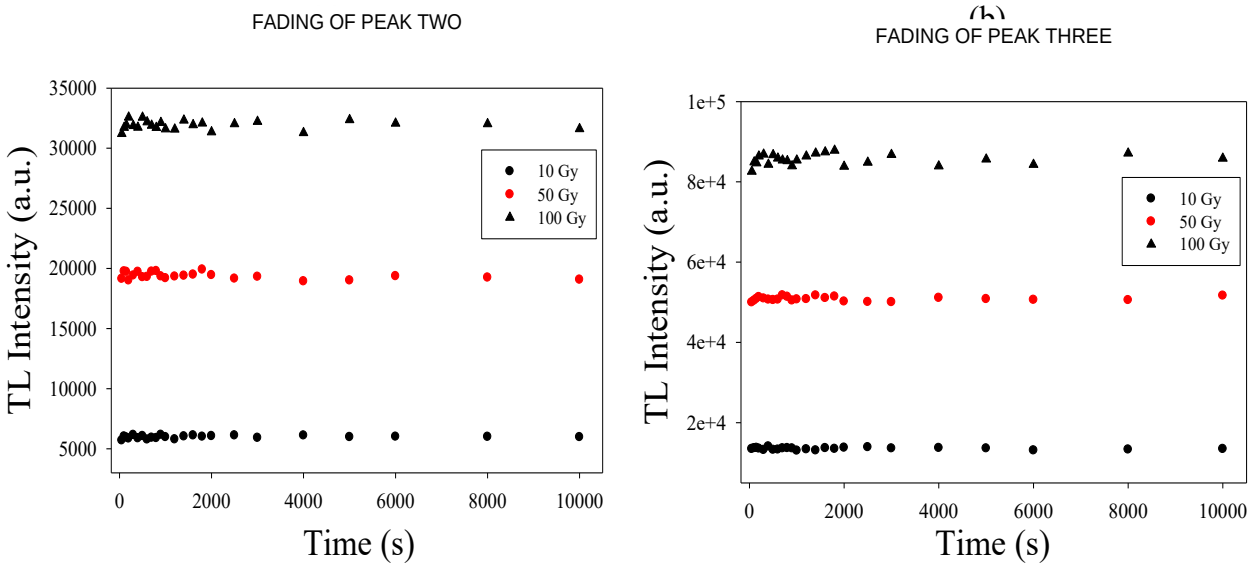

Figure 4.8: TL intensity dependence on delay between irradiation and readout for peak II (a) and peak III (b). The intensity does not change with delay for both peaks.

To account for the type of fading exhibited by peak I, phosphorescence measurement (OSL measurement with LEDs off) was recorded at room temperature for 3,000 s following irradiation to 50 Gy. The sample was thereafter preheated to 500 °C to depopulate all traps, irradiated to 50 Gy, preheated to 96 °C to remove peak I followed by another phosphorescence measurement for 3,000 s. The procedure was repeated while removing both peaks I and II (by preheating to 150 °C) prior to measurement. Figure 4.9 shows a plot of intensity against time when all three peaks are present and compares to when peak I and peaks I-II are removed in succession. The intensity decreases slowly with time when all three peaks are present but the intensity remains stable when peak I is removed prior to phosphorescence measurement. The slow phosphorescence decay is therefore attributed to peak I while peaks II and III show no decay (constant intensity). This implies that peak I is associated with shallow traps that exhibit thermal fading.

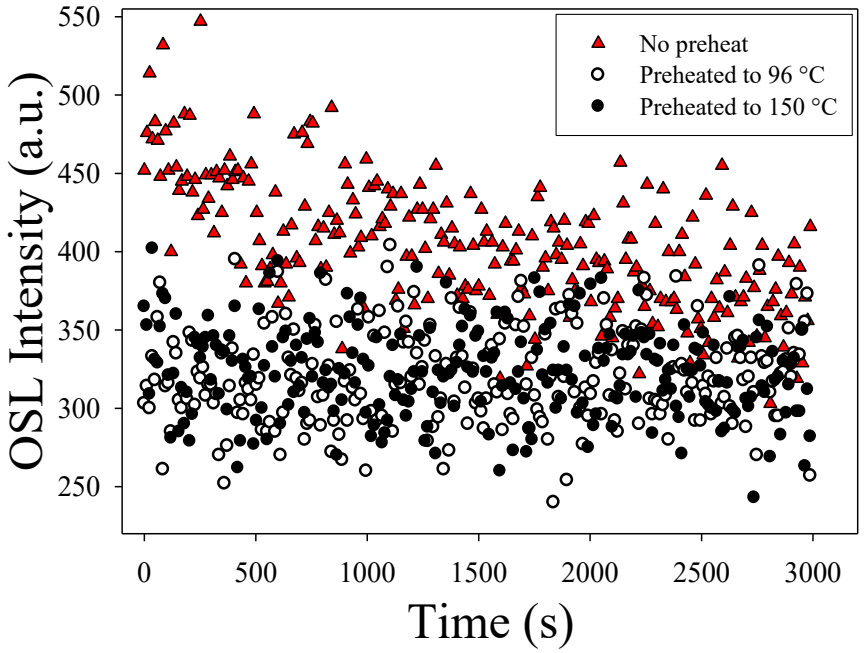

Figure 4.9: Phosphorescence measurement at room temperature. The slow decay (no preheat) is a contribution from peak I and the stable intensities (preheated to 96 and 150 °C) are respectively contributions from both peaks II-III and peak III only.

4.6 Kinetic analysis

The calculated values of the activation energy (E), frequency factor (s) and kinetic order (b) using the initial rise, curve fitting, whole glow peak, phosphorescence decay, phosphorescence area, variable heating rate and peak shape methods of kinetic analysis are presented here. The details of each analytical method have been presented in chapter 2. The kinetic analysis is carried out on all three peaks.

4.6.1 Initial rise method

The activation energy for peak I was evaluated using the initial rise method. The glow curve used for the analysis was recorded following irradiation to 70 Gy. From equation (2.30), a plot of $\ln(I)$ against $1/kT$ will yield a straight line and E can be computed from the gradient. Such a plot for intensity within the rising region of peak I is shown in Figure 4.10. The data points used

for the evaluation correspond to intensity within 5 – 15 % of the maximum TL intensity as suggested elsewhere [19]. The parameter E was evaluated as 0.83 ± 0.03 eV. This value agrees with that reported by Chithambo and Folley [7] as $E = 0.88 \pm 0.04$ eV. The initial rise method was not used to evaluate E for peaks II and III because the intensities at the initial rise region of the peaks are way a

INITIAL RISE METHOD GRAPH

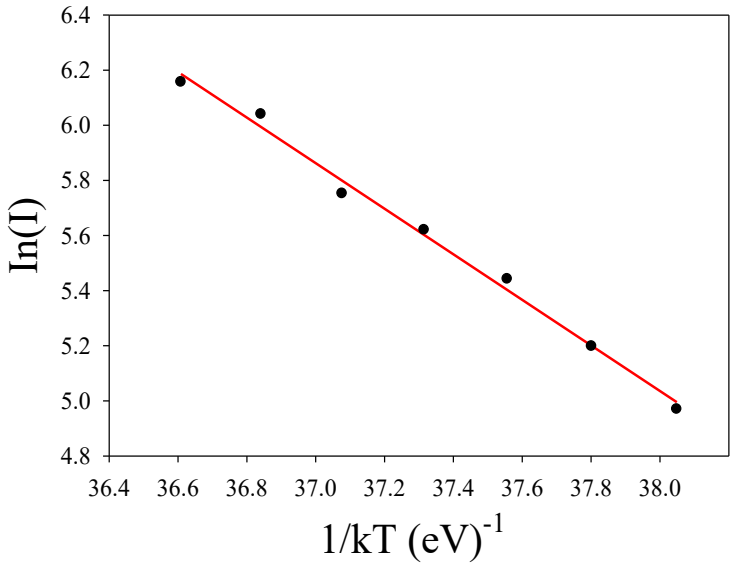

Figure 4.10: A plot of $\ln(I)$ against $1/kT$ for peak I. The continuous line is a linear line through the data points.

4.6.2 Curve fitting method

The Kitis et al. general order curve fitting equation [21], expressed in equation (2.39) was employed to evaluate both E and b for peaks I-III. Following irradiation to 70 Gy, the glow curve was recorded. Figure 4.11 show the fitted experimental data for all the peaks. The best fits were obtained for values of E given as 0.87 ± 0.02, 0.95 ± 0.07 and 1.13 ± 0.01 eV for peaks I-III respectively. The value of E for peak I is comparable to 0.860 ± 0.004 reported by Chithambo and Folley [7]. The kinetic order b yielded 0.96 ± 0.01 for peak I and 1.2 ± 0.01 for both peaks II and III. All the peaks are hence of first order kinetics. The activation energies were substituted in turn into equation (2.41) to calculate the frequency factor for each peak. The resulting values are

4.3×10^{11}, 3.4×10^{10} and 1.4×10^{11} s^{-1} for the respective peaks. These values are comparable to the order of the lattice vibration frequency which is about 10^{12} s^{-1}.

The figure of merit (FOM) was calculated from equation (2.40) for each peak to confirm the goodness of the fits. They are 3.4 % for peak I, 3.3 % for peak II and 3.2 % for peak III. Values of FOM less than 3.5 % are generally acceptable [23] hence the fit for each peak is deemed good.

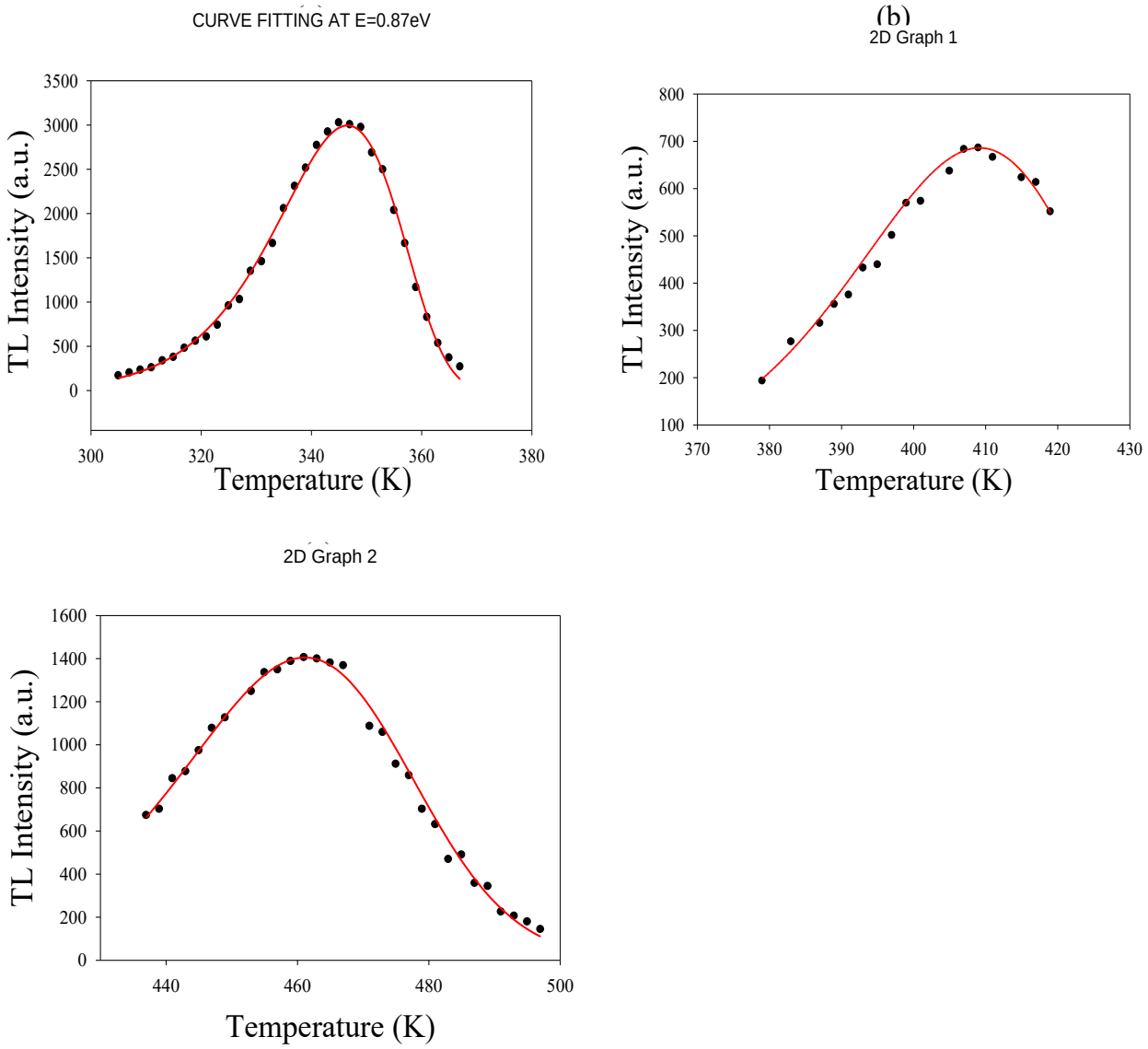

Figure 4.11: Curve fitting of peak I (a), peak II (b) and peak III (c) using Kitis et al. general order curve fitting equation. The solid lines are the fits. The FOM value of each peak is less than 3.5 % hence the fits are good.

4.6.3 Whole glow peak method

The kinetic parameters E, s and b for peaks I-III were calculated using the whole glow peak method. A TL glow curve corresponding to 70 Gy was used for the analysis. From equation (2.35), values of b from 0.8 to 1.2 were used in a plot of $\ln(I/n^b)$ versus $1/kT$ as shown in Figure 4.12(a) for peak I. The most linear line corresponded to $b = 0.9$ with coefficient of determination (r^2) value of 0.9977. The parameters E and s were computed respectively from the gradient and intercept of this line. The plots for peaks II and III are shown in Figures 4.12(b) and 4.12(c). The highest r^2 (with values of 0.9967 and 0.9804) were from the lines $b = 1.3$ for both peaks. This suggest all the peaks are of first order kinetics. The values of E for the respective peaks are 0.77 ± 0.01, 1.03 ± 0.02 and 1.20 ± 0.04 eV. The frequency factor s was calculated as 1.3×10^{10} s^{-1} for peak I, 1.7×10^{10} s^{-1} for peak II and 2.8×10^{10} s^{-1} for peak III. These values compare well with the lattice vibration frequency.

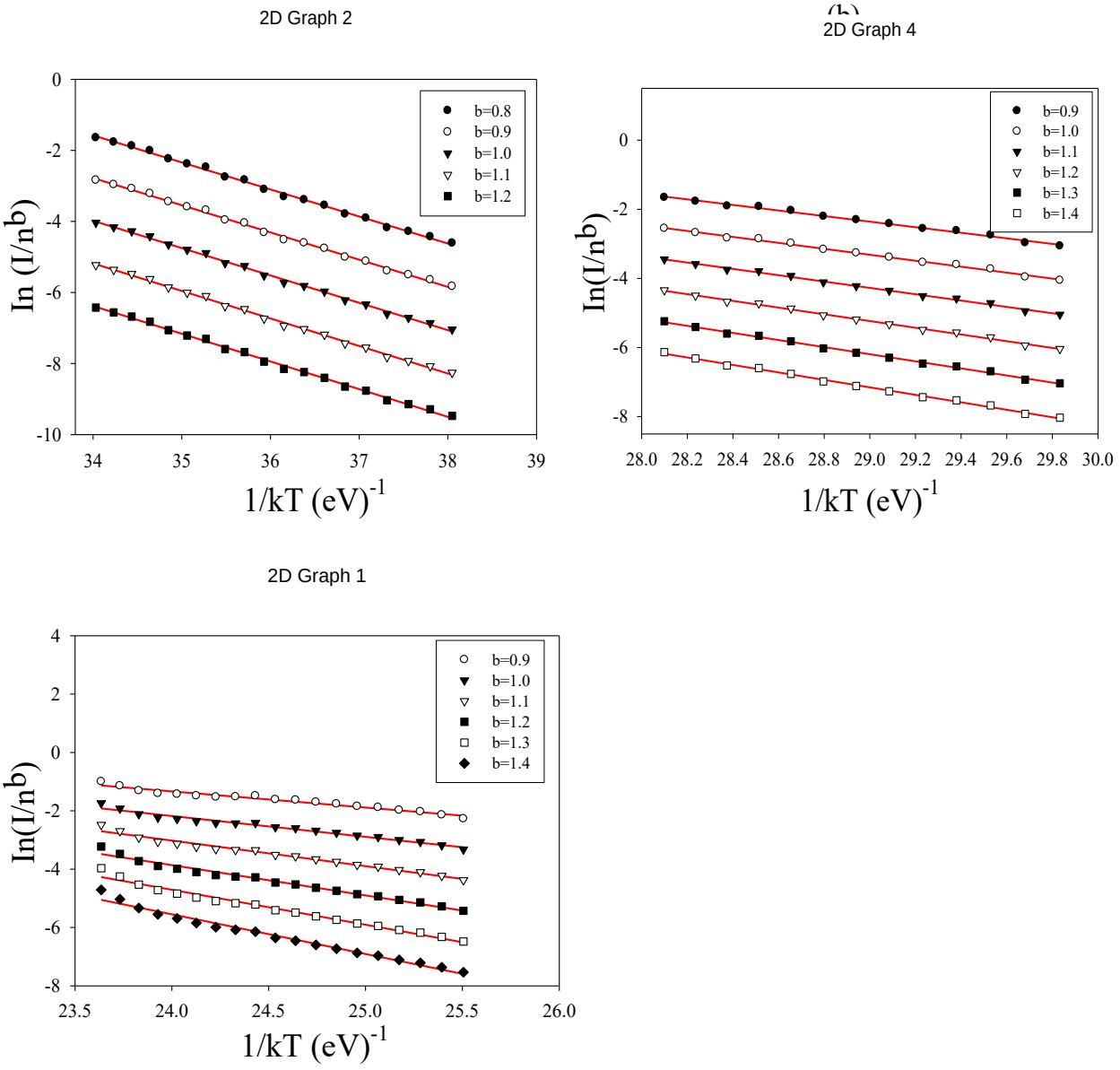

Figure 4.12: Plot of $\ln(I/n^b)$ against $1/kT$ for peaks I (a), II (b) and III (c). The continuous lines are straight lines through the data points. The lines with the highest r^2 values are 0.9 for peak I and 1.3 for both peaks II and III.

4.6.4 Phosphorescence decay method

Phosphorescence measurements were recorded to evaluate the activation energy E and frequency s factor for all the three peaks. For peak I, the phosphorescence was measured in turn at 5 °C

intervals from 40 to 70 °C following irradiation to 50 Gy each time. The measurement duration was 100 s at each temperature. The intensity was calculated by integrating the area under the phosphorescence decay. According to equation (2.48), a plot of $\ln(m)$ against $(1/T)$ will yield a straight line where E and s can be evaluated from the gradient and intercept respectively. Such a plot for peak I is shown in Figure 4.13(a). Each data point represents the mean of three measurements. The kinetic parameters E and s are 0.86 ± 0.01 eV and 1.7×10^{11} s^{-1}.

Peak II followed the same experimental procedure above except that the sample was preheated to 96 °C prior to each measurement, and the measurement temperature ranged from 105 to 130 °C. Figure 4.13(b) shows the plot for peak II. The activation energy E and frequency factor s were evaluated as 0.66 ± 0.05 eV and 3.5×10^{6} s^{-1}. These values are underestimated when compared to the results from the whole glow peak and curve fitting methods. The intensity of peak II is low hence the electron traps are emptied within few seconds of phosphorescence measurement. The TL intensity of peak III was noted to slightly decrease following phosphorescence measurement of peak II within 115 to 130 °C. This means peak III may have contributed to the phosphorescence decay recorded for peak II hence the reason for the inaccurate values of E and s.

Phosphorescence measurement for peak III was recorded in turn from 155 to 180 °C following irradiation to 50 Gy and preheating to 150 °C each time. From Figure 4.13(c), E was calculated as 1.05 ± 0.04 eV and s yielded 1.1×10^{10} s^{-1} for peak III.

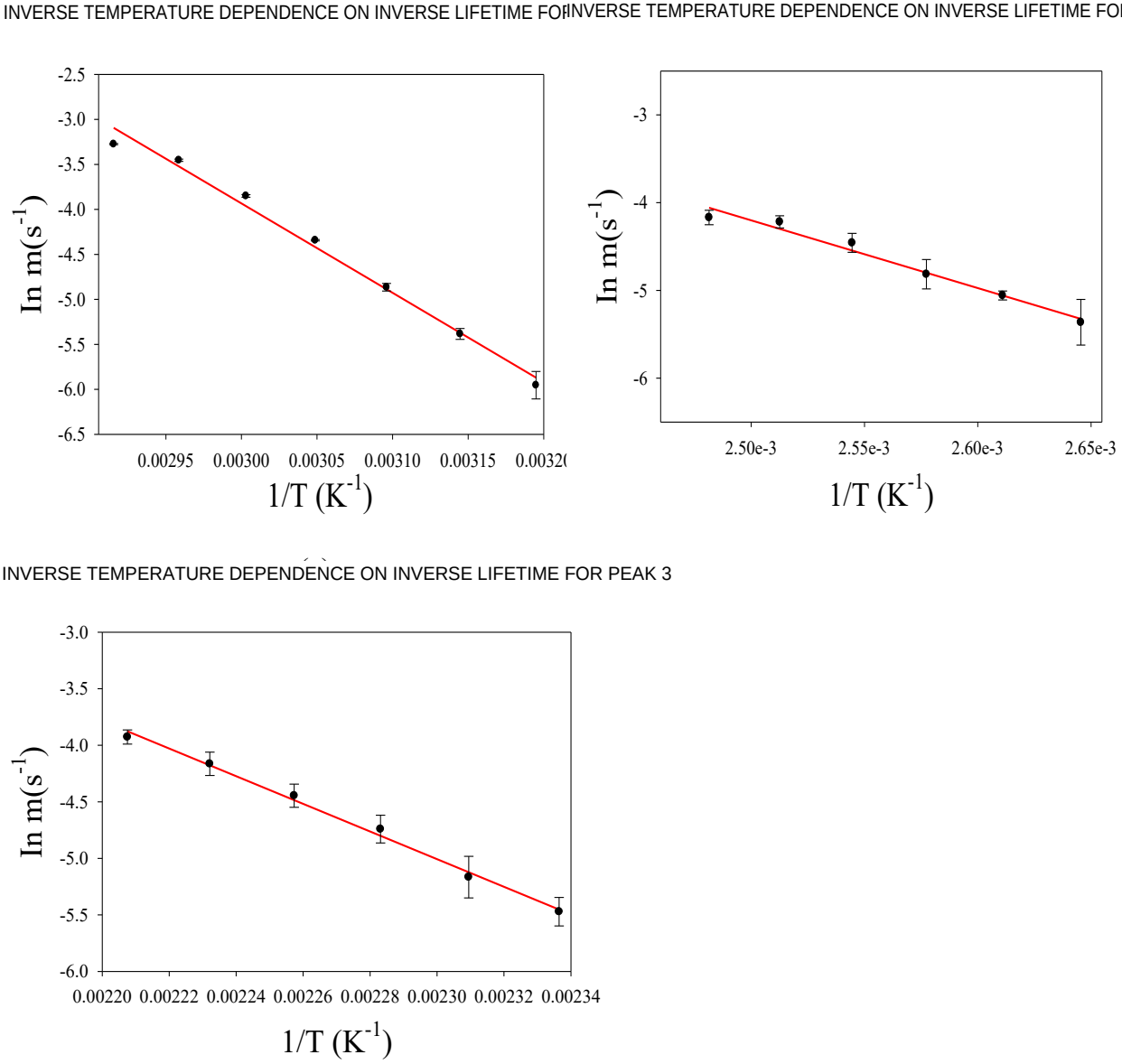

Figure 4.13: Plot of $In(m)$ against $(1/T)$ for peak I (a), peak II (b) and peak III (c). Each data point is the mean of three measurements. The continuous lines are linear lines through the data points.

4.6.5 Phosphorescence area method

The phosphorescence area method has been used to calculate the activation energy E, kinetic order b and the frequency factor s for peak I. Following irradiation to 50 Gy, phosphorescence measurements were recorded in turn at 5 °C intervals from 35 to 90 °C for 10 s each time. The

short measurement time was to ensure the validity of the approximation $e^x = (1 + x)$ applied to arrive at equation (2.62). The area under the phosphorescence decay curve was calculated to represent the intensity. Figure 4.14 shows a pseudo glow peak generated from the plot of intensity against temperature. The pseudo glow curve has been fitted with the Kitis et al. general order curve fitting equation [21]. The kinetic parameters E and b from the fit are 0.88 ± 0.01 eV and 1.00 ± 0.08. The value of b further confirms that peak I is of first order kinetics. The value of E was inserted into equation (2.41) to compute the frequency factor which gave 7.4×10^{11} s^{-1}. The frequency factor is

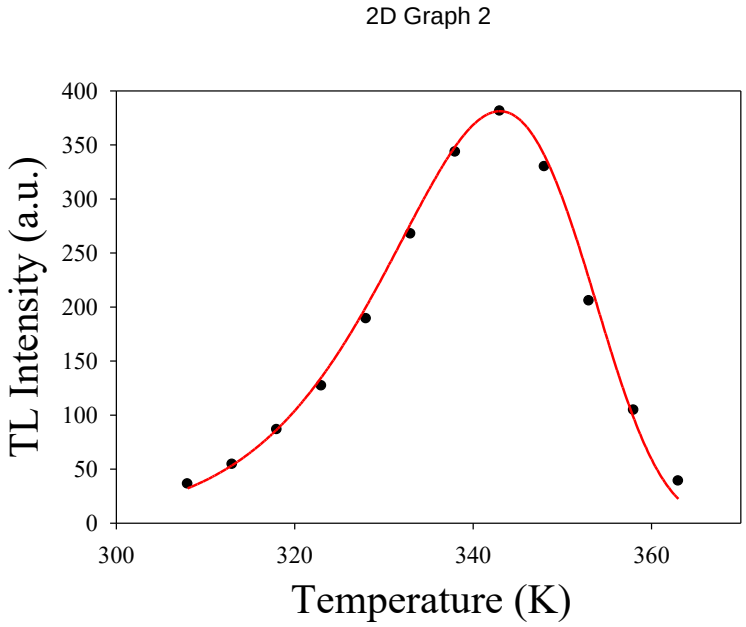

Figure 4.14: Pseudo glow curve of peak I fitted with the Kitis et al. general order curve fitting equation [21]. The continuous line represents the fit.

4.6.6 Variable heating rate method

The changes in the position of the peaks at different heating rates β was employed to calculate the activation energy E and frequency factor s for peaks I-III. The TL intensity was measured in turn at variable heating rates from 0.5 to 4.5 °C s^{-1} following irradiation to 70 Gy each time. The position of each peak was noted thereafter. In all, three TL measurements were made at each heating rate and the average peak position T_m was computed. With reference to equation (2.65), a plot of $\ln(T_m^2/\beta)$ against $1/kT_m$ will be linear as seen in Figure 4.15 for peaks I-III. The

kinetic parameter E was deduced from the slope as 0.78 ± 0.02 eV for peak I, 1.01 ± 0.06 eV for peak II and 1.39 ± 0.11 eV for peak III. From the y-intercept, the calculated values of s are 1.6×10^{10} s^{-1} for

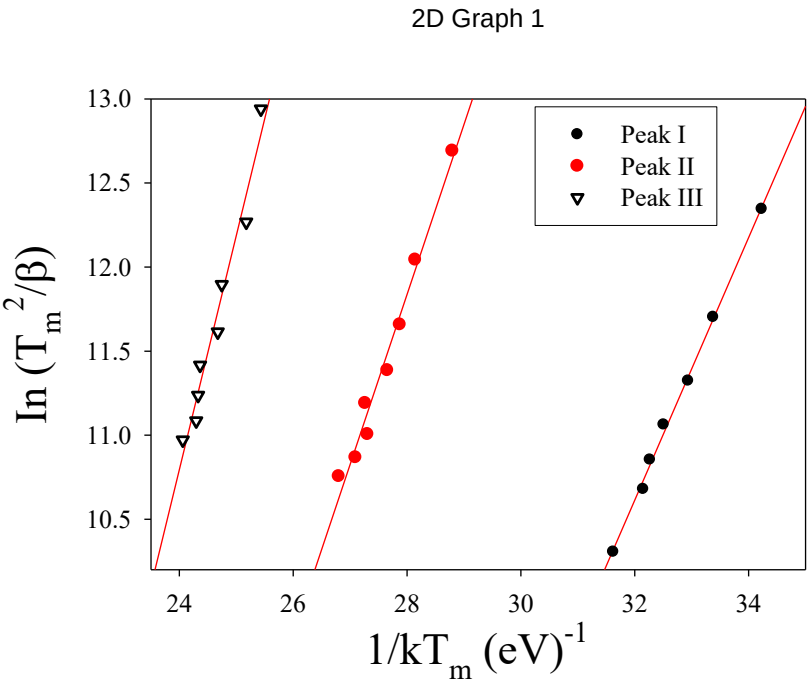

Figure 4.15: Plot of $\ln(T_m^2/\beta)$ against $1/kT_m$ for peaks I-III. The continuous lines are linear lines through the data points.

4.6.7 Peak shape method

The activation energy E and kinetic order b for peak I were again estimated using the peak shape method. The shapes of peaks II and III are not well defined for this procedure. A glow curve corresponding to 70 Gy was used for the analysis. From equation (2.71), the geometric shape factor μ for peak I was calculated as 0.40 ± 0.05 using the values of the half-width (δ) and the total half-width (ω) determined from the glow peak. The value of μ is comparable to that of first order kinetics (μ = 0.42). The activation energies were evaluated from equation (2.72) as E_τ = 0.87 ± 0.01 eV, E_δ = 0.83 ± 0.01 eV and E_ω = 0.86 ± 0.01 eV. These values agree with the activation energy from all the other methods of kinetic analysis for peak I. The peak shape analysis poses a challenge due to the subjectivity involved in locating the parameters $I_M/2$, T_1

and T_2. These parameters are used in deriving the half-widths and the geometric shape factor of the glow peak.

4.7 Thermal quenching

The presence of thermal quenching has been analysed from the relationship between the heating rate and the TL intensity. The details of thermal quenching mechanism have already been given in section 2.4 of chapter 2. The TL intensity was recorded at different heating rates from 0.5 to 4.5 °C s^{-1} following irradiation to 70 Gy each time. The integral of the area under each peak was evaluated to represent the TL intensity (in counts $°C^{-1}$). Figure 4.16 shows a plot of the intensity against heating rate for peaks I-III. The intensity of each peak decreases with increasing heating rate which is an inc

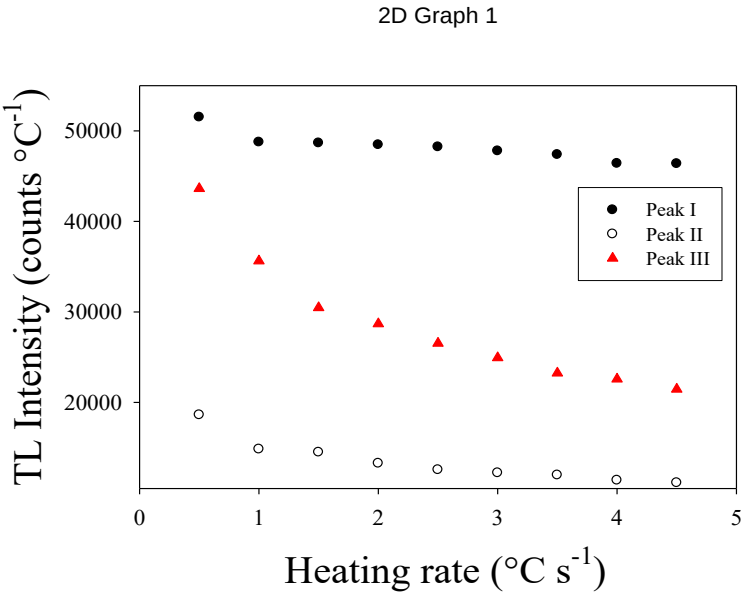

Figure 4.16: Plot of TL Intensity (in counts $°C^{-1}$) at variable heating rates from 0.5 to 4.5 °C s^{-1} for peaks I-III. The intensity reduces with heating rate for all three peaks.

The activation energy of thermal quenching W for each peak has been quantified with reference to equation (2.86). Figure 4.17 shows a plot of $\ln(I_{un}/I_{qn} - 1)$ versus $1/kT_m$ for peaks I-III. The parameter W was computed from the gradient as 0.36 ± 0.08 eV for peak I, 0.72 ± 0.10 eV for peak II and 1.62 ± 0.12 eV for peak III. These values imply that the recombination pathway

for the TL mechanism is different for each peak. The value of W for peak I compares well with 0.34 ± 0.02 reported by Chithambo and Folley [7] whereas that of peak III was reported by the authors as 1.10 ± 0.08 eV.

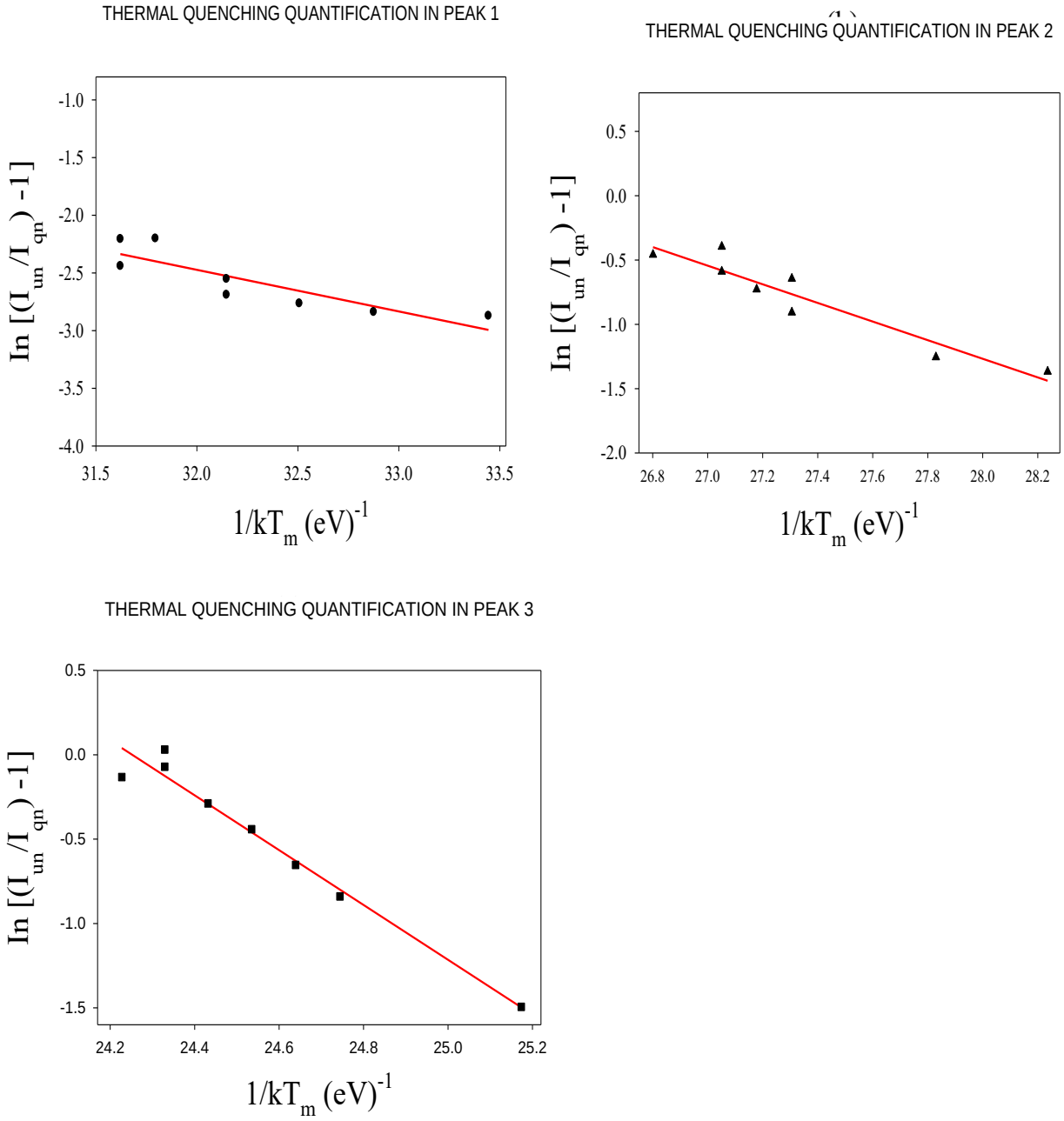

Figure 4.17: Plot of $\ln(I_{un}/I_{qn} - 1)$ versus $1/kT_m$ for peak I (a), peak II (b) and peak III (c). The continuous lines are linear lines through the data points.

4.8 Summary of kinetic parameters

Table 1 shows the computed kinetic parameters for peaks I-III. The results from all the analytical methods agree for the respective peaks except in the case of the phosphorescence decay method in relation to peak II, and a slight overestimation of peak III from the variable heating rate method. The activation energy E is averagely 0.84 eV for peak I, 1.00 eV for peak II and 1.19 eV for peak III. The mean values of the frequency factor s are 3×10^{11}, 7×10^{10} and 3×10^{13} s^{-1} for the respective peaks and these figures are comparable to the lattice vibration frequency. The values of E and s for peak II from the phosphorescence decay method were not included in the averages because these values are greatly underestimated. All the peaks are of first order kinetics since b approaches 1. The kinetic parameters for peak I are consistent with the results from literature. For peak II, except for the phosphorescence decay method, the values of the kinetic parameters are reliable since they are comparable to each other. Also, those of peak III are reliable except for the variable heating rate method.

Table 1. Kinetic parameters for peaks I-III.

Peaks	Analytical Method	E (eV)	s (s^{-1})	b	Reference
Peak I	Initial rise	0.83 ± 0.03			Fig. 4.10
		0.88 ± 0.04			Chithambo and Folley [7]
	Curve fitting	0.87 ± 0.02	4.3×10^{11}	0.96 ± 0.01	Fig. 4.11(a)
		0.860 ± 0.004	2.0×10^{11}	0.970 ± 0.003	Chithambo and Folley [7]
	Whole glow peak	0.77 ± 0.01	1.3×10^{10}	0.9	Fig. 4.12(a)
		0.85 ± 0.01	3.0×10^{11}	1.1 ± 0.1	Chithambo and Folley [7]
	Phosphorescence decay	0.86 ± 0.01	1.7×10^{11}		Fig. 4.13(a)
		0.87 ± 0.05	2.6×10^{11}		Chithambo and Folley [7]
	Phosphorescence area	0.88 ± 0.01	7.4×10^{11}	1.00 ± 0.08	Fig. 4.14
		0.85 ± 0.03		1.1 ± 0.1	Chithambo and Folley [7]
	Variable heating rate	0.78 ± 0.02	1.6×10^{10}		Fig. 4.15
		0.86 ± 0.03	3.0×10^{11}		Chithambo and Folley [7]
	Peak shape	0.87 ± 0.01 (τ)			Sect. 4.5.7
		0.83 ± 0.01 (δ)			
		0.86 ± 0.01 (ω)			
Peak II	Curve fitting	0.95 ± 0.07	3.4×10^{10}	1.20 ± 0.01	Fig. 4.11(b)
	Whole glow peak	1.03 ± 0.02	1.7×10^{10}	1.3	Fig. 4.12(b)
	Phosphorescence decay	0.66 ± 0.05	3.5×10^{6}		Fig. 4.13(b)
	Variable heating rate	1.01 ± 0.06	1.7×10^{11}		Fig. 4.15
Peak III	Curve fitting	1.13 ± 0.01	1.4×10^{11}	1.20 ± 0.01	Fig. 4.11(c)
	Whole glow peak	1.20 ± 0.04	2.8×10^{10}	1.3	Fig. 4.12(c)
	Phosphorescence decay	1.05 ± 0.04	1.1×10^{10}		Fig. 4.13(c)
	Variable heating rate	1.39 ± 0.11	1.0×10^{14}		Fig. 4.15

Chapter 5

Optically stimulated luminescence (OSL)

The aim for carrying out optically stimulated luminescence (OSL) measurements is to supplement the TL and PTTL analysis. Specifically, OSL provides a means of investigating both thermal assistance and quenching of luminescence signal, as well as evaluating the decay constant of the components contributing to the luminescence, which cannot be carried out in TL measurements. Moreover, a comparative analysis of thermal assistance and quenching from the OSL measurements and the PTTL measurements shall be made in the next chapter.

In this chapter, the results of the continuous wave optically stimulated luminescence (CW-OSL) measurement on tanzanite are reported. The shape of the decay curve from the CW-OSL measurement is first presented, followed by an evaluation of the decay constants of the various components associated with the decay curve. The response of the OSL intensity with variable doses has also been investigated. The final part presents the effect of variable temperatures and irradiation doses on the kinetic parameters activation energy of thermal assistance and quenching.

5.1 CW-OSL measurement

The background signal was first cleared by preheating to 500 °C. The sample was then irradiated to 50 Gy and subsequently illuminated with 470 nm blue LEDs for 1000 s while recording the luminescence signal. The measurement was done at room temperature and the power of the blue LEDs was set at 90% and kept constant throughout. Figure 5.1 shows a plot of the OSL intensity against the stimulation time. The intensity decreases rapidly by about 50% within the first 9 s of measurement following which a slow decay is observed from 9 to 200 s. A much slower decay is observed post 200 s. As discussed in section 2.5.1.1.1 of chapter 2, a convenient way of describing the shape of the OSL decay curve is to fit the curve with a sum of several exponential

components although each component may not necessarily be attributed to any physical mechanism. The decay curve has been fitted with a sum of three exponentials given as:

$$I_{OSL} = I_1 \exp(-\lambda_1 t) + I_2 \exp(-\lambda_2 t) + I_3 \exp(-\lambda_3 t) \quad (5.1)$$

where I_{OSL} is the intensity at time t; I_1, I_2 and I_3 are the scaling parameters of the first, second and third component respectively, and λ_1, λ_2, λ_3 represent the decay constant of the respective components. The values of λ_1, λ_2 and λ_3 from the fit are 0.48, 0.01 and 0.0002 s^{-1} respectively. This result implies that the first component exhibits the most rapid decay, followed by the second component and then the third one. The terms fast, medium and slow component have been adopted in a number of literature [5, 45, 72] to represent the exponentials in descending order of magnitude of the de

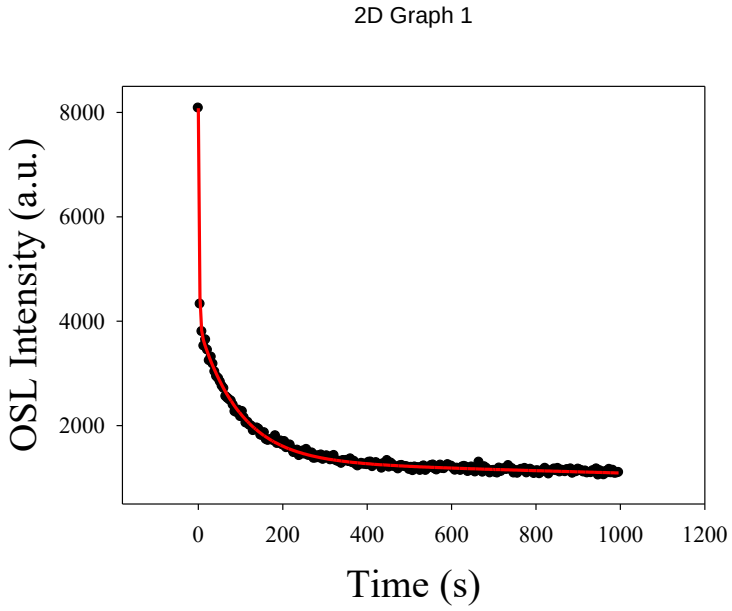

Figure 5.1: CW-OSL decay curve of tanzanite corresponding to 50 Gy. The solid line is the best fit of equation (5.1).

The contribution of each component to the total luminescence intensity can be examined by comparing the ratio of each component's intensity to the total luminescence intensity [5, 37]. Figure 5.2 shows the relative contribution of the respective components with time. The initial intensity is dominated by the first component (fast component) which accounts for 51% of the total intensity and quickly falls to 2% in the first 8 s. At 13 s, the second component (medium component) contributes to 63% of the total intensity and gradually reduces to 4% at 390 s.

Following 520 s, the third component's (slow component) contribution is dominant and essentially the only signal recorded.

To obtain information on the optical properties associated with each component, the photoionization cross section (σ), which indicates a trap's stability to optical stimulation [43] has been evaluated from the relation

$$\sigma = \frac{1}{\tau \Phi} \tag{5.2}$$

where τ represents the inverse of the decay constant i.e $\tau = 1/\lambda$ and Φ is the light intensity [43]. The values of τ are 2.083, 100.00 and 5000 s for fast, medium and slow component respectively. The parameter $\Phi = 9.5\times10^{16}$ cm^{-2} s^{-1} for blue LEDs operated at 90% of its power [5]. The computation of σ yielded 5.1×10^{-18}, 1.1×10^{-19} and 2.1×10^{-21} cm^2 for fast, medium and slow component resp

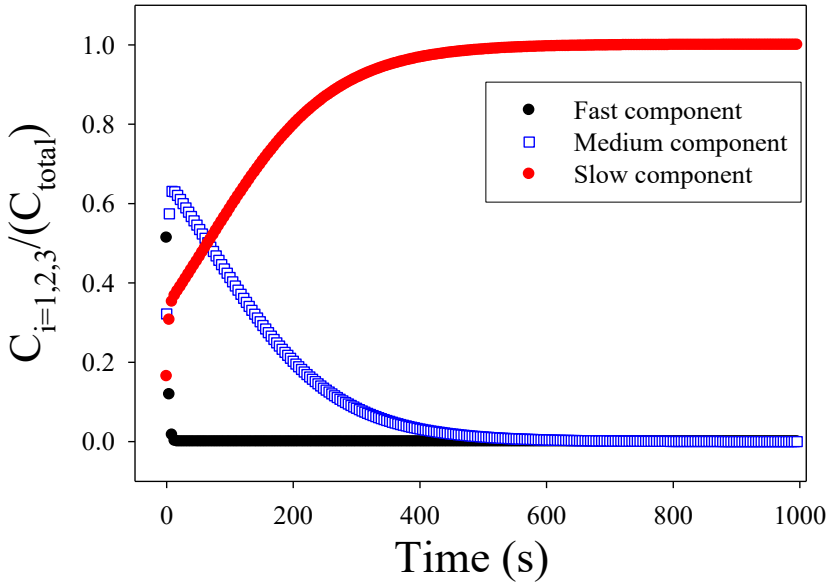

Figure 5.2: Contributions of the slow, medium and fast components to the total OSL intensity. The symbol C_{total} represents the total intensity and C_i represents the intensity of either the fast (C_1) medium (C_2) or slow (C_3) component.

5.2 OSL source traps

The analysis for the OSL source traps is concerned with identifying the temperature range of the electron traps that are contributing to the OSL process. The procedure adopted is similar to that used elsewhere [37] for the same purpose and includes the following steps:

1- Sample irradiation to 50 Gy.
2- Preheating the sample to temperature T_j.
3- CW-OSL measurement for 50 s at temperature T_j.
4- Residual TL measurement at 1 °C s^{-1}.

In step 2, trapped electrons that are present at the preheat temperature T_j are depleted and the measurement of CW-OSL in step 3 will appear as a significant decrease in OSL intensity. As such, the temperature range corresponding to the trap regions can be visually identified. In step 4, the residual TL is measured to monitor the TL intensity following each OSL measurement in step 3. The whole procedure is repeated for different values of temperature T_j in steps 2 and 3. The preheat temperature ranged from 30 to 220 °C at 5 °C intervals. Figure 5.3 shows the plot of the OSL intensity against the preheat temperature. Each data point represents the integral under the OSL decay curve. Within preheat temperatures of 30 to 40 °C, the OSL intensity shows a relative stability. The intensity goes through a rapid reduction from 45 to 90 °C followed by a relative stability up to 170 °C. Within 170 to 220 °C, the intensity shows another significant reduction. The intensity reduces due to depopulation of trapped electrons during preheating. The OSL source traps are therefore located within the regions of 40 to 90 °C and 170 to 220 °C.

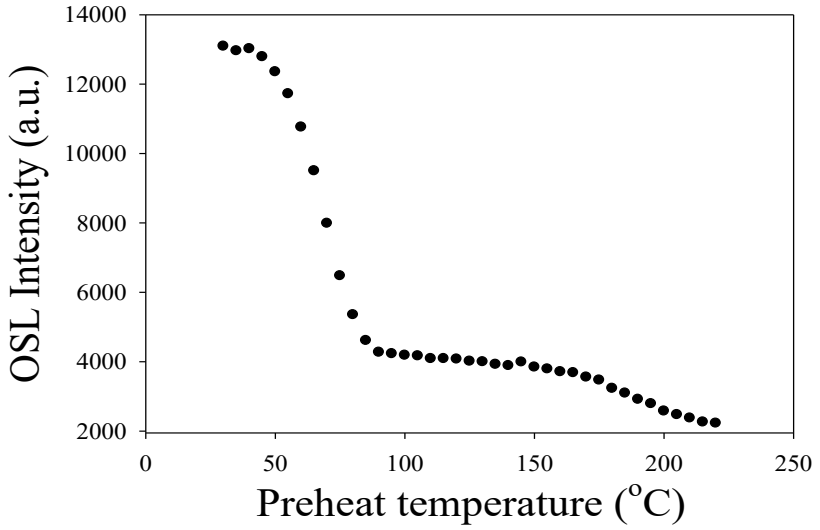

Figure 5.3: OSL intensity against preheat temperatures from 30 to 220 °C. The intensities within 40 to 90 °C and 170 to 220 °C show significant losses.

Figure 5.4(a) shows the plot of residual TL intensity against preheat temperature. The intensity was evaluated as the integral of the area under the TL glow peaks. The TL analysis presented in section 4.1 of chapter 4 revealed three peaks at 74 °C (peak I), 138 °C (peak II) and 186 °C (peak III). All three peaks were revealed in the residual TL measurements as shown in Figure 5.4(b). From Figure 5.4(a), the intensity of peak I reduces within preheat temperatures of 40 to 90 °C and remains stable afterwards. Peak II shows a stable intensity within 30 to 110 °C. A significant intensity loss occurs following 110 °C up to 145 °C and remains relatively stable afterwards. Peak III shows a stable TL intensity within 20 to 155 °C followed by a rapid decline up to 220 °C. The OSL trap regions are noted to occur within temperature ranges of 40 to 90 °C for peak I, 110 to 145 °C for peak II and 160 to 220 °C for peak III. The OSL source traps identified in Figure 5.3 are the same as those identified for peaks I and III in Figure 5.4(a). That of peak II in Figure 5.4(a) could not be clearly identified in Figure 5.3 although a general decrease in OSL intensity is observed but not appreciable. The intensity of peak II is low compared to peaks I and III and therefore could account for the less prominent reduction in OSL intensity in Figure 5.3. The OSL source traps are hence within the regions of 40 to 90 °C, 110 to 145 °C and 160 to 220 °C. These are the same as the TL source traps.

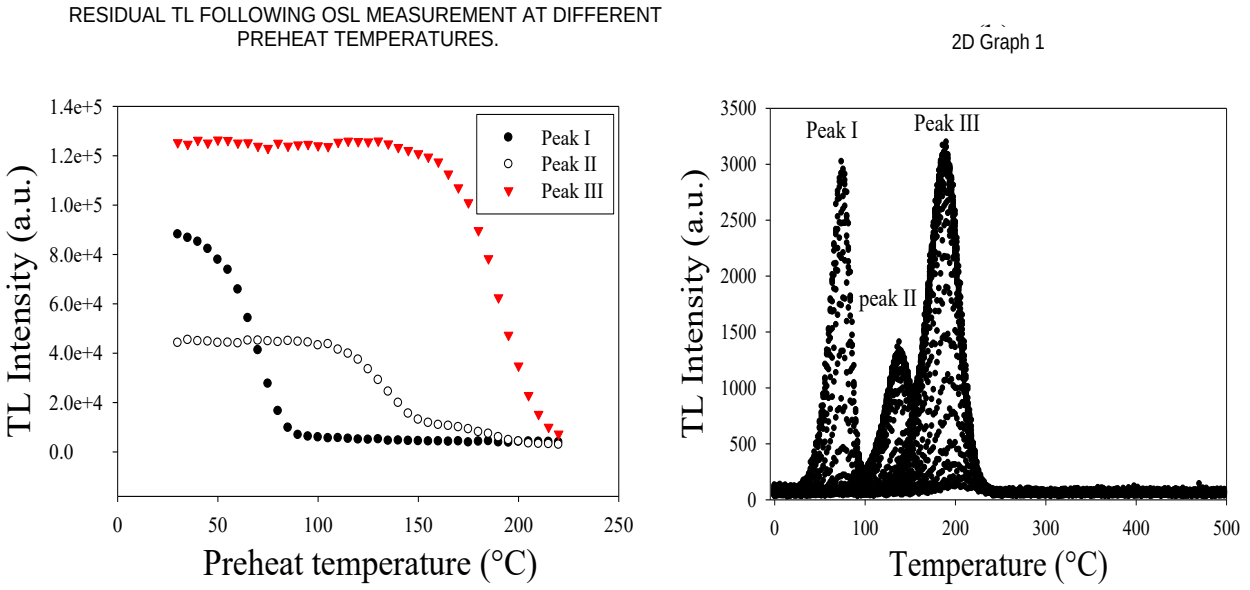

Figure 5.4: Residual TL intensity at variable preheat temperatures (a) and cluster of residual TL glow curves recorded following irradiation to 50 Gy, in turn preheating from 30 to 220 °C and illumination for 50 s each time.

5.3 Dose response

The dependence of the OSL intensity on irradiation dose from 20 to 150 Gy has been studied. The OSL signal was measured for 50 s each time following in turn irradiation from 20 to 150 Gy. The measurements were made at room temperature. The intensity was calculated by integrating the area below the OSL decay curves. Figure 5.5(a) shows the plot of the intensity against dose. The intensity increases non-linearly with dose and has been fitted with the empirical expression

$$y(D) = aD^b \tag{5.3}$$

where y is an empirical function dependent on dose D, and a, b are constants.

The dose response was further analysed using the supralinearity index function *f(D)* [69] given in equation (4.2). Figure 5.5(b) shows a plot of *f(D)* against dose. The value of *f(D)* decreases continuously from 1 to a minimum of 0.456 at 150 Gy hence a sublinear dose response is shown.

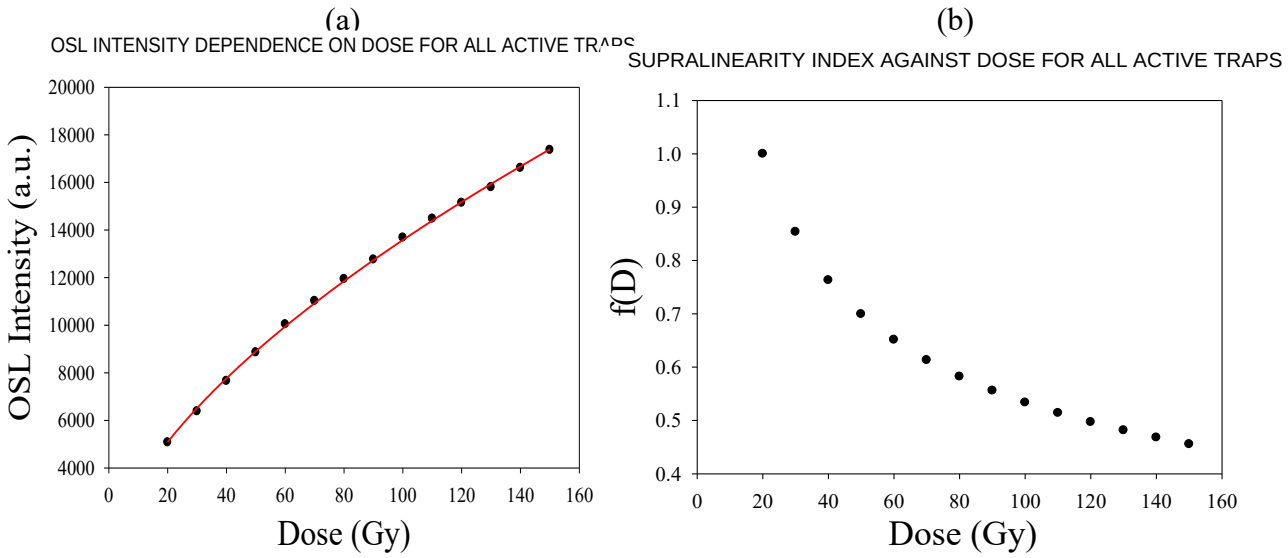

Figure 5.5: OSL intensity dependence on dose for all active traps (a). The continuous line is the fit of equation (5.3). Plot of supralinearity index function *f(D)* against dose (b). The parameter *f(D)* < 1 indicating a sublinear dose response.

The experimental procedure was repeated while preheating the sample to 95 °C prior to each OSL measurement. Preheating was to cause the depletion of trapped charges within 40 to 90 °C. The active luminescence traps are therefore within 110 to 145 °C and 160 to 220 °C. Figure 5.6(a) shows the plot of intensity against dose for the two active trap regions. The intensity increases with dose. The plot is best fitted with equation (5.3).

Figure 5.6(b) shows the plot of *f(D)* against dose for the luminescence traps within 110 to 145 °C and 160 to 220 °C. The function *f(D)* is less than 1 from 30 Gy up to 150 Gy. The response to the dose is therefore sublinear.

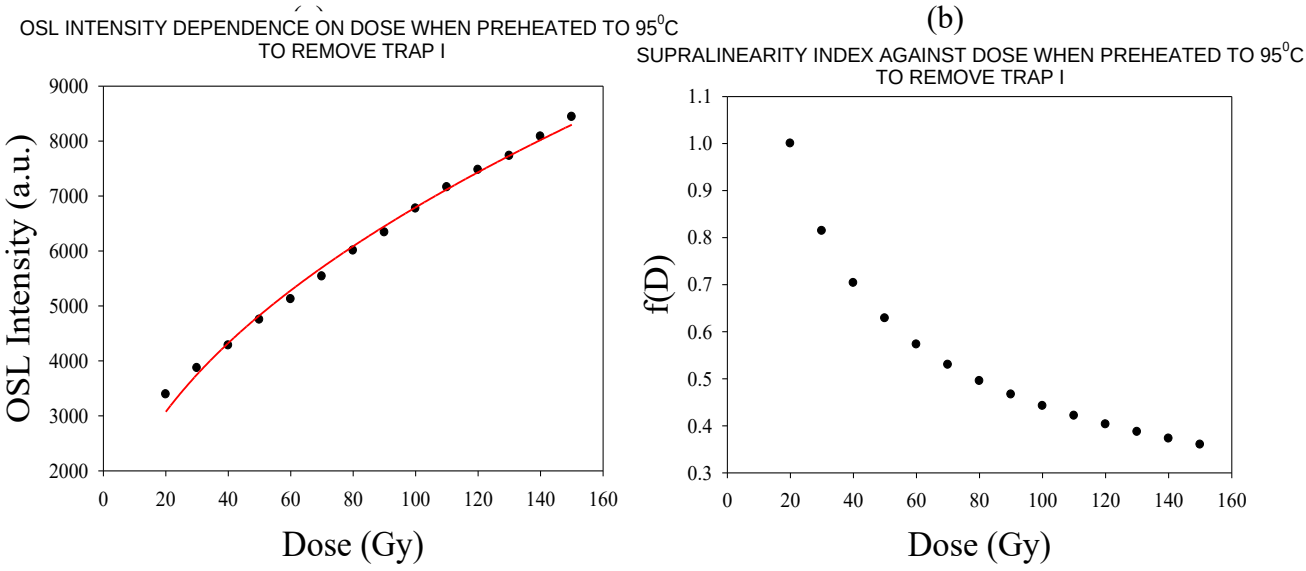

Figure 5.6: OSL intensity dependence on dose for luminescence traps within 110 to 145 °C and 160 to 220 °C (a). The continuous line is the best fit of equation (5.3). Plot of supralinearity index function *f(D)* against dose (b). The value of *f(D)* < 1 indicating a sublinear dose response.

The dose response for the traps within 160 to 220 °C was also analysed by preheating the sample to 145 °C prior to recording the OSL signal for the various doses. The plot of the OSL intensity versus dose is shown in Figure 5.7(a). The intensity once again increases non-linearly with dose. The empirical function that best fit the data is given by

$$y(D) = c + aD^b \tag{5.4}$$

where *c* is a constant and all other parameters are as previously defined.

The plot of *f(D)* against dose for the luminescence traps within 160 to 220 °C is displayed in Figure 5.7(b). A sublinear dose response is shown since *f(D)* < 1.

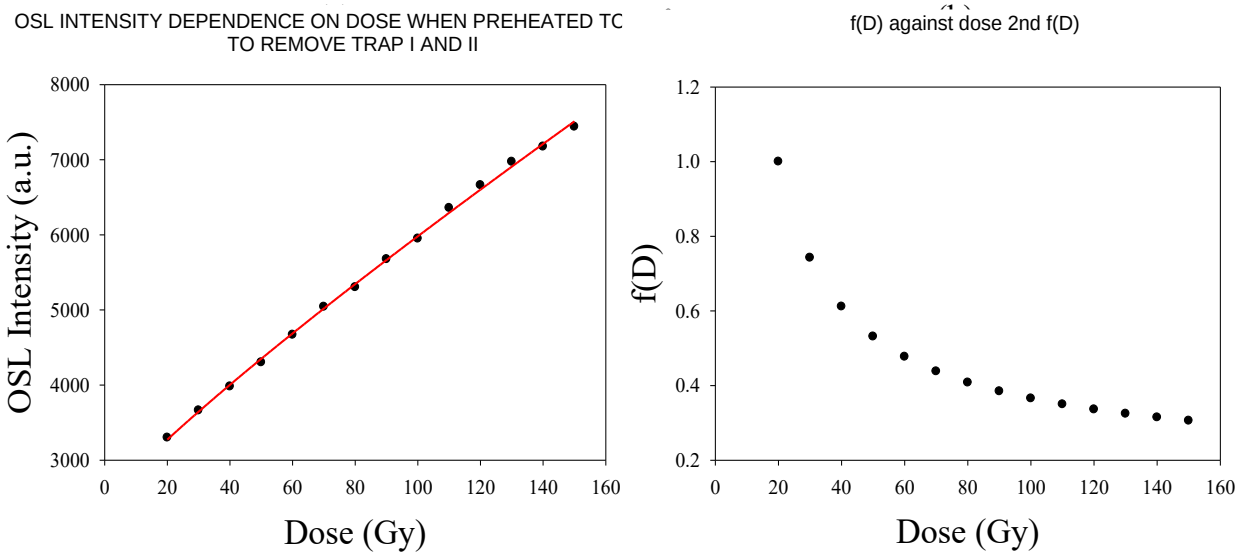

Figure 5.7: A plot of OSL intensity dependence on dose for luminescence traps within 160 to 220 °C (a). The continuous line is the best fit of equation (5.4). Plot of supralinearity index function *f(D)* against dose (b). The value of *f(D)* < 1 hence the response to the dose is sublinear.

5.4 Thermal assistance and thermal quenching of OSL signal

Thermal assistance and thermal quenching respectively describe temperature assisted increase and decrease in measured luminescence signal. The effect of thermal assistance is observed in OSL measurement where the intensity recorded at higher temperature is greater than that measured at room temperature. For thermal quenching, the OSL intensity measured at a higher temperature is less compared to that measured at room temperature. The thermal quenching mechanism has been detailed in section 2.4 of chapter 2 using the Mott-Seitz configurational coordinate model. The dependence of luminescence lifetime on temperature can be expressed as

$$\frac{1}{\tau} = \frac{1}{\tau_{rad}} + \gamma coth\left(\frac{h\omega}{kT}\right) + \nu exp\left(\frac{\Delta E}{kT}\right) \qquad (5.5)$$

where τ represents the lifetime of the excited state, τ_{rad} is the radiative lifetime, γ is a constant, h is Planck's constant, ω is the vibration frequency of the phonon, ν is the frequency factor of the non-radiative process, k is the Boltzmann's constant, T is temperature and ΔE is the activation

energy for the non-radiative recombination [73]. When contribution from phonons is ignored and the effect of thermal assistance is introduced, equation (5.5) can be written as

$$\frac{1}{\tau} = \frac{1}{\tau_{rad}} + \left[v exp\left(\frac{\Delta E}{kT}\right)\right] exp\ \left(\frac{E_a}{kT}\right) \tag{5.6}$$

where E_a is the activation energy of thermal assistance [37]. Equation (5.6) means that both radiative and non-radiative recombination pathways are available for the luminescence process. The OSL intensity dependence on temperature is given as

$$I(T) = \frac{I_0 exp\left(\frac{E_a}{kT}\right)}{1 + C exp\left(\frac{-\Delta E}{kT}\right)} \tag{5.7}$$

where I_0 is initial intensity, C is a constant and all other symbols are as previously defined. The parameters E_a, ΔE, I_0 and C are simultaneously evaluated by fitting equation (5.7) to the experimental OSL intensity recorded at different temperatures.

5.4.1 OSL measurement at different temperatures

The OSL intensity dependence on the measurement temperature is of interest in this section. The decay curves were measured in turn from 20 to 190 °C following irradiation to 50 Gy each time. Each measurement duration lasted 50 s. The intensity has been evaluated as the integral below the decay curves. Figure 5.8 shows the plot of OSL intensity against the temperature of measurement. There are three noticeable intensity peaks at 60, 130 and 180 °C. These peaks resemble the shape of the TL glow curve measured within the same temperature range as shown in Figure 4.2. Moreover, the source traps of the OSL decay are the same as those of the TL source traps as identified earlier hence the OSL intensity peaks are most probable to occur within the temperature range of the source traps.

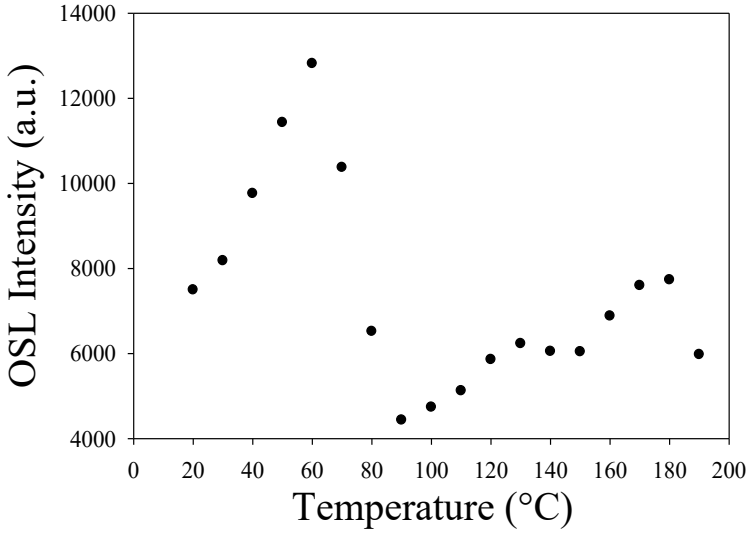

Figure 5.8: OSL intensity measured from 20 to 190 °C following sample irradiation to 50 Gy each time. Each data point represents the integral under the decay curve. Three intensity peaks are noted at 60, 130 and 180 °C.

The rising and falling regions of the intensity peaks are attributed to thermal assistance and thermal quenching respectively. This was verified by comparing the measurements of OSL intensities at room temperature to those measured at increasing temperatures. For the former, the sample was irradiated to 50 Gy and 34 consecutive OSL measurements were made for 50 s at each run. For the latter, the OSL signal was consecutively measured from 35 to 200 °C with each run lasting for 50 s. For both procedures, irradiation to 50 Gy was sufficient to ensure luminescence above background throughout the measurement period. The area under the decay curves was computed to represent the OSL intensity. Figure 5.9 compares the plot of 34 consecutive OSL measurement at room temperature to that measured at variable temperatures. The intensity measured at increasing temperature (from 35 to 160 °C) is observed to be higher than those measured at room temperature (from measurement number 1 to 26) and this is due to thermal assistance. From measurement number 27 to 34, the intensity is observed to be higher than those measured from 165 to 200 °C. The decrease in the luminescence intensity measured at higher temperatures in comparison with those measured at room temperature is attributed to the effect of thermal quenching.

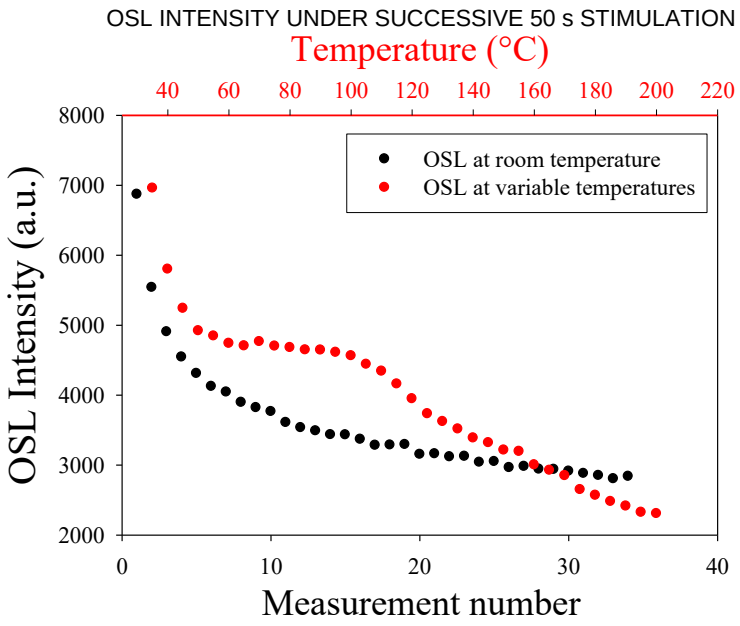

Figure 5.9: Consecutive OSL measurement at room temperature and at variable temperatures. Irradiation to 50 Gy preceded each consecutive measurement. Each data point represents the area under the decay curve.

The kinetic parameters activation energy of thermal assistance E_a and activation energy of thermal quenching ΔE associated with the OSL signal have been computed from temperature ranges of 30 to 80 °C, 95 to 145 °C and 145 to 195 °C since the OSL source traps are located within those regions. The OSL signal was measured each time for 50 s following in turn sample irradiation to 10, 50 and 70 Gy. Recording the OSL signal at different temperatures following in turn irradiation to variable doses generally affect the shape of the OSL curve, the luminescence intensity and the kinetic parameters activation energy of thermal assistance and quenching which are important factors to consider in the choice of a material for dosimetry application.

Firstly, the OSL was measured in turn from 30 to 80 °C following irradiation to 10 Gy each time. The intensity at each temperature was evaluated by integrating the curve below the recorded signal. The whole procedure was repeated for sample irradiated to 50 and 70 Gy. The luminescence signal in this procedure is from all the OSL source traps earlier identified. Figure 5.10 shows the plot of OSL intensity measured at different temperatures corresponding to 10, 50 and 70 Gy. The intensity for sample irradiated to 70 Gy is the highest in all the measurement, followed by 50 Gy and then 10 Gy. Higher doses ensure sufficient trap filling which lead to

higher luminescence signal upon liberation from traps and subsequent recombination with holes at the recombination centre. As pointed out earlier in this section, the rising regions are ascribed to the effect of thermal assistance while the descending regions are ascribed to thermal quenching. Equation (5.7) is fitted to the data points. The coefficient of determination (r^2) is 0.978, 0.844 and 0.983 for the respective doses. The kinetic parameter E_a from the fits are 0.121 ± 0.002 eV for sample irradiated to 10 Gy, 0.171 ± 0.001 eV for sample irradiated to 50 Gy and 0.153 ± 0.001 eV for sample irradiated to 70 Gy. These figures are consistent and averagely computed as 0.15 eV. The values of ΔE are 0.80 ± 0.01, 0.81 ± 0.01 and 0.82 ± 0.01 eV for the respective doses. These values are also comparable, and the average is 0.81 eV. The recombination site is the same for all the doses since the kinetic parameter activation energy of thermal quenching is comparable. The constant C are 2.9×10^{11}, 7.1×10^{11} and 1.4×10^{12} for sample irradiated to 10, 50 and 70 Gy respectively. The fit corresponding to 50 Gy is, however, not optimal and adjusting the initial fitting parameters did little to improve it.

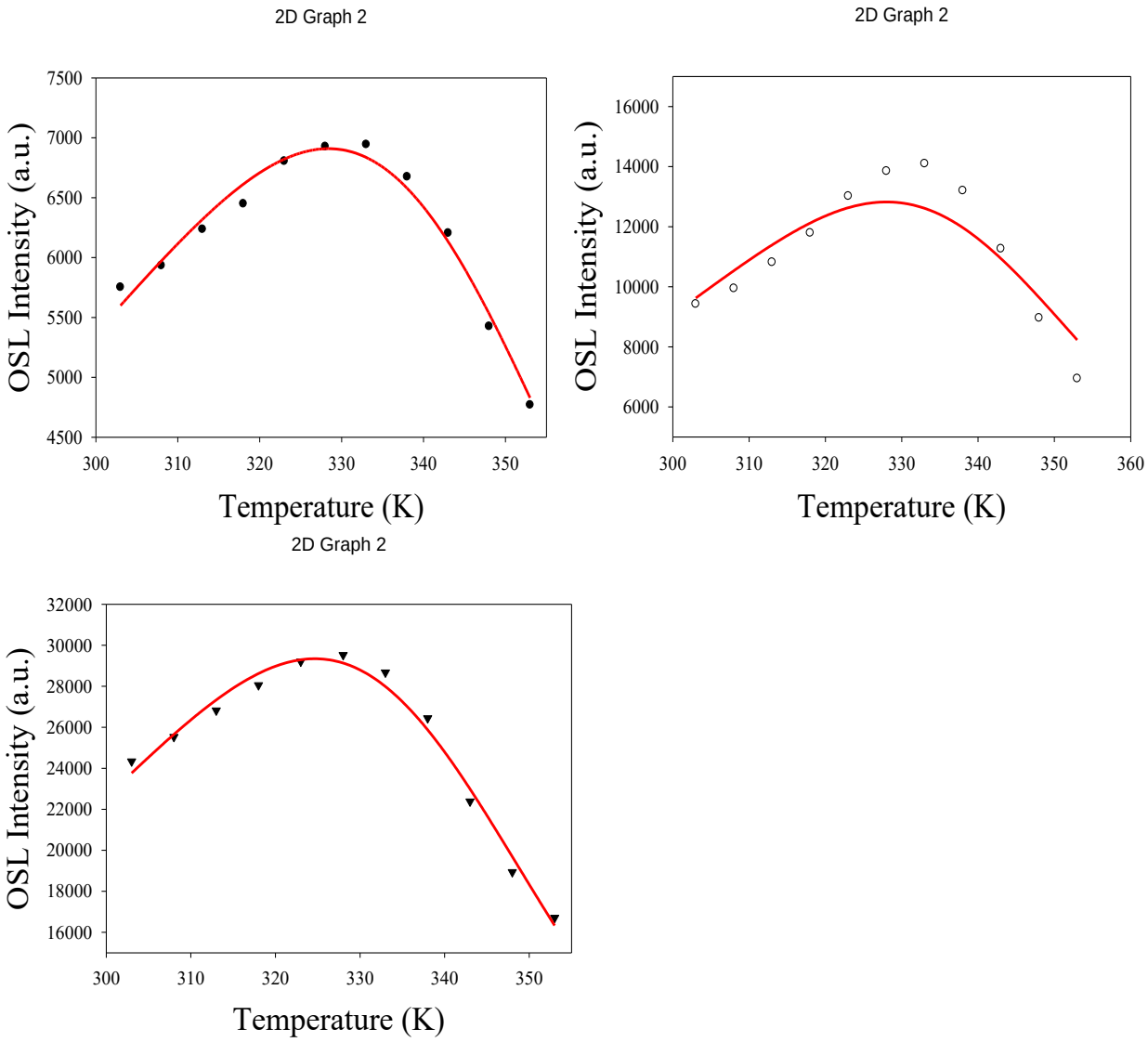

Figure 5.10: OSL intensity measured at variable temperatures from 30 to 80 °C following in turn irradiation to 10 Gy (a), 50 Gy (b) and 70 Gy (c). The integral of the area under the OSL decay represents the intensity. The solid lines are the best fits of equation (5.7). All three OSL trap regions within 40 to 220 °C contribute to the intensity.

Following in turn irradiation to 10, 50 and 70 Gy, the sample was each time preheated to 95 °C and the OSL was recorded from 95 to 145 °C. The preheating was to ensure depletion of the source traps within 40 to 90 °C prior to optical stimulation and measurement. Figure 5.11 shows the plot of OSL intensity measured from 95 to 145 °C for the various doses. The data has been fitted with equation (5.7) to compute for E_a, ΔE and C. The parameter r^2 from the fits are 0.983,

0.982 and 0.996 for the respective doses. The values of E_a are 0.10 ± 0.01, 0.20 ± 0.01 and 0.19 ± 0.01 eV for irradiation to 10, 50 and 70 Gy respectively. The figures for sample irradiated to 50 and 70 Gy are comparable but that obtained for 10 Gy is comparatively lower. The parameter ΔE was computed as 0.69 ± 0.01, 0.71 ± 0.01 and 0.72 ± 0.01 eV for the respective doses. These values are consistent and the average is approximately 0.71 eV. This result suggests that the recombination pathway is the same for all doses. The values of the constant *C* from the fits are 5.3×10^7, 2.9×10^8 and 3.9×10^8 for the respective doses.

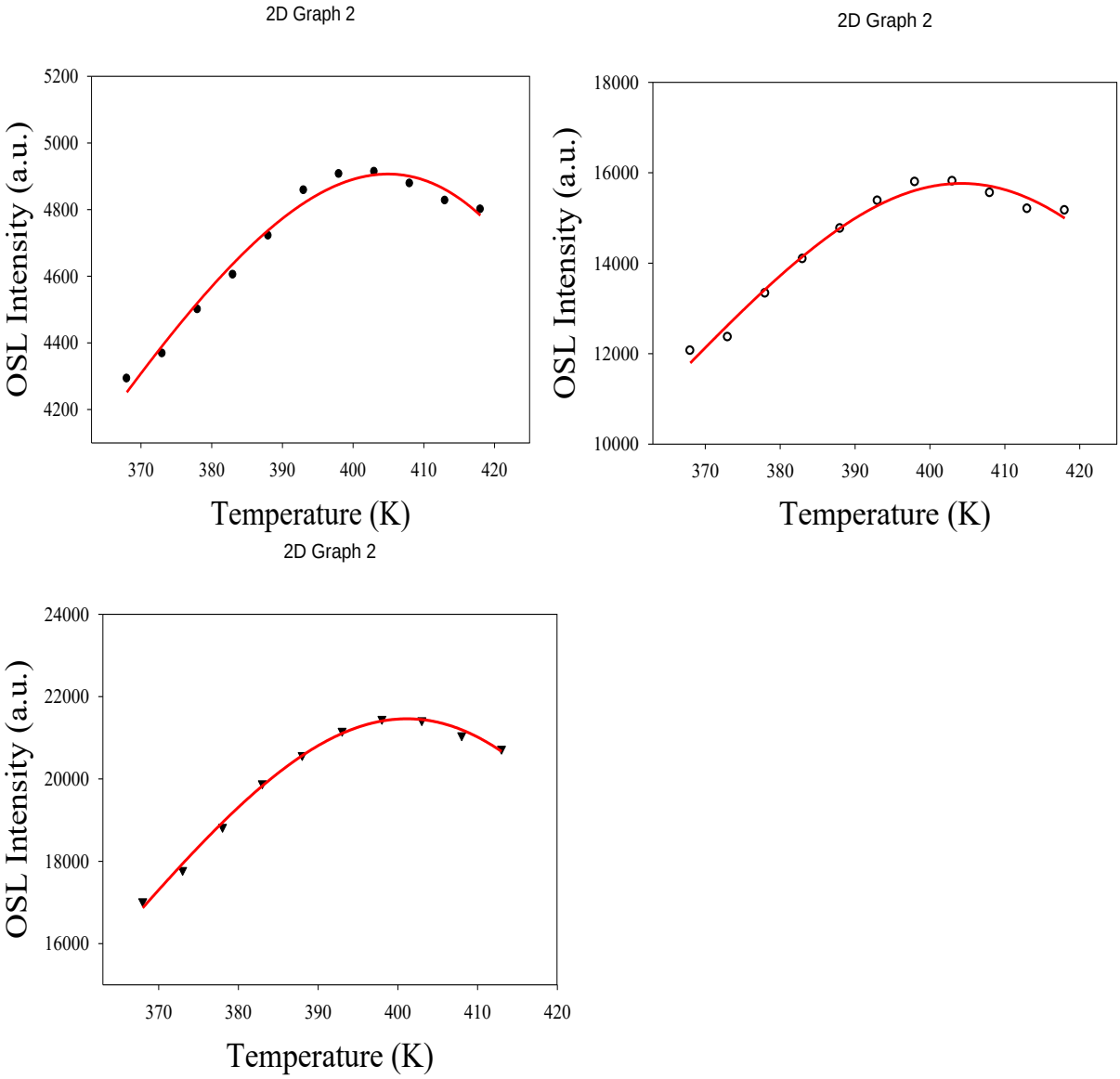

Figure 5.11: OSL intensity measured at variable temperatures from 95 to 145 °C corresponding to 10 Gy (a), 50 Gy (b) and 70 Gy (c). Each data point represents the area under the OSL decay curve. The solid lines are the best fits of equation (5.7). The source traps contributing to the luminescence are within 110 to 220 °C.

The experimental procedure was repeated but the preheat temperature this time was 145 °C and the OSL measurement temperature ranged from 145 to 195 °C. The active luminescence traps are hence within 160 to 220 °C. Figure 5.12 shows the plot of OSL intensity measured from 145 to 195 °C for sample irradiated in turn to 10, 50 and 70 Gy. From the fits of equation 5.7, the

activation energy of thermal assistance E_a gave 0.22 ± 0.01 eV for irradiation to both 10 and 50 Gy, and 0.26 ± 0.01 eV for irradiation to 70 Gy. These values are consistent with dose. The average of E_a is about 0.23 eV. The activation energy of thermal quenching ΔE is 1.04 ± 0.03, 1.08 ± 0.01 and 1.081 ± 0.003 eV for the respective doses and these values agree. The mean of ΔE was computed as 1.07 eV. The constant C are 2.7×10^{11}, 9.8×10^{11} and 1.6×10^{12} for the respective doses and these are also consistent. All the parameters are each consistent for all doses. The values of r^2 from the fits are 0.979, 0.932 and 0.953 for the respective doses. The figure for ΔE is comparable to that reported by Chithambo and Folley [7] as 1.10 ± 0.08 eV for the TL peak III.

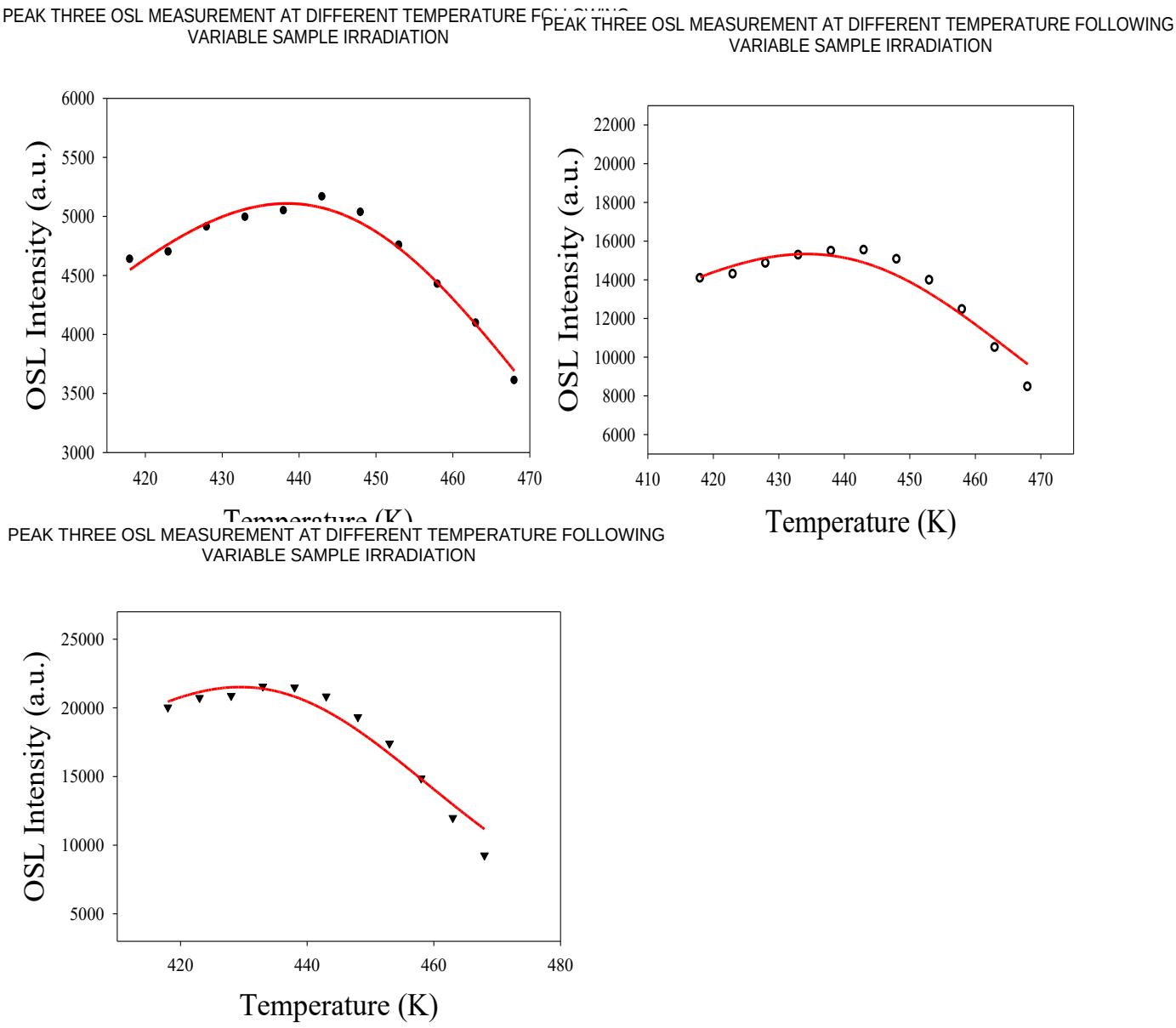

Figure 5.12: OSL intensity recorded at variable temperatures from 145 to 195 °C corresponding to 10 Gy (a), 50 Gy (b) and 70 Gy (c). Each data point represents the area under the OSL decay curve. The solid lines are the best fits of equation (5.7). The OSL source traps are within 160 to 220 °C.

5.5 Optically induced fading of TL peaks

The influence of light exposure on trapped charges following sample irradiation determines the stability of the electron traps to illumination. The OSL measurements in the previous section

suggest that all the TL peaks are susceptible to optical stimulation. In this section, the optically induced fading of all the TL peaks is investigated by measuring the TL following sample irradiation and optical stimulation for variable time intervals. The sample was irradiated to 50 Gy and the OSL was recorded at 20 °C for 10 s after which the TL was measured at a heating rate of 1 °C s^{-1}. The whole procedure was repeated but the duration of OSL measurement was varied up to 800 s. The area under the TL glow curve was integrated to represent the residual TL intensity. Figure 5.13 shows the plot of TL intensity against the OSL measurement duration. The intensity decreases for all the peaks as expected. Peak I however shows about 92% intensity loss within the first 200 s as compared to 16% intensity loss for peaks II and III each. By 800 s, only 3% of peak I intensity remains while that of peaks II and III are 47 and 57% respectively. Peak I is affected most by optical fading. All the peaks have been fitted with an empirical exponential decay equation

$$I(t) = a + I_0 exp^{-\lambda t} \tag{5.8}$$

where I is luminescence intensity at time t, a is a constant, I_0 is initial intensity and λ is the decay constant. The values of the decay constant λ from the fits are 1.8×10^{-2}, 1.0×10^{-3} and 1.01×10^{-3} for peaks I-III respectively which further confirms that peak I fades faster than peaks II and III.

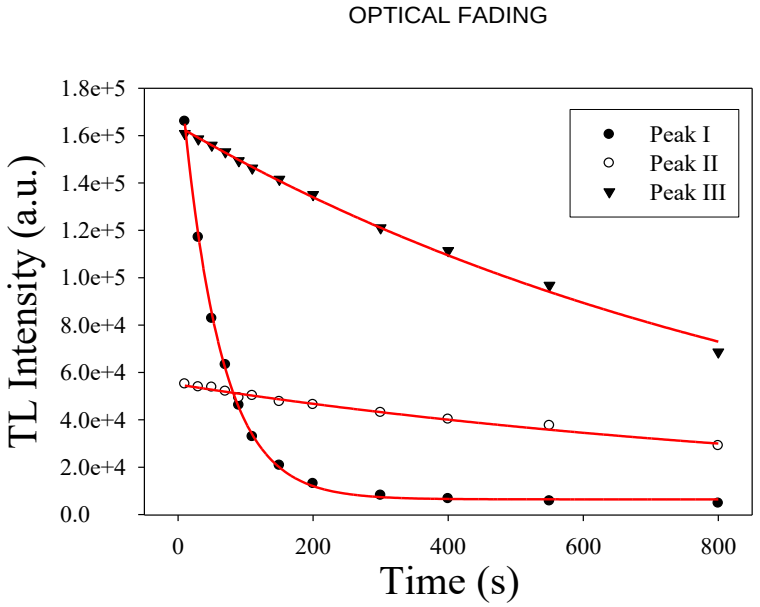

Figure 5.13: TL intensity dependence on duration of optical illumination. The intensity represents the area under the TL peaks I-III. The solid lines are the best fits of equation (5.8). Peak I is most susceptible to optical exposure.

5.6 Conclusion

The effect of variable temperatures and doses on optically stimulated luminescence (OSL) of tanzanite has been analysed. Comparison of 34 consecutive OSL measurement at room temperature to those measured at increasing temperatures shows that thermal assistance and quenching of luminescence signal are present. The source traps of the OSL occur within temperature ranges of 40 to 90 °C, 110 to 145 °C and 160 to 220 °C, and these are noted to be the same as those associated with the TL peaks I (74 °C), II (138 °C), and III (186 °C) respectively. The dose response for all three active traps, or those within 110 to 220 °C, or those within 160 to 220 °C only shows a sublinear response. The computed values of E_a and ΔE for the OSL from all the source traps, recorded from 30 to 80 °C are each comparable for all doses (10, 50 and 70 Gy) and are averagely estimated as 0.15 and 0.81 eV respectively. For the OSL from traps within 110 to 220 °C, recorded from 95 to 145 °C, ΔE is comparable for all doses, averaging 0.71 eV. The parameter E_a is comparable for 50 and 70 Gy irradiation and the mean value is 0.195 eV but that for 10 Gy, evaluated as 0.10 ± 0.01 eV is comparatively lower. The average values of ΔE for all the source traps and for those within 110 to 220 °C are comparable which suggest that the recombination site for the OSL mechanism in both procedures is the same. The parameters E_a and ΔE are each comparable for the OSL from traps 160 to 220 °C, recorded from 145 to 195 °C for all doses and are averagely estimated as 0.23 and 1.07 eV respectively. This implies that the recombination site for traps within 160 to 220 °C is different from those within 40 to 220 °C and 110 to 220 °C. Optically induced fading analysis shows that the TL peak I is most susceptible to illumination by 470 nm blue LEDs.

Chapter 6

Phototransferred thermoluminescence (PTTL)

This chapter presents the results from the phototransferred thermoluminescence (PTTL) analysis of tanzanite. The findings on the optically stimulated luminescence (OSL) measurements in chapter 5 indicate that tanzanite is sensitive to optical stimulation of luminescence. This means that tanzanite can produce PTTL. The PTTL analysis in this chapter seeks to investigate how electrons from traps can be transferred to other traps under optical stimulation by 470 nm blue LEDs. The glow curve features corresponding to a high irradiation dose (150 Gy) are first presented, followed by the glow curve characteristics from the PTTL measurements. The kinetic order and the dose response of the PTTL peaks have also been analysed and compared with those of the conventional TL peaks. The final part presents the PTTL time response profiles, and thermal quenching analysis of the PTTL signal.

6.1 Introduction

Phototransferred thermoluminescence mechanism describes the transfer of electrons from stable deep traps to empty shallow traps by means of optical stimulation [43]. In the literature, only one work on the PTTL of tanzanite has been reported, namely, by Chithambo [8]. In that work, peak I (at 86 °C) was noted to reappear under phototransfer when the sample was irradiated to 120 Gy and preheated to remove either peak I only or both peaks I and II. Blue LEDs were used as the stimulation source and the TL was recorded at 1 °C s^{-1}. The donors (peaks II and III) were each observed to comprise of multiple collocated peaks. This finding is of relevance to our study, as we will demonstrate later. The PTTL mechanism of tanzanite was ascribed to a system of one acceptor and multiple donors. The phenomenological model of Chithambo et al. [51], imposed to describe the PTTL response with illumination time is of great utility here since the experimental result dictates the number of acceptor and donor traps. This model has been used to describe the PTTL intensity dependence on illumination time for tanzanite [8], quartz [54], CaF_2 [55] and α-

Al_2O_3:C [51]. The theoretical framework of the phenomenological model has been elaborated in chapter 2.

The focus of this chapter is to study the mechanism of PTTL in tanzanite. The PTTL intensity dependence on illumination time has been examined with the phenomenological model of Chithambo et al. [51]. The results from optical stimulation of very deep electron traps (those occurring after 500 °C) intended to cause transfer of charges to shallow empty ones have been reported as well.

6.2 Glow curve features

The sample was preheated to 500 °C to clear the background signal. Irradiation to 150 Gy preceded the measurement of the TL signal at 1 °C s^{-1}. The high dose was to ensure sufficient trap population leading to sufficient electron transfer from deep traps to shallow ones. Figure 6.1 shows the TL glow curve corresponding to 150 Gy. There are three noticeable peaks at positions 74, 136 and 186 °C. The peaks are referenced as I-III respectively. Thermal cleaning procedure [1], as detailed in section 2.3.1 did not show any other peaks. Four additional TL measurements gave the average peak positions as 74, 137.2 ± 1.1 and 187.2 ± 1.1 for peaks I-III. The percentage difference of the maximum and minimum intensity is less than 1% for each peak. The peaks are therefore reproducible.

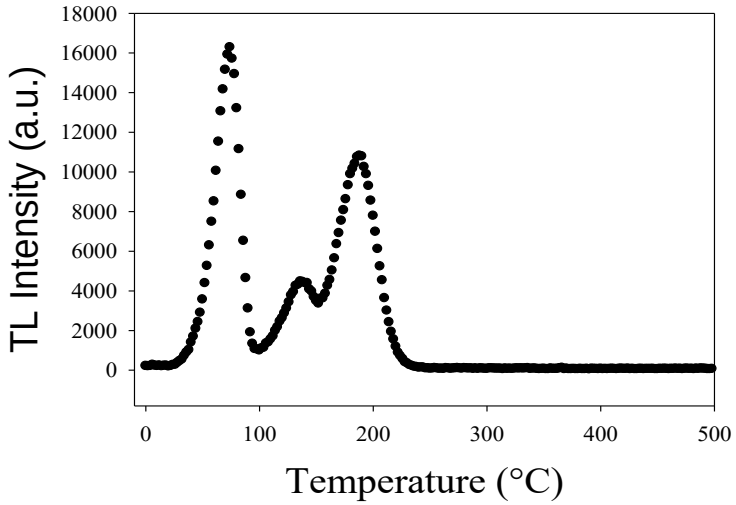

Figure 6.1: A TL glow curve of tanzanite recorded at 1 °C s^{-1} following 150 Gy irradiation. Three peaks occur at 74, 136 and 186 °C.

6.3 Glow curve features from PTTL measurement

The sample was first irradiated to 150 Gy followed by preheating to 158 °C, optical exposure for 120 s and finally heating to 500 °C to record the TL glow curve. Preheating to 158 °C was to depopulate the electron traps for both peaks I and II. Figure 6.2(a) shows the measured TL glow curve on a semi-log scale to aid in visual clarity. Only peak I reappears with a low intensity under phototransfer. When the duration of the optical stimulation was extended to 3000 s, peak II was reproduced under phototransfer. The PTTL peak II is shown in Figure 6.2(b). Peak II was not visually spotted under phototransfer for illumination period of 120 s because the high intensity peak III and the low PTTL peak II were collocated. It is only when the intensity of peak III has reduced following a longer illumination period, of about 3000 s, that the PTTL peak II is seen. No PTTL was observed when the preheat temperature was changed to 100 °C to remove only peak I. Moreover, when preheated to 500 °C to analyse electron transport from very deep traps to shallow traps, no PTTL peak was observed. Chithambo [8] reported three TL peaks at 86, 160 and 320 °C (peaks I-III) of which only peak I was reproduced under phototransfer for an irradiation dose of 120 Gy, illumination time of 200 s and preheat temperature of either 120 or 230 °C. The observation of peak II under phototransfer in this work is an important finding that illustrates how the illumination period can influence the observed PTTL mechanism.

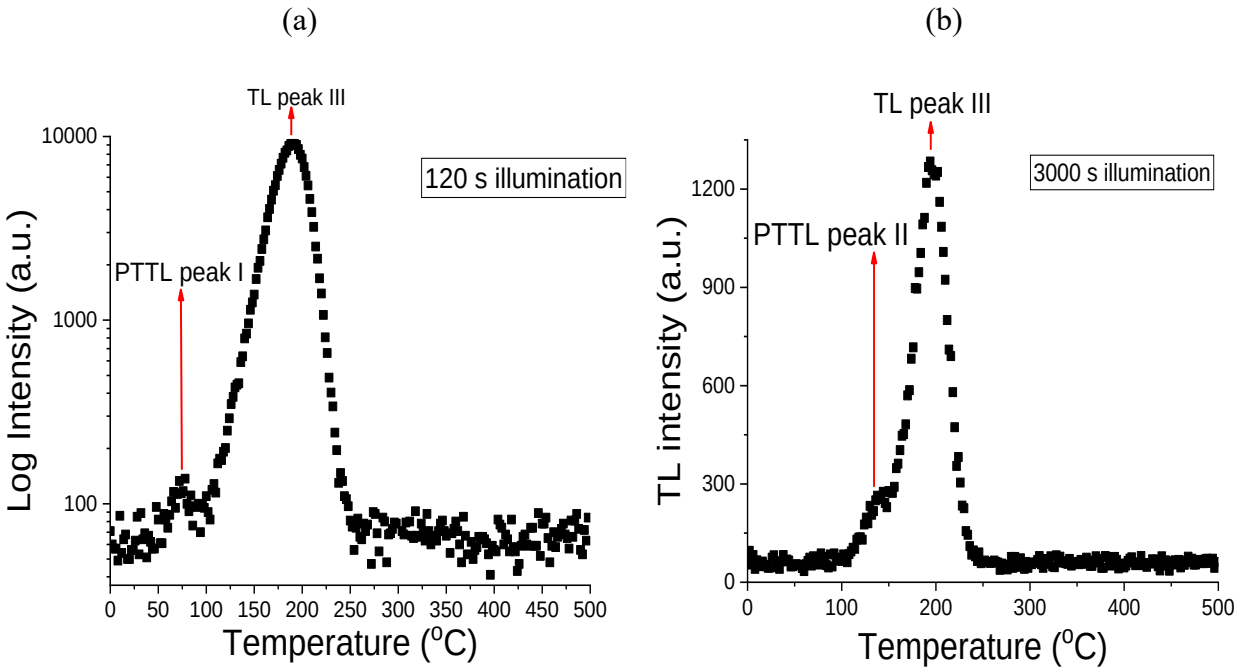

Figure 6.2: A TL glow curve of tanzanite recorded at 1 °C s^{-1} following irradiation to 150 Gy, preheating to 158 °C and illumination period of 120 s showing that the TL peak I reappears under phototransfer (a). For illumination period of 3000 s, the TL peak II reappears under phototransfer (b).

6.4 Pulse annealing procedure

Pulse annealing [74, 75] was carried out to identify which of the traps play the roles of donors and acceptors. This procedure is primary conducted to gain insight into the ways in which the various traps contribute to the PTTL mechanism. A dose of 150 Gy was administered to the sample followed by preheating to 20 °C, illumination for 100 s and then TL measurement at 1 °C s^{-1}. The procedure was iterated while varying the preheat temperature at 10 °C intervals up to 240 °C. The TL intensity was computed from the area under the peaks at each preheat. Figure 6.3 shows the plot of the TL intensity for peaks I-III against the preheating temperature. Peak I decreases sharply between 40 to 100 °C. This is attributed to the detrapping of electrons due to preheating. The intensity following 100 °C, although not high, decreases slowly and consistently. These intensities are due to electrons transferred from donor traps yet to be identified, to acceptor traps (peak I). The intensity of peak II within 100 to 150 °C decreases consistently while that of

peak III remains stable. Hence, peak II act as a donor to peak I within preheat temperature of 100 to 150 °C. Following 150 to 200 °C, the intensities of peaks I and II are due to electrons transferred from the donor traps of peak III to acceptor traps of peaks I and II since both peaks are removed by preheating to 150 °C prior to optical stimulation. The pulse annealing procedure indicates that peak III plays the role of a donor whereas peaks I and II act as acceptors within preheat temperature range of 150 to 200 °C. Also, peak II acts as a donor to peak I at preheat temperatures below 100 °C. Hence, peaks I and II are acceptors whereas peak III is a donor in the PTTL mechanism.

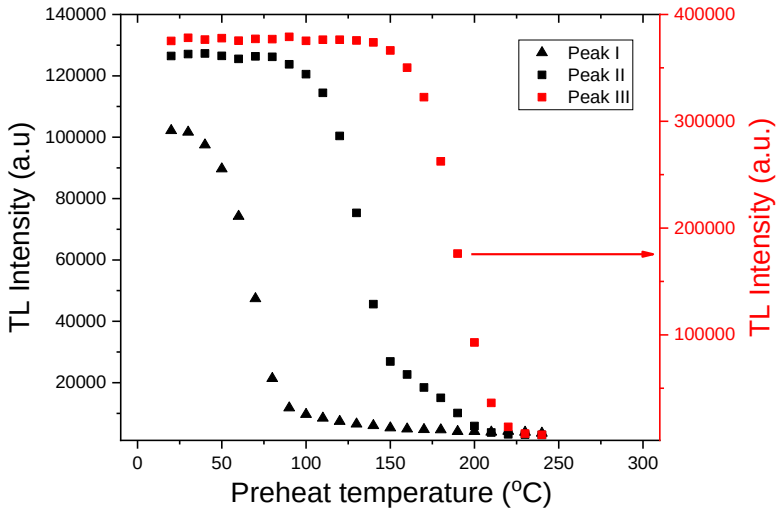

Figure 6.3: The variation in TL intensity of peaks I-III with preheating temperature during a pulse annealing procedure.

6.5 Dose response of PTTL peaks

The PTTL intensity response to varying doses ranging from 10 to 240 Gy has been analysed. For the PTTL peak I intensity measurement, the sample was irradiated, preheated to 158 °C, illuminated for 120 s and then heated to 500 °C to measure the PTTL signal. The area beneath the glow peak was used to quantify the intensity. Figure 6.4(a) is a plot of the PTTL peak I intensity against dose. The intensity shows a steady rise in correlation with the dose. The data is best fitted with the empirical function

$$y(D) = aD^b \tag{6.1}$$

where y is the PTTL intensity, D is dose and a, b are constants.

For the PTTL peak II, the measurement procedure remained the same, but the duration of optical illumination was 3000 s. The plot in Figure 6.4(b) illustrates how the PTTL peak II intensity changes in response to the dose. A consistent trend of increasing intensity is observed as the dose increases. The data is best fitted with a linear function given as

$$y(D) = mD + c \tag{6.2}$$

where m and c are constants, and all other symbols retain their previous definitions.

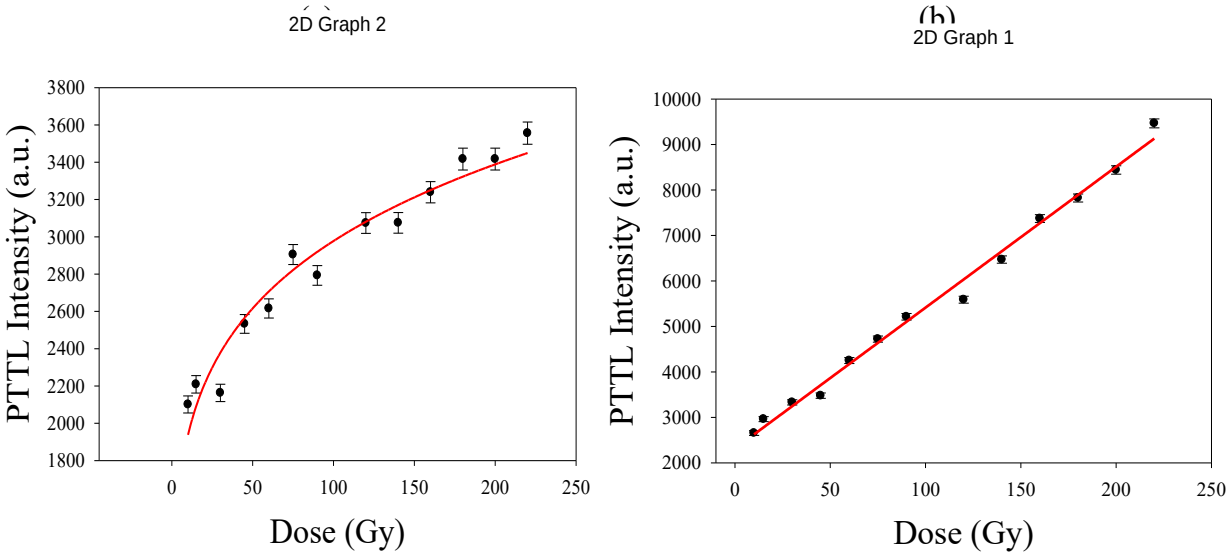

Figure 6.4: Variation of PTTL peak I intensity on dose (a), and PTTL peak II intensity on dose (b). The error bars for the individual data points are derived from the square root of the intensity since photon counts are random events. The continuous lines represent the fits of equations (6.1) and (6.2) respectively.

Qualitative analysis of the dose response with the supralinearity index function $f(D)$ expressed in equation (4.2) has been conducted and the plots are shown in Figure (6.5) for the respective PTTL peaks. The function $f(D) < 1$ in both plots signifying a sublinear dose response [69]. A similar result was seen for the conventional peaks I and II.

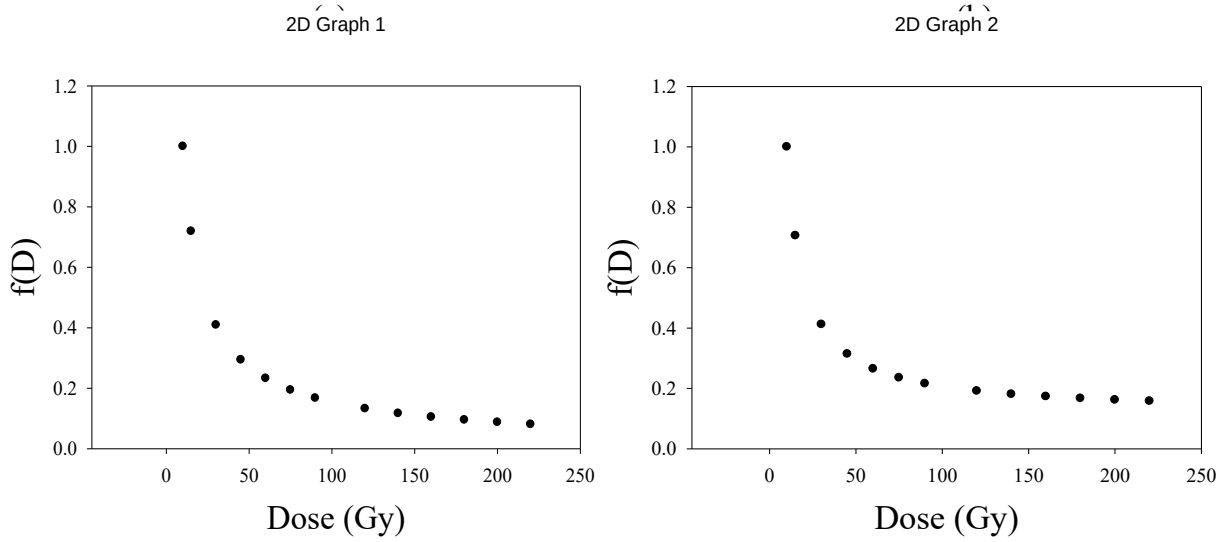

Figure 6.5: Plot of $f(D)$ against dose for PTTL peak I (a) and peak II (b). The dose response is sublinear for each PTTL peak as indicated by the inequality $f(D) < 1$.

6.6 Analysis for order of kinetics

The order of kinetics for the PTTL peaks I and II has been determined by assessing the peak position dependence on dose (T_m – dose) and on partial heating ($T_m - T_{stop}$).

6.6.1 Peak position (T_m) dependence on dose

The experimental procedure used for the dose response analysis was carried out three times after which the PTTL peak positions were extracted. Nevertheless, the dose range was extended to 300 Gy. Figure 6.6 shows the positions of the PTTL peaks I and II at the various doses. Each data is an average of the three measurements and the error bars represent the standard deviations. The variable doses do not produce any systematic shifts in the peak positions. The mean values of T_m are 74.5 ± 2.8 and 141.0 ± 3.3 °C for PTTL peaks I and II respectively. The PTTL peaks are characterized by first order kinetics since T_m does not vary systematically with dose [1]. Moreover, the PTTL peak positions are consistent with the conventional TL peaks I and II, as presented in section 4.3.1, which were evaluated as 73.3 ± 1.0 and 137.6 ± 2.7 °C.

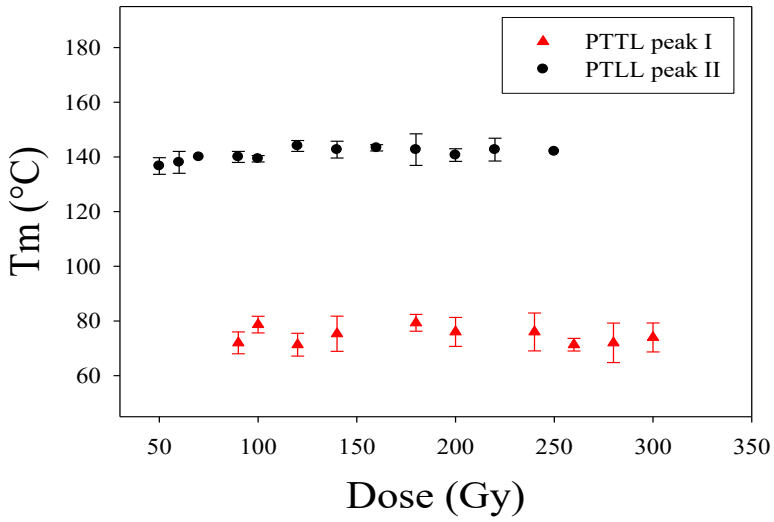

Figure 6.6: Peak position T_m dependence on dose for PTTL peaks I and II. The position of each PTTL peak is stable with dose. Each data point is the mean of three measurements and the error bars are the standard deviations.

6.6.2 Peak position dependence on partial heating ($T_m - T_{stop}$)

The sample was irradiated to 150 Gy, preheated to 158 °C, illuminated for 120 s, preheated in turn from 20 to 60 °C followed by TL measurement at 1 °C s^{-1} after each preheat (T_{stop}). The measurements were conducted three times and the average position of PTTL peak I was determined. That of PTTL peak II was recorded for an illumination period of 3000 s and at preheat temperatures from 100 to 130 °C. The plot of T_m against T_{stop} for the respective PTTL peaks are shown in Figure 6.7. No systematic variation of T_m on T_{stop} is observed for each PTTL peak, and the average positions are 75.5 ± 4.2 and 141 ± 3.0 °C. The stability of T_m with T_{stop} for the PTTL peaks is indicative of first order kinetics [1].

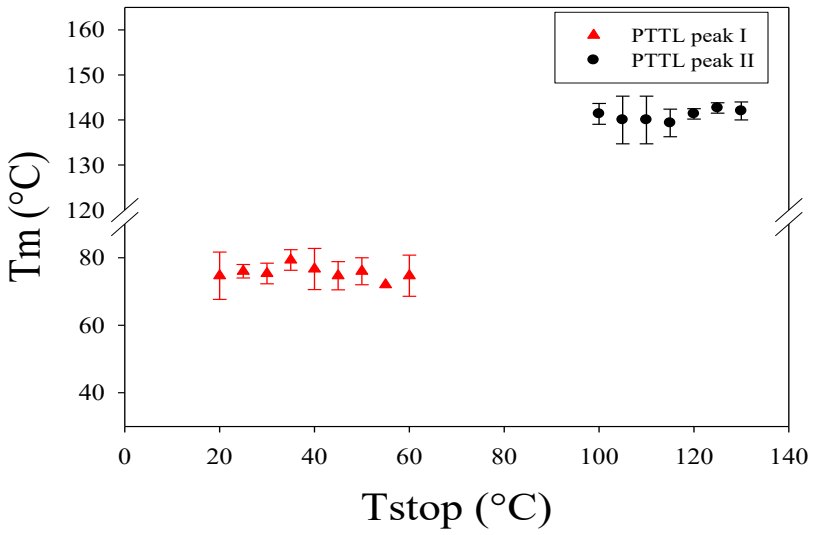

Figure 6.7: Peak position T_m dependence on partial heating ($T_m - T_{stop}$) for PTTL peaks I and II. The PTTL peak positions are stable with partial heating. The average of 3 measurements yielded the value of each data point.

6.7 Fading of PTTL peaks

The reduction in the PTTL signal when thermal stimulation to measure the glow curve is delayed at variable intervals has been analysed. For the PTTL peak I, thermal stimulation was delayed in turn between 0 to 5000 s after the sample was irradiated to 150 Gy, preheated to 158 °C and illuminated for 120 s each time. The TL was measured immediately the delay elapsed. The area under the peaks was integrated to derive the PTTL intensity. Figure 6.8(a) shows the plot of the intensity versus delay for the PTTL peak I. The intensity exhibits a decreasing trend with time. At 5000 s, about 70% of the initial intensity remains. When the delay was extended to a longer duration of 6000 s, the PTTL peak could no longer be observed. Thus, PTTL peak I fades. Fading analysis of the PTTL peak II was carried out for delay between 0 to 10000 s following irradiation to 150 Gy, preheating to 158 °C and illumination for 3000 s each time. The plot in Figure 6.8(b) illustrates the dependence of intensity on delay for the PTTL peak II. A stable intensity is observed with time. The PTTL peak II is hence unaffected by delay and shows no fading. For each data point, the error bar represents the square root of the intensity since the measurements are based on photon counts which are random events.

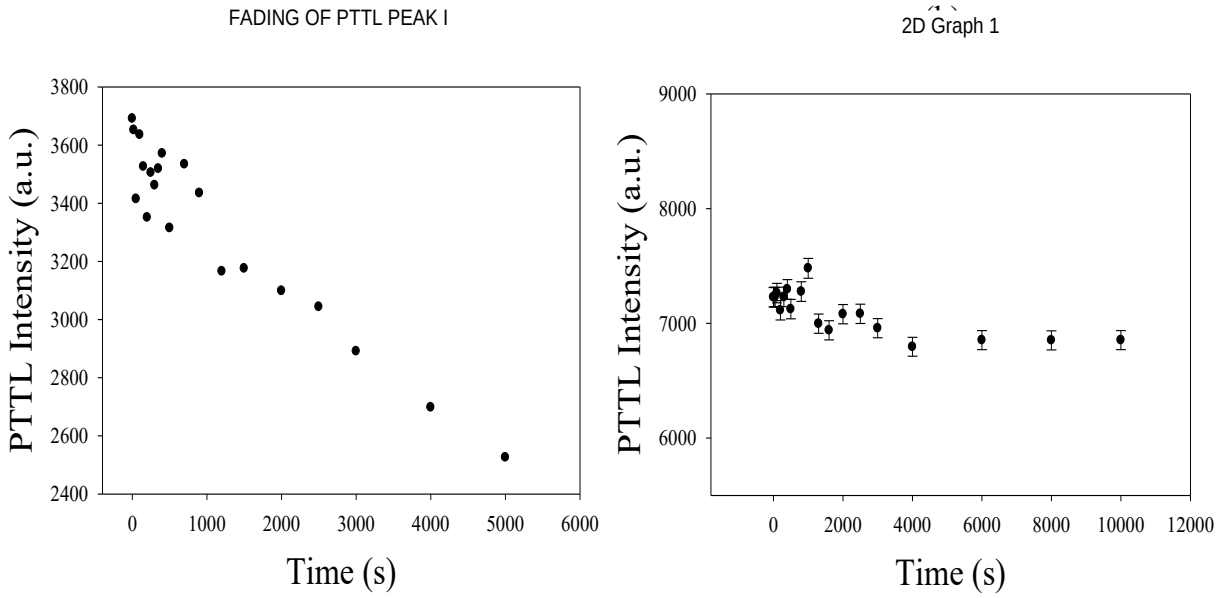

Figure 6.8: Intensity dependence on delay between shallow trap population and readout for PTTL peaks I (a) and II (b). The PTTL peak I fades with time, whereas PTTL peak II is stable.

6.8 PTTL intensity dependence on illumination period

The change in the PTTL intensity with varying illumination periods is of interest in this section. A mathematical model that suitably describes the PTTL intensity variation in response to the duration of illumination has been presented.

6.8.1 PTTL following preheating to remove peaks I and II

The sample was illuminated in turn for variable periods between 5 to 9000 s following irradiation to 150 Gy and preheating to 158 °C each time. The TL was recorded after each illumination. Figure 6.9(a) shows a plot of the intensity for the PTTL peak I against the illumination time. The intensity increases to a maximum at 120 s. The increase is because within this period (5 to 120 s), the amount of electrons captured into the acceptor traps is significantly higher than those detrapped at the time of illumination [51]. The intensity thereafter reduces to a minimum at 8000 s which implies that electron detrapping is more prominent than trapping within this period. Such behaviour of PTTL intensity increasing to a maximum value within a

short period, followed by a continuous decrease is a common experimental observation (e.g. [8, 53, 54]).

The PTTL intensity for peak II is seen after a longer illumination period from 1500 to 8000 s as shown in Figure 6.9(b). The intensity shows a continuous reduction with time. The intensity of the donor, which is, peak III is shown in Figure 6.9(c). Over time, the intensity declines as a result of electron loss to the acceptor traps of peaks I and II.

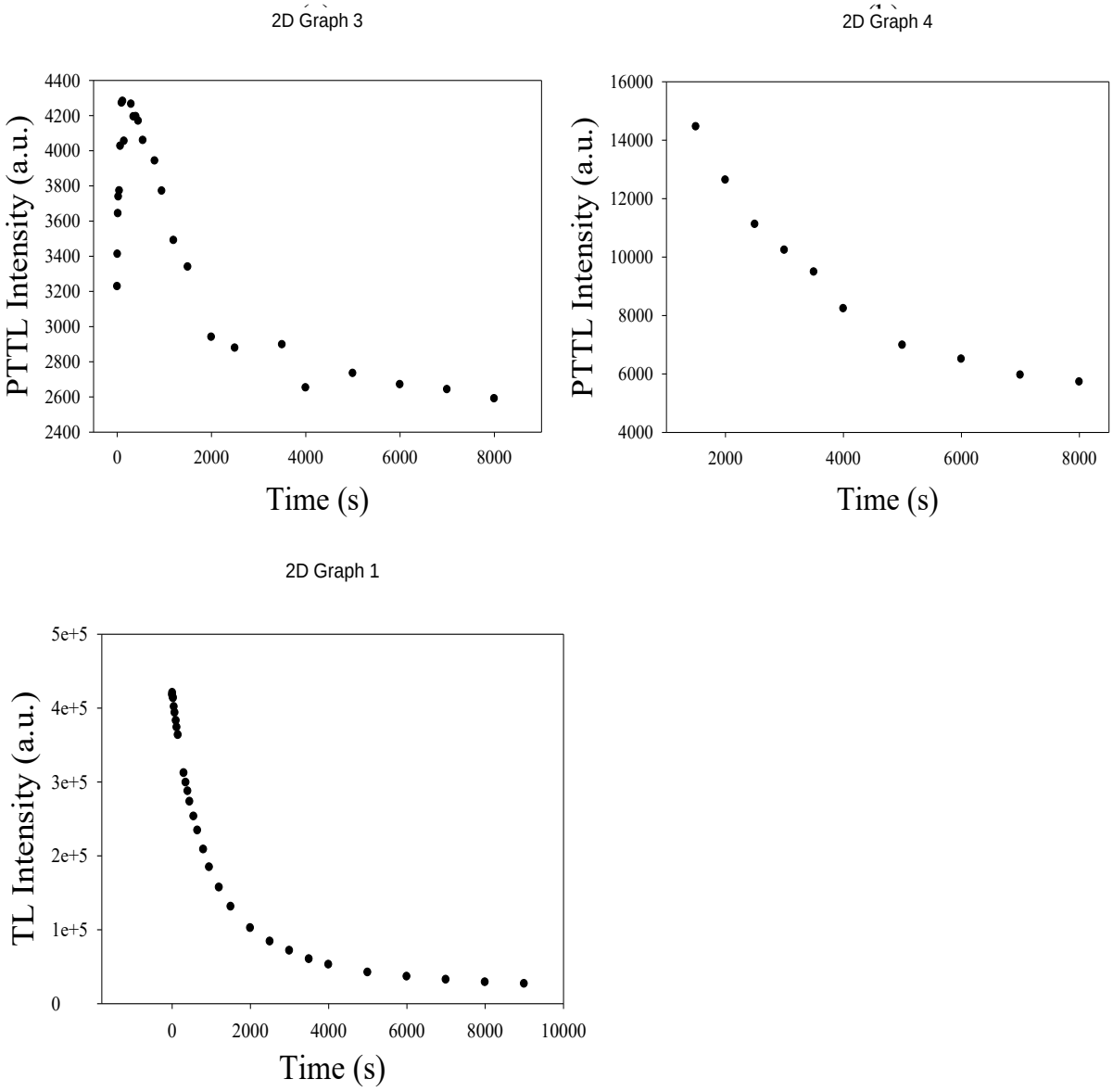

Figure 6.9: Plot of intensity against duration of illumination for PTTL peaks I (a) and II (b), and the changes in the intensity of the donor (peak III) with illumination time (c).

6.8.2 Mathematical model of PTTL intensity dependence on illumination period

The phenomenological model of Chithambo et al. [51] is adopted to elucidate the time response profiles. For this model, a system of linear differential equations is created, and solutions are generated for any number of donors and acceptors. Section 2.6.1.2 provides the theoretical framework of the phenomenological model.

When the sample is preheated to 158 °C, peak III plays the role of a donor while peaks I and II are acceptors. A system of one donor and two acceptors is hence considered. Figure 6.10 shows an energy band diagram for a system consisting of a single donor and two acceptors. The shallow acceptor traps are denoted as I and II. The donor trap is denoted as III and the recombination site is represented as R. Electron concentrations in traps I-III are indicated by n_1, n_2 and n_3 respectively. The parameters f_1, f_2 and f_3 denote the rates of optical stimulation of electrons from the respective traps. Electron recapturing by donor trap is ignored.

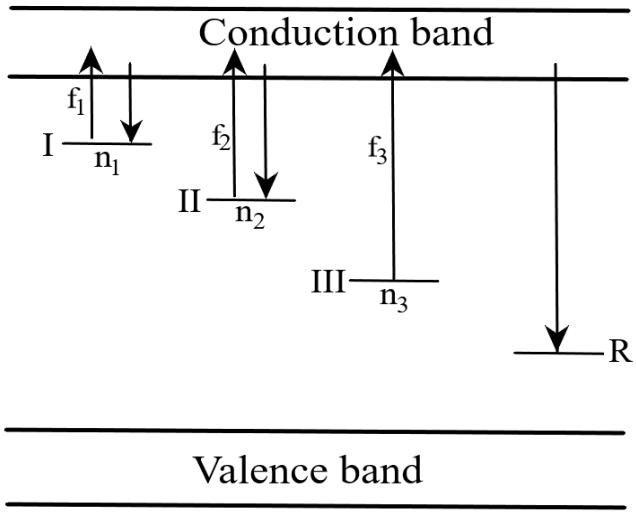

Figure 6.10: An energy level diagram showing the PTTL mechanism for a system of two acceptors (traps I and II) and one donor (trap III). The traps are respectively those of peaks I-III. The arrows indicate the electron transitions. All symbols are defined in the text.

We first analyse the flow of charges from donor trap III to acceptor trap I during the illumination stage. In this context, the focus is on a system with one acceptor and one donor. The set of differential equations for such a system is represented as

$$\frac{dn_3}{dt} = -f_3 n_3 \tag{6.3}$$

$$\frac{dn_1}{dt} = -f_1 n_1 + \varrho_3 f_3 n_3 \tag{6.4}$$

where ϱ_3 is proportionality constant. Equation (6.3) represents electron detrapping from donor trap III into the conduction band. The parameters $f_1 n_1$ in equation (6.4) represent electron detrapping from acceptor trap I, and the term $\varrho_3 f_3 n_3$ is the proportion of charges recaptured at the acceptor trap. The solution to the first-order linear differential equation (6.4) that represents the PTTL is given by

$$n_1 = A_3(e^{-f_3 t} - e^{-f_1 t}) \tag{6.5}$$

where A_3 is a constant expressed as $A_3 = (\varrho_3 f_3 n_{ci})/(f_1 - f_3)$. The parameter n_{ci} denotes the initial concentration of electrons in trap III.

Equation (6.5) however did not give an appropriate fit to the experimental data. A similar finding was reported by Chithambo [8] where the donor peaks, occurring at 160 and 320 °C were each noted to be a collocation of an unknown number of peaks hence a solution in the form of equation (6.5) could not model the experimental time-response profile. The failure was because the donor peaks were each initially considered to consist of a single peak. Peak separation procedures ($T_m - T_{stop}$ and thermal cleaning) were not successful in segregating the individual peaks. The PTTL mechanism in tanzanite is hence considered as a system of one acceptor and multiple imprecise donors [8].

A new set of differential equations is defined to satisfactorily describe the experimental data. The donor traps are increased to three, creating a system of one acceptor and three donors. A system of one acceptor and two donors could not satisfactorily fit the PTTL peak I data either. Figure 6.11 shows an energy level diagram for such a system. The flow of electrons at the illumination stage is governed by the set of differential equations:

$$\frac{dn_3}{dt} = -f_3 n_3 \tag{6.6}$$

$$\frac{dn_4}{dt} = -f_4 n_4 \tag{6.7}$$

$$\frac{dn_5}{dt} = -f_5 n_5 \tag{6.8}$$

$$\frac{dn_1}{dt} = -f_1 n_1 + Б_3 f_3 n_3 + Б_4 f_4 n_4 + Б_5 f_5 n_5 \tag{6.9}$$

where $Б_3$, $Б_4$ and $Б_5$ are proportionality constants. Electron detrapping from donor traps III-V is represented by equations (6.6) to (6.8) respectively. The term $f_1 n_1$ in equation (6.9) describes the liberation of electrons from acceptor trap I and the remaining parameters represents electron recapture. The solution to the first-order linear differential equation (6.9) is given as

$$n_1 = B_1(e^{-f_3 t} - e^{-f_1 t}) + B_2(e^{-f_4 t} - e^{-f_1 t}) + B_3(e^{-f_5 t} - e^{-f_1 t}) \tag{6.10}$$

where B_1, B_2 and B_3 are constants respectively expressed as $(Б_3 f_3 n_{ai})/(f_1 - f_3)$, $(Б_4 f_4 n_{bi})/(f_1 - f_4)$ and $(Б_5 f_5 n_{ci})/(f_1 - f_5)$. The symbols n_{ai}, n_{bi} and n_{ci} are the initial concentrations of electrons at the respective donor traps. The mathematical methods followed to arrive at equation (6.10) are detailed in section 2.6.1.2. The experimental data for the PTTL peak I has been satisfactorily fitted with equation (6.10) and the plot is shown in Figure 6.12(a). The photoionization cross section (σ) which determines a trap's stability under optical excitation has been calculated from the relation $\sigma = f_1/\Phi$ [43], where Φ is the light intensity and its value is 9.5×10^{16} cm^{-2} s^{-1} for blue LEDs operated at 90% of its power [5]. The parameter σ was evaluated as 1.3×10^{-19} cm^2 for the PTTL peak I. This is the first time σ for the PTTL peak I is being reported for tanzanite. When the number of donors were increased beyond three, the error margins of the parameters were very high, making them unreliable for consideration.

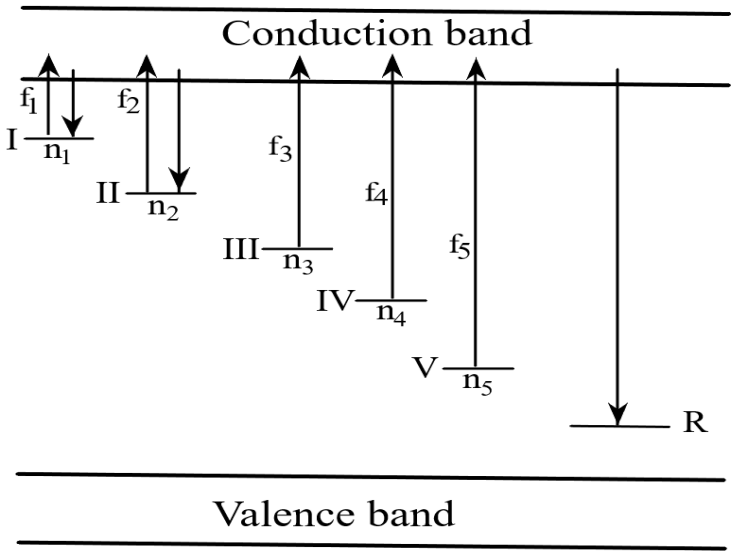

Figure 6.11: An energy level diagram illustrating the PTTL mechanism for a system of two acceptors (I and II) and three donors (III-V). The donor traps III-V are aggregated into a single broad peak.

We now consider the case where trap II is the acceptor and traps III-V remain donors. The differential equations governing the transfer of charges during optical excitation can be represented as follows:

$$\frac{dn_3}{dt} = -f_3 n_3 \tag{6.11}$$

$$\frac{dn_4}{dt} = -f_4 n_4 \tag{6.12}$$

$$\frac{dn_5}{dt} = -f_5 n_5 \tag{6.13}$$

$$\frac{dn_2}{dt} = -f_2 n_2 + \alpha_3 f_3 n_3 + \alpha_4 f_4 n_4 + \alpha_5 f_5 n_5 \tag{6.14}$$

where α_3, α_4 and α_5 are constants of proportionality and all other parameters retain their previous definitions. The solution for the PTTL at peak II can hence be written as

$$n_2 = D_1(e^{-f_3 t} - e^{-f_2 t}) + D_2(e^{-f_4 t} - e^{-f_2 t}) + D_3(e^{-f_5 t} - e^{-f_2 t}) \tag{6.15}$$

where D_1, D_2 and D_3 are constants respectively expressed as $(\alpha_3 f_3 n_{ai})/(f_2 - f_3)$, $(\alpha_4 f_4 n_{bi})/(f_2 - f_4)$ and $(\alpha_5 f_5 n_{ci})/(f_2 - f_5)$. The fit of equation (6.15) for the PTTL peak II is shown in Figure 6.12(b). The photoionization cross section for the PTTL peak II was evaluated as 2.8×10^{-18} cm^2.

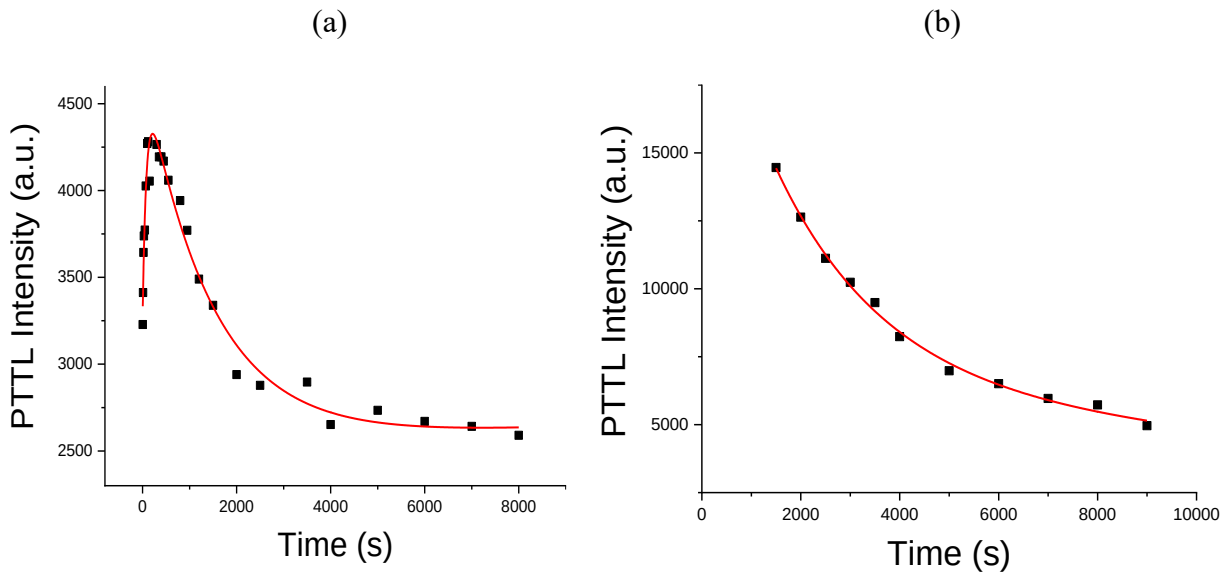

Figure 6.12: Plot of intensity against duration of illumination for PTTL peaks I (a) and II (b). The solid lines are respectively the fits of equations (6.10) and (6.15).

6.9 Effect of illumination temperature on PTTL signal

The variation in the PTTL intensity as a function of the optical stimulation temperature has been studied for both PTTL peaks I and II. The stimulation temperature during illumination determines the amount of electrons available in the conduction band that can take part in the PTTL process [76, 77]. The primary goal is to investigate the temperature assisted increase (thermal assistance) and decrease (thermal quenching) in PTTL intensity. The influence of thermal assistance becomes apparent in measurements where intensity levels recorded at elevated temperatures are higher than those measured at room temperature. On the other hand, the intensity measured at higher temperatures is diminished in comparison to those recorded at room temperature due to thermal quenching.

The irradiated sample was preheated to remove peaks I and II followed by illumination at 25 °C for 120 s. The PTTL signal for peak I was recorded afterwards by heating to 500 °C. The illumination temperature was varied for subsequent measurements up to 90 °C. The recorded PTTL intensity was however noted to reduce to background levels from 40 to 90 °C. Moreover, the intensity from 25 to 40 °C reduced continuously. The intensity loss is as a result of thermal quenching.

The duration of optical stimulation was extended to 3000 s to analyse the temperature effect on the PTTL peak II. The illumination temperature ranged from 25 to 120 °C this time. The plot of the intensity against the illumination temperature is shown in Figure 6.13. A continuous decline in intensity is generally observed as the temperature increases due to thermal quenching.

In PTTL measurements, thermal quenching is typically noticeable at temperatures farther away from room temperature, in contrast to thermal assistance which is observed close to room temperature (e.g. [55, 76]) but this is not the case for the PTTL peaks I and II. The intensities closer to room temperature are quenched. The OSL measurement at different temperatures in chapter 5 revealed both thermal assistance and quenching of luminescence signal. However, this is not the case for optical stimulation at different temperatures in the PTTL measurements made. Only thermal quenching is consistently observed. The reason for this is that as the illumination temperature increases, the number of electrons detrapped from the donor (peak III) into the conduction band although increases, the number of electrons detrapped from the acceptors (peaks I and II) also increases significantly hence the continuous decrease in the PTTL intensities. The number of electrons transitioned to the acceptors due to thermal assistance is very small to circumvent against the loss. This implies that a sufficient amount of electrons greater than those trapped at the acceptors is required to observe any appreciable increase in luminescence signal due to thermal assistance. The thermal quenching mechanism has been elaborated in section 2.4 using the Mott-Seitz configurational coordinate model.

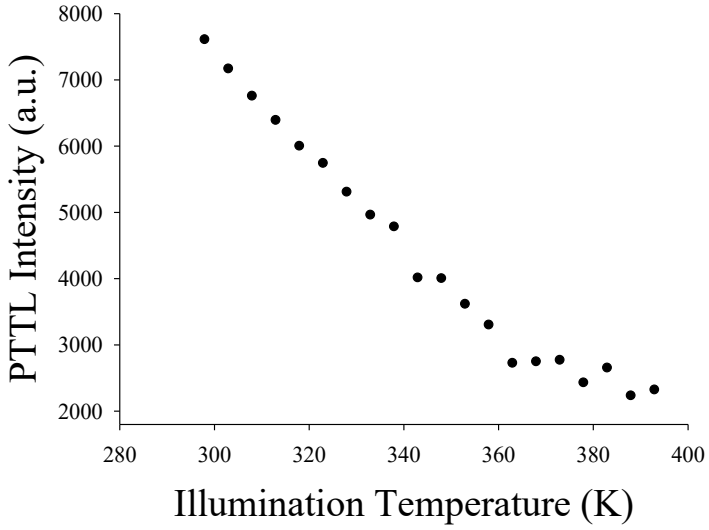

Figure 6.13: A plot of intensity against illumination temperature for PTTL peak II. The intensity reduces continuously with time.

6.10 Conclusion

The phototransferred thermoluminescence (PTTL) mechanism of tanzanite has been studied. For a dose of 150 Gy, the thermoluminescence (TL) signal recorded at 1 °C s^{-1} shows a prominent peak at 74 °C and two other peaks at 136 and 186 °C referenced respectively as peaks I-III. Peaks I and II reappear under phototransfer caused by 470 nm blue LEDs. No PTTL peak was seen when electron transfer from very deep traps (those occurring after 500 °C) to empty traps was analysed. The PTTL peaks I and II are of first order kinetics. The response of the intensity at variable doses from 10 to 240 Gy is qualitatively sublinear for both PTTL peaks I and II. Fading of the luminescence signal for the PTTL peak I occurs between shallow trap population and readout whereas that of PTTL peak II is stable. The PTTL intensity variation in response to the duration of optical exposure has been modelled using sets of first-order linear differential equations. The fits of the solutions to the differential equations suggest that the mechanism of phototransfer involves a system of one acceptor and three donors. The photoionization cross section was computed as 1.3×10^{-19} cm^2 for the PTTL peak I and 2.8×10^{-18} cm^2 for the PTTL peak II. The PTTL signals are quenched from the relation between the illumination temperature and the PTTL intensity.

Chapter 7

Conclusions and suggestions for future work

This work has focused on the thermoluminescence and phototransferred thermoluminescence dynamics in tanzanite. The summary of the main findings is presented in this section. The latter part outlines some recommendations for future areas of study.

7.1 Conclusions

A TL glow curve corresponding to 70 Gy and recorded at 1 °C s^{-1} displayed a prominent peak at 74 °C (peak I) and two others at 138 °C (peak II) and at 186 °C (peak III). First order kinetics features were evident for all the peaks, with their positions showing no variation with changes in either dose or partial heating ($T_m - T_{stop}$). The response of the TL intensity of each peak with dose is qualitatively sublinear as determined from the supralinearity index analysis. The intensity of peak I reduced when stimulation was delayed following irradiation whereas peaks II and III remained stable. Peak I exhibited thermal fading at room temperature hence associated with shallow electron traps unlike peaks II and III which are deep electron traps. The activation energy for the respective peaks is approximately 0.84, 1.00 and 1.19 eV. The kinetic parameter activation energy of thermal quenching was calculated as 0.36 ± 0.08, 0.72 ± 0.10 and 1.62 ± 0.12 eV for peaks I-III respectively. These values imply that the peaks have distinct recombination sites.

OSL measurements at different temperatures have been utilized to compute the kinetic parameters activation energy of thermal assistance (E_a) and quenching (ΔE). The value of the parameter E_a for all the source traps (within 40 to 220 °C) is consistent, as it does not depend on variable irradiation to 10, 50 or 70 Gy. The activation energy of thermal quenching is also consistent with dose (10, 50 and 70 Gy). Also, for the source traps within 110 to 220 °C, ΔE is comparable to that from all the source traps. This implies that the recombination site for the OSL mechanism for the two trap regions (40 to 220 °C and 110 to 220 °C) is the same. For source

traps within 160 to 200 °C, ΔE and E_a are each comparable with dose (10, 50 and 70 Gy) but higher than those of the other traps. This important finding indicates that the recombination sites for the OSL mechanism are different.

The PTTL signal induced by 470 nm blue LEDs revealed that the conventional TL peaks I and II reappear under phototransfer. This is the first time the TL peak II is being reported to be reproduced under phototransfer. No transfer of electrons from very deep traps (those occurring after 500 °C) was observed under phototransfer. The dose response of the PTTL peaks I and II exhibits a sublinear pattern. A first order kinetics characterizes the PTTL peaks. The changes in the PTTL intensity with optical stimulation time have been modelled using set of coupled linear differential equations, and the PTTL mechanism is ascribed to a system of one acceptor and three donors. The donor peak III however consists of an unknown number of collocated peaks. The photoionization cross section for the respective PTTL peaks was evaluated as 1.3×10^{-19} and 2.8×10^{-18} cm^2, and this is the first time these values are being reported for tanzanite. Evidence of thermal quenching is observed as the intensity of the PTTL signal decreases with an increase in the optical stimulation temperature above room temperature.

7.2 Recommendations for future study

The following areas could be explored to gain more insight into the luminescence mechanism of tanzanite:

- Spectral analysis of tanzanite to probe defects that are contributing to the TL and OSL mechanisms. The values of the activation energy of thermal quenching for the TL peaks suggest that each peak has a distinct recombination site. Also, depending on the source traps contributing to the OSL signal, the values of the activation energy of thermal quenching were found to be different which is an indication of distinct recombination sites.
- The influence of annealing on the TL, OSL and PTTL properties of tanzanite. In silicate luminescence materials such as quartz, annealing is known to have an effect on the kinetic parameters, including activation energy of thermal assistance and quenching [54].

The sensitivity of tanzanite to thermal stimulation may also be affected by annealing as in the case of quartz.

- TR-OSL analysis to compute the lifetimes of the OSL mechanism in order to investigate recombination processes.
- The effect of different light wavelengths on the OSL and PTTL mechanisms since the eviction of trapped electrons is dependent on the energy of the illumination source.
- The factors that affect the sensitivity of tanzanite to thermal stimulation of luminescence. During the sample preparation stage, it was noted that tanzanite with different blue colour and grain size respond differently to thermal stimulation.
- A probe into the possible use of tanzanite for dating with a focus on TL peaks II and III, which do not fade over long periods of delayed stimulation. The study could explore sensitivity changes and lifetimes of the trapped charges.

References

[1] S. W. S. McKeever, *Thermoluminescence of Solids*. Cambridge University Press, 1985. doi: 10.1017/CBO9780511564994.

[2] R. Chen and S. W. S. McKeever, *Theory of Thermoluminescence and Related Phenomena*. World Scientific, Singapore, 1997. doi: 10.1142/2781.

[3] G. Kitis, G. S. Polymeris, and V. Pagonis, "Stimulated luminescence emission: From phenomenological models to master analytical equations," *Applied Radiation and Isotopes*, vol. 153, Nov. 01, 2019. doi: 10.1016/j.apradiso.2019.05.041.

[4] S. W. S. McKeever, M. Moscovitch, and P. D. Townsend, *Thermoluminescence dosimetry materials: properties and uses*. Nuclear Technology Pub, 1995.

[5] J. M. Kalita, Kaya-Keleş, G. Çakal, N. Meriç, and G. S. Polymeris, "Thermoluminescence and optically stimulated luminescence properties of ulexite mineral," *J Lumin*, vol. 230, Feb. 2021, doi: 10.1016/J.JLUMIN.2020.117759.

[6] E. G. Yukihara and S. W. McKeever, "Optically stimulated luminescence (OSL) dosimetry in medicine.," *Physics in medicine and biology*, vol. 53, no. 20. 2008. doi: 10.1088/0031-9155/53/20/R01.

[7] M. L. Chithambo and D. E. Folley, "Dosimetric features, kinetics and mechanisms of thermoluminescence of tanzanite," *Physica B Condens Matter*, vol. 598, Dec. 2020, doi: 10.1016/j.physb.2020.412435.

[8] M. L. Chithambo, "Phototransferred thermoluminescence of tanzanite: A matrix-based analysis of time-response profiles and competition effects," *J Lumin*, vol. 234, Jun. 2021, doi: 10.1016/j.jlumin.2021.117969.

[9] K. A. Opoku, "Kinetic analysis and dosimetric features of thermoluminescence of tanzanite," in *67 Annual Conference of the South African Institute of Physics*, 2023, pp. 26–32.

[10] S. W. S. McKeever and E. G. Yukihara, *Optically Stimulated Luminescence : Fundamentals and Applications.* John Wiley & Sons, 2011.

[11] C. Kittel, *Introduction to Solid State Physics*. Vol. 8. John Wiley & Sons, 2004.

[12] R. Chen and V. Pagonis, *Thermally and optically stimulated luminescence: a simulation approach*. John Wiley & Sons, 2011.

[13] A. J. J. Bos, "Theory of thermoluminescence," *Radiat Meas*, vol. 41, suppl. 1, pp. S45–S56, Dec. 2006, doi: 10.1016/J.RADMEAS.2007.01.003.

[14] L. Bøtter-Jensen, "Luminescence Techniques: Instrumentation and Methods," *Radiat Meas*, vol. 27, no. 5/6, 1997.

[15] S. W. S. McKeever, *A course in luminescence measurements and analyses for radiation dosimetry*. Wiley, 2022.

[16] J. T. Randall and M. H. F. Wilkins, "Phosphorescence and electron traps - I. The study of trap distributions," *Proc R Soc Lond*, *Series A*, *Math & Phys Sci*, vol. 184, no. 999, pp. 365–389, Nov. 1945, doi: 10.1098/RSPA.1945.0024.

[17] G. F. J. Garlick and A. F. Gibson, "The Electron Trap Mechanism of Luminescence in Sulphide and Silicate Phosphors," *Proceedings of the Physical Society*, vol. 60, no. 6, p. 574, Jun. 1948, doi: 10.1088/0959-5309/60/6/308.

[18] C. E. May and J. A. Partridge, "Thermoluminescent kinetics of alpha-irradiated alkali halides," *J Chem Phys*, vol. 40, no. 5, pp. 1401–1409, 1964, doi: 10.1063/1.1725324.

[19] V. Pagonis, G. Kitis, and C. Furetta, *Numerical and practical exercises in thermoluminescence*. Springer, New York, 2006.

[20] G. Kitis, "TL glow-curve deconvolution functions for various kinetic orders and continuous trap distribution: Acceptance criteria for E and s values," *J Radioanal Nucl Chem*, vol. 247, no. 3, pp. 697–703, 2001, doi: 10.1023/A:1010688122988/METRICS.

[21] G. Kitis, J. M. Gomez-Ros, and J. W. N. Tuyn, "Thermoluminescence glow-curve deconvolution functions for first, second and general orders of kinetics," *J Phys D Appl Phys*, vol. 31, no. 19, p. 2636, Oct. 1998, doi: 10.1088/0022-3727/31/19/037.

[22] H. G. Balian and N. W. Eddy, “Figure-of-merit (FOM), an improved criterion over the normalized chi-squared test for assessing goodness-of-fit of gamma-ray spectral peaks,” *Nuclear Instruments and Methods*, vol. 145, no. 2, pp. 389–395, Sep. 1977, doi: 10.1016/0029-554X(77)90437-2.

[23] R. K. Gartia and L. L. Singh, “Evaluation of trapping parameter of quartz by deconvolution of the glow curves,” *Radiat Meas*, vol. 46, no. 8, pp. 664–668, Aug. 2011, doi: 10.1016/J.RADMEAS.2011.06.036.

[24] J. T. Randall and M. H. F. Wilkins, “Phosphorescence and electron traps II. The interpretation of long-period phosphorescence,” *Proc R Soc Lond*, *Series A*, *Math & Phys Sci*, vol. 184, no. 999, pp. 390–407, Nov. 1945, doi: 10.1098/RSPA.1945.0025.

[25] M. L. Chithambo, “A method for kinetic analysis and study of thermal quenching in thermoluminescence based on use of the area under an isothermal decay-curve,” *J Lumin*, vol. 151, pp. 235–243, Jul. 2014, doi: 10.1016/J.JLUMIN.2014.02.037.

[26] A. H. Booth, “Calculation of Electron Trap Depth from Thermoluminescence Maxima,” *Can J Chem*, vol. 32, no. 2, pp. 214–215, Feb. 2011, doi: 10.1139/V54-027.

[27] A. Bohun, “Thermoemission und Photoemission von Natriumchlorid,” *Czechoslovak Journal of Physics*, vol. 4, no. 1, pp. 91–93, Feb. 1954, doi: 10.1007/BF01688114/METRICS.

[28] H. Willey, “Electron Traps in Zinc-Sulphide Phosphors,” *Philips Research Report*, vol. 13, pp. 515–693, 1958.

[29] R. Chen, “On the calculation of activation energies and frequency factors from glow curves,” *J Appl Phys*, vol. 40, no. 2, pp. 570–585, 1969, doi: 10.1063/1.1657437.

[30] A. G. Wintle, “Thermal Quenching of Thermoluminescence in Quartz,” *Geophys J Int,* vol. 41, no. 1, pp. 107-113, 1975.

[31] S. Vincellér, G. Molnár, A. Berkane-Krachai, and P. Iacconi, “Influence of thermal quenching on the thermostimulated processes in α-Al_2O_3. Role of F and F+ centres,” *Radiat Prot Dosimetry*, vol. 100, no. 1–4, pp. 79–82, 2002, doi: 10.1093/OXFORDJOURNALS.RPD.A005940.

[32] R. Nanjundaswamy, K. Lepper, S. W. S. Mckeever, Y. S. Horowitz, and L. Oster, "Thermal quenching of thermoluminescence in natural quartz," *Radiat Prot Dosimetry*, vol. 100, no. 1–4, pp. 305–308, 2002, doi: 10.1093/OXFORDJOURNALS.RPD.A005874.

[33] V. Pagonis *et al.*, "Modelling the thermal quenching mechanism in quartz based on time-resolved optically stimulated luminescence," *J Lumin*, vol. 130, no. 5, pp. 902–909, May 2010, doi: 10.1016/J.JLUMIN.2009.12.032.

[34] M. A. Reshchikov, "Mechanisms of Thermal Quenching of Defect-Related Luminescence in Semiconductors," *physica status solidi (a)*, vol. 218, no. 1, p. 2000101, Jan. 2021, doi: 10.1002/PSSA.202000101.

[35] M. L. Chithambo, *An introduction to time-resolved optically stimulated luminescence*. Morgan & Claypool Publishers, California, 2018.

[36] I. D. Venevtsev, V. Khanin, P. A. Rodnyi, H. Wieczorek, and C. Ronda, "Temperature quenching of radio- and photoluminescence of $Y_3(Ga,Al)_5O_{12}:Ce^{3+}$ and $Gd_3(Ga,Al)_5O_{12}:Ce^{3+}$ Garnet Ceramics," *IEEE Trans Nucl Sci*, vol. 65, no. 8, pp. 2090–2096, Aug. 2018, doi: 10.1109/TNS.2018.2810894.

[37] M. L. Chithambo, "Thermal assistance in the optically stimulated luminescence of superluminous $Sr_4Al_{14}O_{25}$: Eu^{2+},Dy^{3+}," *Physica B Condens Matter*, vol. 603, Feb. 2021, doi: 10.1016/j.physb.2020.412722.

[38] B. Subedi, G. Kitis, and V. Pagonis, "Simulation of the influence of thermal quenching on thermoluminescence glow-peaks," *Physica Status Solidi (A) Applications and Materials Science*, vol. 207, no. 5, pp. 1216–1226, May 2010, doi: 10.1002/PSSA.200925588.

[39] G. Kitis, J. G. Gapadopoulos, S. Charalambous, and J. W. N. Tuyn, "The Influence of Heating Rate on the Response and Trapping Parameters of Alpha-Al_2O_3:C," *Radiat Prot Dosimetry*, Oct. 1994, doi: 10.1093/OXFORDJOURNALS.RPD.A082391.

[40] D. E. Folley and M. L. Chithambo, "Influence of annealing on thermoluminescence of natural quartz: Kinetic analysis and experimental study of apparent inverse thermal quenching," *Radiat Meas*, vol. 120, pp. 53–58, Dec. 2018, doi: 10.1016/J.RADMEAS.2018.04.010.

[41] G. Kitis, G. S. Polymeris, V. Pagonis, and N. C. Tsirliganis, "Thermoluminescence response and apparent anomalous fading factor of Durango fluorapatite as a function of the heating rate," *physica status solidi (a)*, vol. 203, no. 15, pp. 3816–3823, Dec. 2006, doi: 10.1002/PSSA.200622197.

[42] A. Murray *et al.*, "Optically stimulated luminescence dating using quartz," *Nature Reviews Methods Primers*, vol. 1, no. 1, Dec. 2021, doi: 10.1038/S43586-021-00068-5.

[43] L. Bøtter-Jensen, S. W. S. McKeever, and A. G. Wintle, *Optically Stimulated Luminescence Dosimetry*. Elsevier, 2003. doi: 10.1016/B978-0-444-50684-9.X5077-6.

[44] J. H. Choi, G. Duller, and A. G. Wintle, "Analysis of quartz LM-OSL curves," *Ancient TL*, vol. 24, no. 1, 2006.

[45] R. M. Bailey, "The slow component of quartz optically stimulated luminescence," *Radiat Meas,* vol. 32, no. 3, pp. 233-246, 2000.

[46] M. L. Chithambo and R. B. Galloway, "On the slow component of luminescence stimulated from quartz by pulsed blue light-emitting diodes," *Nucl Instrum Methods Phys Res B*, vol. 183, no. 3-4, pp. 358-368, 2001.

[47] E. Bulur, "An alternative technique for optically stimulated luminescence (OSL) experiment," *Radiat Meas*, vol. 26, no. 5, pp. 701–709, 1996, doi: 10.1016/S1350-4487(97)82884-3.

[48] M. L. Chithambo and R. B. Galloway, "On luminescence lifetimes in quartz," *Radiat Meas*, vol. 32, no. 5–6, pp. 621–626, Dec. 2000, doi: 10.1016/S1350-4487(00)00096-2.

[49] I. K. Bailiff, "Characteristics of time-resolved luminescence in quartz," *Radiat Meas*, vol. 32, no. 5, pp. 401–405, Dec. 2000, doi: 10.1016/S1350-4487(00)00126-8.

[50] M. L. Chithambo, "The analysis of time-resolved optically stimulated luminescence: I. Theoretical considerations," *J Phys D Appl Phys*, vol. 40, no. 7, p. 1874, Mar. 2007, doi: 10.1088/0022-3727/40/7/006.

[51] M. L. Chithambo, C. Seneza, and J. M. Kalita, "Phototransferred thermoluminescence of α-Al_2O_3:C: Experimental results and empirical models," *Radiat Meas*, vol. 105, pp. 7–16, Oct. 2017, doi: 10.1016/J.RADMEAS.2017.08.009.

[52] C. S. Alexander, M. F. Morris, and S. W. S. McKeever, "The time and wavelength response of phototransferred thermoluminescence in natural and synthetic quartz," *Radiat Meas*, vol. 27, no. 2, pp. 153–159, Apr. 1997, doi: 10.1016/S1350-4487(96)00105-9.

[53] M. L. Chithambo, P. Niyonzima, and J. M. Kalita, "Phototransferred thermoluminescence of synthetic quartz: Analysis of illumination-time response curves," *J Lumin*, vol. 198, pp. 146–154, Jun. 2018, doi: 10.1016/J.JLUMIN.2018.02.029.

[54] R. R. Dawam, "Thermoluminescence and Phototransferred Thermoluminescence of Synthetic Quartz," PhD Thesis, Rhodes University, Grahamstown, South Africa, 2020.

[55] M. L. Chithambo, "Phototransferred thermoluminescence of CaF_2: Principles, analytical methods, and mechanisms," *J Appl Phys*, vol. 132, no. 5, Aug. 2022, doi: 10.1063/5.0091205.

[56] C. H. Edwards, D. E. Penney, and D. Calvis, *Elementary differential equations with boundary value problems*, Sixth Ed. New Jersey: Pearson Education, Inc., 2014.

[57] DTU Physics, "Product Catalogue, 2103a," Assessed: Aug. 20, 2023, online at https://www.fysik.dtu.dk/english/-/media/institutter/fysik/research/radiation-physics/produkter-og-services/radiation_measurement_instruments/tl_osl_reader/brochure/product-catalogue-2103a.pdf?la=da&hash=97FBE3BD05A1520A920064B66757A80FE3E4EE55.

[58] DTU Nutech, "Product specification RISØ TL/OSL Reader," 2014.

[59] Z. Mao, F. Jiang, and T. S. Duffy, "Single-crystal elasticity of zoisite $Ca_2Al_3Si_3O_{12}(OH)$ by Brillouin scattering," *American Mineralogist*, vol. 92, no. 4, pp. 570–576, 2007, doi: 10.2138/am.2007.2329.

[60] W. A. Deer, R. A. Howie, and J. Zussman, *An Introduction to the Rock-Forming Minerals*, Wiley, New York, 1992.

[61] T. Pluthametwisute, B. Wanthanachaisaeng, C. Saiyasombat, and C. Sutthirat, “Cause of Color Modification in Tanzanite after Heat Treatment,” *Molecules*, vol. 25, no. 16, Aug. 2020, doi: 10.3390/molecules25163743.

[62] R. Bocchio, I. Adamo, V. Bordoni, F. Caucia, and V. Diella, “Gem-quality zoisite from Merelani (Northeastern Tanzania): Review and new data,” *Periodico di Mineralogia*, vol. 81, no. 3. Sapienza Universita Editrice, pp. 379–391, 2012. doi: 10.2451/2012PM0022.

[63] T. Armbruster *et al.*, “Recommended nomenclature of epidote-group minerals,” *European Journal of Mineralogy*, vol. 18, no. 5, pp. 551–567, Nov. 2006, doi: 10.1127/0935-1221/2006/0018-0551.

[64] N. R. Barot and E. W. Boehm, “Gem-Quality Green Zoisite,” *Gems & Gemology*, vol. 28, no. 1, pp. 4-15.

[65] D. M. Dirlarn, E. B. Misiorowski, R. Tozer, K. B. Stark, and A. M. Bassett, “Gem Wealth of Tanzania,” *Gems & Gemology*, vol. 28, no. 2, pp. 80-102.

[66] K. Karlschmetzer and H. Bank, “Bluish-Green Zoisite From Merelani, Tanzania,” *Gems & Gemol.*, vol. 16, pp. 121–122, 1979.

[67] C. S. Hurlbut, “Gem zoisite from Tanzania 1,” *American Mineralogist*, vol. 54, pp. 702–709, 1969.

[68] B. Olivier, “The Geology and Petrology of the Merelani Tanzania Deposit, NE Tanzania,” PhD Thesis, University of Stellenbosch, South Africa, 2006.

[69] R. Chen and S. W. S. McKeever, “Characterization of nonlinearities in the dose dependence of thermoluminescence,” *Radiat Meas*, vol. 23, no. 4, pp. 667–673, Oct. 1994, doi: 10.1016/1350-4487(94)90002-7.

[70] A. G. Wintle, “Detailed study of a thermoluminescent mineral exhibiting anomalous fading,” *J Lumin*, vol. 15, no. 4, pp. 385–393, Dec. 1977, doi: 10.1016/0022-2313(77)90037-0.

[71] I. K. Sfampa, G. S. Polymeris, N. C. Tsirliganis, V. Pagonis, and G. Kitis, “Prompt isothermal decay of thermoluminescence in an apatite exhibiting strong anomalous fading,” *Nucl Instrum Methods Phys Res B*, vol. 320, pp. 57–63, Feb. 2014, doi: 10.1016/J.NIMB.2013.12.003.

[72] E. Bulur, L. Bøtter-Jensen, and A. S. Murray, “Optically stimulated luminescence from quartz measured using the linear modulation technique,” *Radiat Meas*, vol. 32, no. 5, pp. 407–411, Dec. 2000, doi: 10.1016/S1350-4487(00)00115-3.

[73] F. Agulló-López, C. R. A. Catlow, and P. D. Townsend, *Point defects in materials*. Academic Press, London, 1988.

[74] E. Bulur and H. Y. Göksu, “Phototransferred thermoluminescence from α-Al_2O_3:C using blue light emitting diodes,” *Radiat Meas*, vol. 30, no. 2, pp. 203–206, Apr. 1999, doi: 10.1016/S1350-4487(99)00035-9.

[75] G. A. T. Duller, “A new method for the analysis of infrared stimulated luminescence data from potassium feldspars,” *Radiat Meas*, vol. 23, no. 2–3, pp. 281–285, Apr. 1994, doi: 10.1016/1350-4487(94)90053-1.

[76] M. L. Chithambo, K. Shinsho, and G. S. Polymeris, “Properties of phototransferred thermoluminescence of Al_2O_3:Cr,” *Physica B Condens Matter*, vol. 650, p. 414576, Feb. 2023, doi: 10.1016/J.PHYSB.2022.414576.

[77] B. G. Markey, S. W. S. McKeever, M. S. Akselrod, L. Bøtter-Jensen, N. Agersnap Larsen, and L. E. Colyott, “The Temperature Dependence of Optically Stimulated Luminescence from Alpha-Al_2O_3:C,” *Radiat Prot Dosimetry*, vol. 65, no. 1–4, pp. 185–189, Jun. 1996, doi: 10.1093/OXFORDJOURNALS.RPD.A031617.

Appendix A

Portions of the result from the thermoluminescence analysis were published in the South Africa Institute of Physics 2023 Conference Proceedings. A reprint of the paper is given in this Appendix.

Kinetic analysis and dosimetric features of thermoluminescence of tanzanite

K A Opoku

Department of Physics and Electronics, Rhodes University, PO 94, Grahamstown, 6140, South Africa

E-mail: **akingsley75@yahoo.com**

Abstract. Tanzanite is a rare gem mineral of high commercial value. It is sensitive to optical and thermal stimulation of luminescence used to study point defects in insulators. Kinetic analysis and dosimetric features of thermoluminescence of tanzanite are reported. A glow curve measured at 1 °C s^{-1} following beta irradiation to 70 Gy shows a high intensity peak at 74 °C and two lower intensity peaks at 138 and 186 °C. The peaks are respectively referred to as I, II and III. The dependence of the peak position on partial heating and on irradiation dose is consistent with first order kinetics. The activation energy for peaks I-III are 0.81, 1.00 and 1.24 eV respectively. The dose response of each peak is sublinear as quantitatively determined using analysis of supralinearity indices.

1. Introduction

Tanzanite is a gem mineral found only at Merelani, Tanzania. The gem has a huge market demand owing to its aesthetic qualities linked to its pleochroism which is evident at different crystallographic orientations. Tanzanite is a type of zoisite [$Ca_2Al_3(Si_2O_7)(SiO_4)O(OH)$], a metamorphic mineral of the epidote group [1,2] and has an orthorhombic crystal structure [3]. The crystal structure is built of octahedral chains connected by single tetrahedra of SiO_4 and double tetrahedra of Si_2O_7 groups.

Zoisite is sensitive to thermal and optical stimulation of luminescence [4,5]. Despite this, there is only one report, namely, that of Chithambo and Folley [6] on the thermoluminescence (TL) of tanzanite. For TL to occur, an insulator or semiconductor is first irradiated with ionizing radiation to induce electron movement into the conduction band. Point defects within the crystal create charge trapping centres. The supply of heat leads to the excitement of trapped electrons into the conduction band followed by their recombination with trapped holes during which luminescence appears [7]. In the study of Chithambo and Folley [6], three TL peaks at 70, 130 and 180 °C were observed in measurements made at 1 °C s^{-1}, after 51 Gy beta irradiation. All peaks were seen to suffer thermal quenching. The TL of peak I ensues from recombination of electron occurring at $[TiO_4\backslash h^+]^0$ sites whereas the TL of peaks II and III appears owing to alkali recombination at $[TiO_4]^-$ sites [6]. Kinetic analysis was conducted only for the prominent peak, that is, peak I and that of peaks II and III was omitted. Fading of peaks II and III, due to delay in readout following irradiation meant that the peaks are not shallow traps, but the activation energy and frequency factor were not reported. To gain deeper insights into the TL of tanzanite, we compute the kinetic parameters and analyze the dose response of all three peaks.

2. Experimental procedure

The sample used was commercially available tanzanite (African Gems and Minerals, Cape Town). Samples were prepared in coarse grain form and used *as received*. TL measurements were made using

a RISØ TL/OSL DA-20 Luminescence Reader. The luminescence was detected by an EMI 9235QB photomultiplier tube through a 7 mm Hoya U-340 filter (transmission band 250 - 390 nm). The sample was irradiated *in-situ* using a $^{90}Sr/^{90}Y$ beta source at a dose rate of 0.10 Gy/s. All measurements were made in a nitrogen atmosphere to ensure good thermal contact between the heater plate and the sample holder. Unless indicated otherwise, all recordings were carried out at 1 °C s^{-1}.

3. Results and discussion

3.1. *Glow curve features*

Figure 1 depicts a glow curve corresponding to 70 Gy. Three peaks at 74 °C, 138 °C and at 186 °C (peaks I-III) are seen. A similar number of peaks and a weaker fourth one were observed by Chithambo and Folley [6]. Thermal cleaning to identify less prominent peaks in the glow curve revealed none.

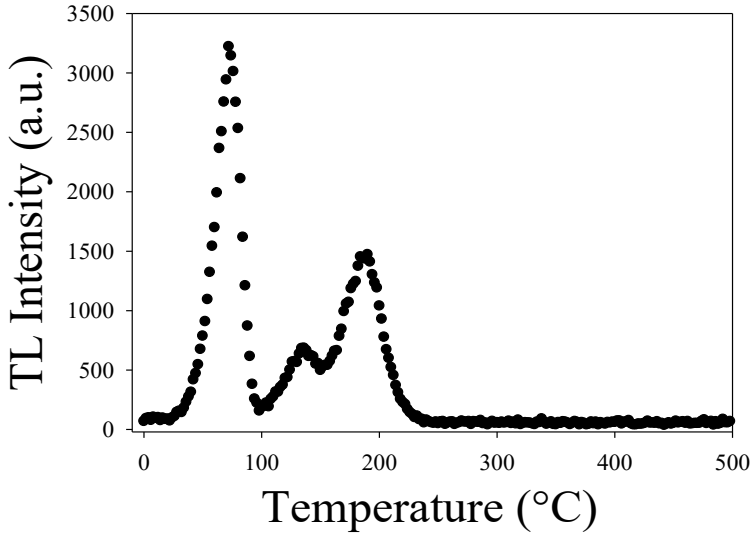

Figure 1. TL glow curve of tanzanite following 70 Gy beta irradiation. Three peaks at 74, 138 and 186 °C can be observed.

3.2. *Analysis for order of kinetics*

The order of kinetics for the peaks was assessed by examining how variable doses and partial heating affect the peak position (T_m). The partial heating procedure (T_m-T_{stop}) monitors the shifts in peak position as the sample undergoes partial heating to a temperature (T_{stop}) each time it is irradiated. For first order kinetics, T_m does not vary with either dose or preheat (T_{stop}) because the initial concentration of trapped charges has no bearing on T_m [7]. For second order kinetics, T_m decreases as dose increases [7]. A graph of T_m against T_{stop} is depicted in figure 2. The position of peaks I-III were determined as 74 ± 1, 139 ± 3 and 191 ± 3 °C. The parameter T_m also shows no dependence on dose at 73 ± 1, 138 ± 3 and 186 ± 2 °C respectively. Therefore all peaks are of first order kinetics.

3.3. *Stability of peaks*

Any change in the TL intensity owing to delay in readout after irradiation was analysed for periods between 0 to 10,000 s following irradiation to 10, 50 and 100 Gy. Figure 3(a) shows the intensity of peak I versus delay in readout corresponding to the three doses. Peak I fades with time for all doses. A similar behaviour was observed before in the literature [6].

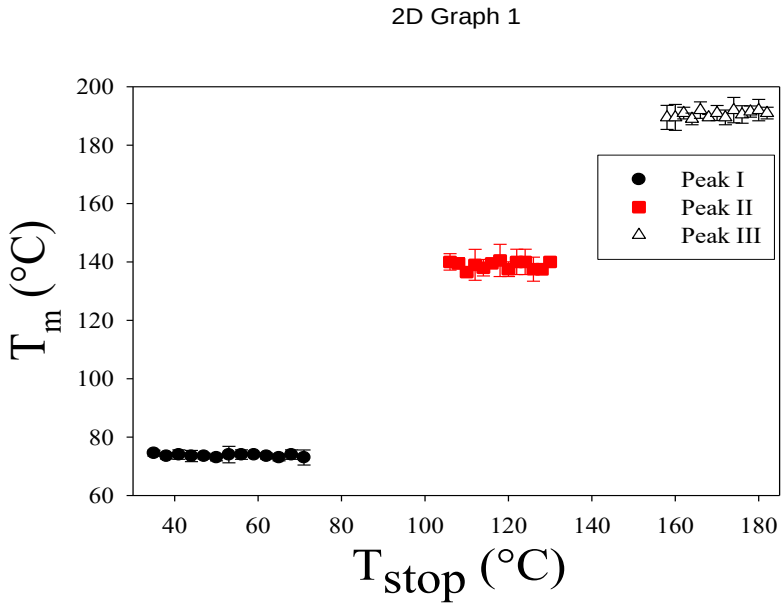

Figure 2. Peak position (T_m) dependence on partial heating (T_{stop}). The peak position remains stable for each peak. The mean of four measurements was evaluated to represent the value of each data point.

An empirical function that best fit the data is given by:

$$I(t) = a + I_0 e^{-\lambda t}, \tag{1}$$

where a is a constant, I_0 is initial intensity, t is delay and λ is decay constant. Figure 3(b) shows the intensity of peak II versus delay. The intensity is stable with time for all doses. A similar result was seen

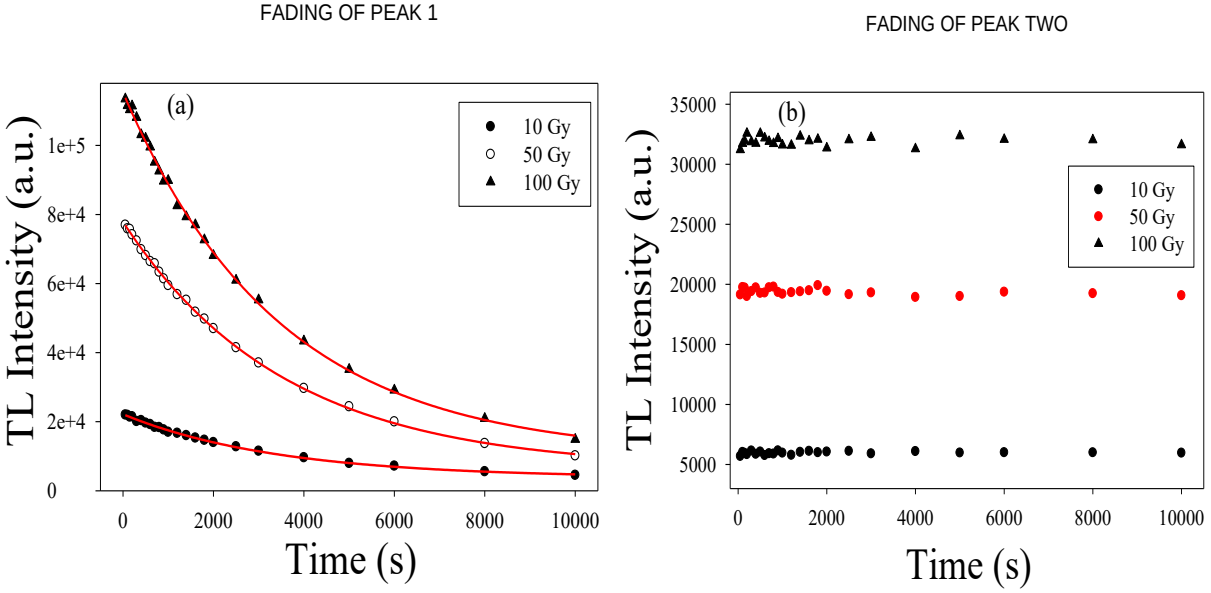

Figure 3. The relationship between intensity and delay in readout after irradiation for peak I (a) and peak II (b). The continuous lines in (a) represent the fits of equation (1).

3.4. *Dose response*

The dose response for all three peaks was analysed for doses from 10 to 200 Gy. The plot in figure 4(a) depicts the dose response for each peak. The intensity increases sublinearly with dose. The data is best fitted with the empirically chosen function:

$$y(D) = a\left(1 - e^{-bD}\right), \tag{2}$$

where a is intensity at saturation level, b is a constant and D is dose. Qualitative analysis of the dose response was carried out with the supralinearity index [7] given as:

$$f(D) = [y(D)/D]/[y(D_1)/D_1], \tag{3}$$

where D_1 represents normalization dose and $y(D_1)$ is a function dependent on the normalization dose. Figure 4(b) depicts the plot of $f(D)$ versus dose for all peaks. In such a test, values of $f(D) < 1$ indicates a sublinear dose response and $f(D) > 1$ shows a supralinearity response [7]. From figure 4(b), $f(D) < 1$

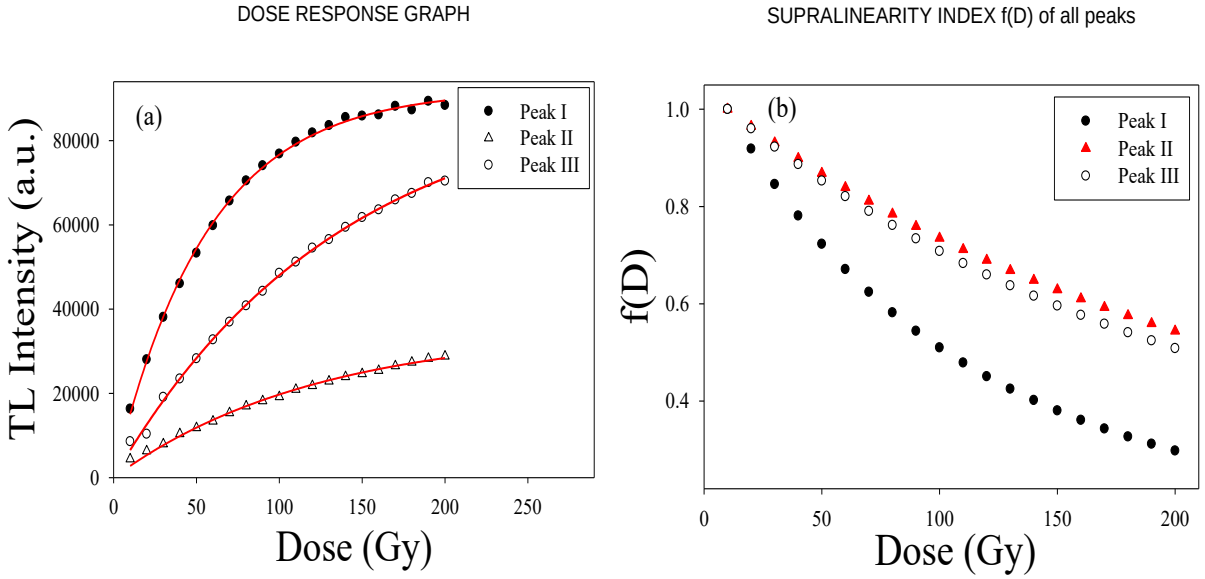

Figure 4. TL dose response for peaks I-III (a), and supralinearity index function $f(D)$ versus dose for peaks I-III (b). The continuous lines in (a) represent the fits of equation (2).

3.5. *Kinetic analysis*

Kinetic parameters such as the activation energy (E), frequency factor (s) and kinetic order (b) provide insight into the luminescence processes. The activation energy is the energy required to detrap an electron into the conduction band. The frequency factor is the number of times per second the electrons interacts with lattice phonons. The parameter b denotes the order of kinetics [7]. Results using various analytical methods used for the kinetic analysis in this work are now presented:

3.5.1. *Curve fitting method (CF).* The glow peaks were fitted with the Kitis et al general order curve fitting equation [8] given as:

$$I(T) = I_m b^{\frac{b}{b-1}} e^{\left(\frac{E}{kT}\frac{T-T_m}{T_m}\right)} \left[1 + (b-1)\frac{2kT_m}{E} + (b-1)\left(1 - \frac{2kT}{E}\right)\frac{T^2}{T_m^2} e^{\left(\frac{E}{kT}\frac{T-T_m}{T_m}\right)}\right]^{-\frac{b}{b-1}}, \tag{4}$$

where I is intensity, T is temperature, k is Boltzmann constant, I_m is maximum intensity and all other parameters retain their usual meanings. The parameter s was evaluated from the expression [7]:

$$s = (\beta E/kT_m^2)e^{(E/kT_m)}, \tag{5}$$

where β is heating rate. As an example, the plot for peak I is depicted in figure 5. The parameter E yielded 0.87 ± 0.02, 0.95 ± 0.07 and 1.13 ± 0.01 eV for peaks I-III respectively. The values of b were 0.96 ± 0.01, 1.2 ± 0.01, and 1.2 ± 0.01 for the respective peaks. Since b for all the peaks are closer to 1,

all peaks are of first order kinetics. From equation (5), s was evaluated as 4.3×10^{11}, 3.4×10^{10} and 1.4×10^{11} s^{-1} respectively. The values of s are comparable to the order of the lattice vibration frequency which is approxin

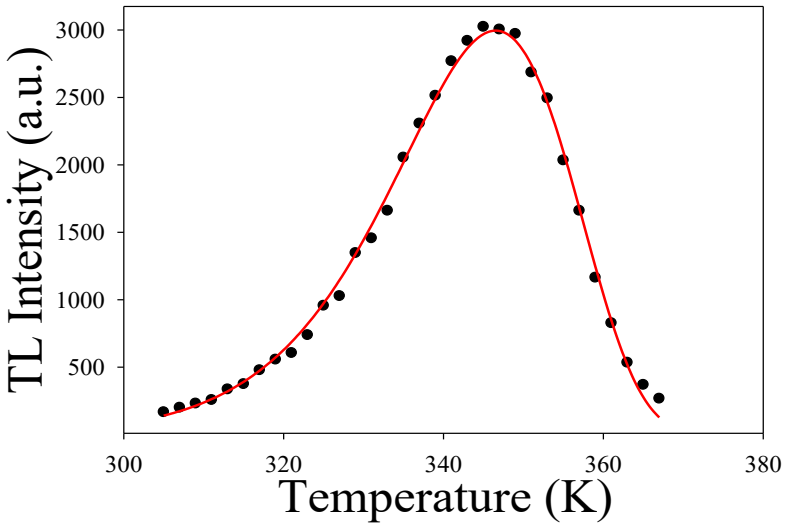

Figure 5. General order curve fitting for peak I. The solid line represents the fit of equation (4).

3.5.2. Variable heating rate method (VHR)

Recording the TL at different heating rates alters the peak position. The TL was recorded at heating rates of 0.5 to 4.5 °C s^{-1} after 70 Gy irradiation each time. The parameters E and s were evaluated using the expression [7]:

$$\ln(T_m^2/\beta) = E/(kT_m) + \ln(E/sk). \quad (6)$$

A plot of $\ln(T_m^2/\beta)$ against $1/(kT_m)$is linear as shown in figure 6. The slope of the plot is equal to E, evaluated as 0.78 ± 0.02, 1.01 ± 0.06 and 1.39 ± 0.11 eV for the respective peaks. The parameter s was evaluated from the

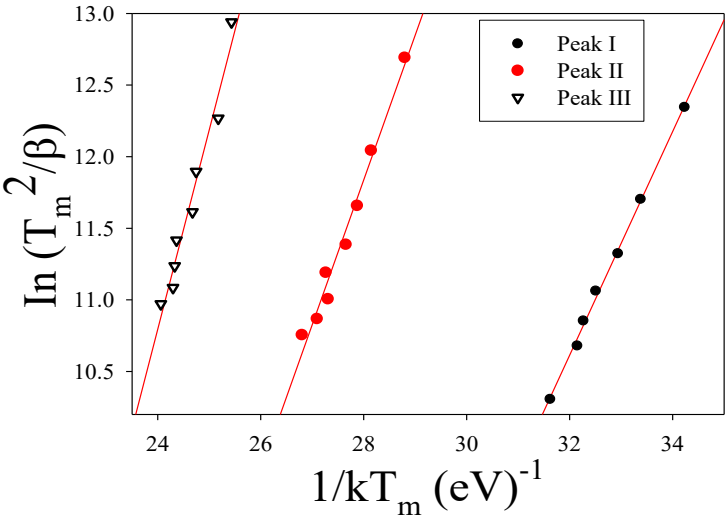

Figure 6. Plot of $\ln(T_m^2/\beta)$ versus $1/(kT_m)$ for peaks I-III. Measurement of the TL was done at different β from 0.5 to 4.5 °C s^{-1} after 70 Gy irradiation each time. The continuous lines are the most linear trends through the data points.

3.5.3. *Whole glow peak method (WGP)*
The integral of the area (A) beneath a peak can be written as a function of temperature as:

$$\ln(I/A^b) = \ln(s/\beta) - E/kT, \quad (7)$$

where a graph of $\ln(I/A^b)$ versus $1/kT$ will yield a linear line for an appropriate value of b [7]. The parameters E and s are computed from the gradient and y-intercept accordingly. Figure 7 depicts such plot for various values of b for peak I. The line with the highest coefficient of determination (r^2) value of 0.9977 corresponds to b=0.9. For peaks II and III, b=1.3 yields the most linear line. The values of E hence found are 0.77 ± 0.01, 1.03 ± 0.02 and 1.20 ± 0.04 eV for the respective peaks. The parameter s was evaluated as 1. I.

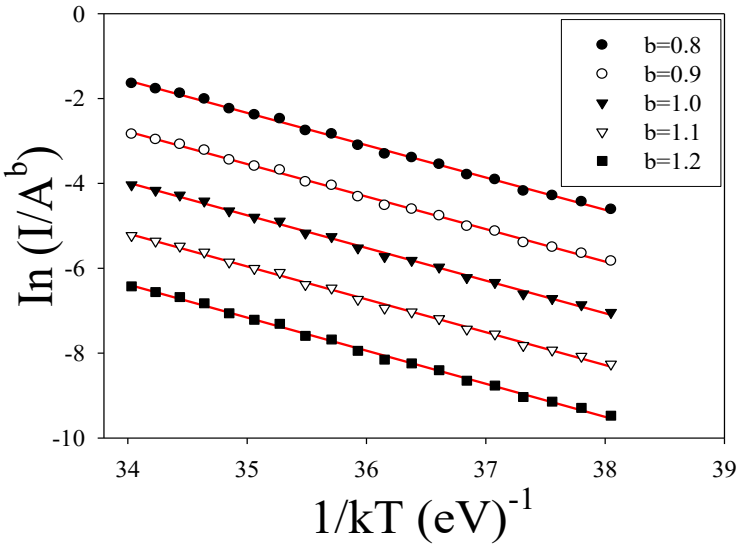

Figure 7. Graph of $\ln(I/A^b)$ against $1/kT$ for peak I. The continuous lines are the most linear trends through the data points.

3.5.4. *Summary of kinetic parameters*
Table 1 depicts the evaluated kinetic parameters for all peaks. The kinetic parameters for peak I are compared with those reported in literature. The parameters compare favourably. Also, the results derived from the different analytical methods are comparable. The mean of the activation energy E is 0.81, 1.00 and 1.24 eV for the respective peaks. The kinetic parameter E for peaks II and III suggest the peaks are not shallow electron traps. This is corroborated by the fact that the peaks do not show any phosphorescence at room temperature. The full meaning of CF, VHR and WGP as used in the table has been specified in sections 3.5.1 to 3.5.3 respectively.

4. Conclusion

We have observed three TL peaks in tanzanite at 74, 138 and 186 °C for a glow curve measured at 1 °C s^{-1} after 70 Gy beta irradiation. All peaks are of first order kinetics. Peak I fades with delay in readout after irradiation, in contrast to peaks II and III which do not. The dose response of peaks I-III is sublinear. The activation energy for peaks I-III are about 0.81, 1.00 and 1.24 eV respectively. The frequency factor is within the order of 10^{11}, 10^{10} and 10^{13} s^{-1} for the respective peaks.

Table 1. Kinetic parameters for peaks I, II and III.

Peaks	Analytical Method	E (eV)	s (s^{-1})	b	Reference
Peak I	CF	0.87 ± 0.02	4.3×10^{11}	0.96 ± 0.01	Figure 5
		0.860 ± 0.004	2.0×10^{11}	0.970 ± 0.003	Chithambo and Folley [6]
	VHR	0.78 ± 0.02	1.6×10^{10}		Figure 6
		0.86 ± 0.03	3.0×10^{11}		Chithambo and Folley [6]
	WGP	0.77 ± 0.01	1.3×10^{10}	0.9	Figure 7
		0.85 ± 0.01	3.0×10^{11}	1.1	Chithambo and Folley [6]
Peak II	CF	0.95 ± 0.07	3.4×10^{10}	1.20 ± 0.01	Current work
	VHR	1.01 ± 0.06	1.7×10^{11}		
	WGP	1.03 ± 0.02	1.7×10^{10}	1.3	
Peak III	CF	1.13 ± 0.01	1.4×10^{11}	1.20 ± 0.01	
	VHR	1.39 ± 0.11	1.0×10^{14}		
	WGP	1.20 ± 0.04	2.8×10^{10}	1.3	

Acknowledgement
This research was conducted under the supervision of Prof. M L Chithambo and was generously funded by Rhodes University and the National Research Foundation of South Africa.

References

[1] Mao Z, Jiang F and Duffy T S 2007 *Am. Min*. **92** 570-576
[2] Pluthametwisute T, Wanthanachaisaeng B, Saiyasombat C and Suthirat C 2020 *Molecules* **25** 3743
[3] Xu J, Zhang D, Fan D, Wu X, Shi F and Zhou W 2019 *Phys. Chem. Miner*. **46** 333–341
[4] Chithambo M L 2021 *J. Lumn*. **234** 117969
[5] Ccallata H J and Watanabe S 2010 *AIP Conf. Proc.* (Santiago) Vol 1265, 391-394
[6] Chithambo M L and Folley D E 2020 *Phys. Condens. Matter* B **598** 412435
[7] Chen R and Pagonis V 2011 *Thermally and optically stimulated luminescence: a simulation approach* (Chichester: John Wiley & Sons)
[8] Kitis G, Gomez-Ros J M and Tuyn J W N 1998 *J. Phys.* D **31** 2636–2641